

**NORTH AMERICAN MONSOON VARIABILITY FROM
PALEOCLIMATE ERA TO CLIMATE CHANGE PROJECTION: A
MULTIPLE DATASET PERSPECTIVE**

By

Carlos Mauricio Carrillo Cruz

Copyright © Carlos Mauricio Carrillo Cruz 2014

A Dissertation Submitted to the Faculty of the

DEPARTMENT OF ATMOSPHERIC SCIENCES

In Partial Fulfillment of the Requirements

For the Degree of

DOCTOR OF PHILOSOPHY

In the Graduate College

THE UNIVERSITY OF ARIZONA

2014

UMI Number: 3667939

All rights reserved

INFORMATION TO ALL USERS

The quality of this reproduction is dependent upon the quality of the copy submitted.

In the unlikely event that the author did not send a complete manuscript and there are missing pages, these will be noted. Also, if material had to be removed, a note will indicate the deletion.



UMI 3667939

Published by ProQuest LLC (2014). Copyright in the Dissertation held by the Author.

Microform Edition © ProQuest LLC.

All rights reserved. This work is protected against unauthorized copying under Title 17, United States Code



ProQuest LLC.
789 East Eisenhower Parkway
P.O. Box 1346
Ann Arbor, MI 48106 - 1346

THE UNIVERSITY OF ARIZONA
GRADUATE COLLEGE

As members of the Dissertation Committee, we certify that we have read the dissertation prepared by Carlos Mauricio Carrillo Cruz, titled **North American monsoon variability from paleoclimate era to climate change projection: a multiple dataset perspective** and recommend that it be accepted as fulfilling the dissertation requirement for the Degree of Doctor of Philosophy.

_____ Date: 11/14/2014
Christopher L. Castro

_____ Date: 11/14/2014
Connie A. Woodhouse

_____ Date: 11/14/2014
Gregg Garfin

_____ Date: 11/14/2014
Francina Dominguez

Final approval and acceptance of this dissertation is contingent upon the candidate's submission of the final copies of the dissertation to the Graduate College.

I hereby certify that I have read this dissertation prepared under my direction and recommend that it be accepted as fulfilling the dissertation requirement.

_____ Date: 11/14/2014
Dissertation Director: Christopher L. Castro

STATEMENT BY AUTHOR

This dissertation has been submitted in partial fulfillment of the requirements for an advanced degree at the University of Arizona and is deposited in the University Library to be made available to borrowers under rules of the Library.

Brief quotations from this dissertation are allowable without special permission, provided that an accurate acknowledgement of the source is made. Requests for permission for extended quotation from or reproduction of this manuscript in whole or in part may be granted by the copyright holder.

SIGNED: Carlos Mauricio Carrillo Cruz

ACKNOWLEDGEMENTS

I would like to acknowledge the continued support from my major professor, Dr. Christopher L. Castro, who guide me in the whole process of this investigation and also help me in the transition to become a better scientist. Also, I want to thank Drs. Connie A. Woodhouse, Gregg Garfin, and Francina Dominguez for serving on my committee. Their expertise in the field has helped to polish this investigation and their continuous advice was critically important to clarify and motivate many of the ideas presented in here.

The first year of this research was funded by the National Science Foundation under grants ATM-0813656 and the Atmospheric Sciences Department through the Graduates Incentives for Growth Award (GIGA), in Hydrometeorology related research. The second year was funded by the City of Tucson Office of Conservation and Sustainable Development and the National Science Foundation. Additional funding was provided by the Climate Assessment for the Southwest (CLIMAS) at the University of Arizona. The last two years of this research were founded by a multi institutional project among the Department of Interior, Bureau of Reclamation, Salt River Project, and Central Arizona Project. Additional funding for the last year was provided by the Water Sustainability Graduate Student Fellowship Program at the University of Arizona. Also many anonymous contributors. Thanks to all of them.

I am grateful to Dr. Hsin-I Chang for her support and long hours of conversation debugging modeling codes in these years at the University of Arizona. I am especially grateful to Dr. Daniel Griffin for his continuous motivation, informal lectures, and encourage on pursuing the tree-ring part of this research. I also want to thank to Drs. Eylon Shamir and Melissa S. Bukovsky for their collaboration and support in this stage of my career. This research was possible only through an extensive collaboration: Drs. Dave Meko, Steve Leavitt, Ramzi Touchan, and Sharon Megdal. Also, my student colleagues: Brittany Ciancarelli, Thang Luong, Jeremy Mason, Timothy Lahmers, and Megan Jares.

Thanks also to all of my fellow students, Koichi, Gouri, Lesley, Lindsay, Maria, Bill S., Bill, Susan, Kerry, Huancui, James, Michael, Michael S., Diana, Zhao, Alejandro, Ewan, and Aishwarya for working and solving problems together. Especially thank to Dr. Erick Rivera who helped me in all the academic part of this program such as homeworks, mid-terms, and the qualifying examination and comprehensive evaluation. Thanks for your partnership and guidance on these issues, Erick, I could not make it without your help. I am also thankful to Dr. Patrick Broxton, my friend and office mate, for sharing long hours on the bike preparing for the 2014 Tour de Tucson. I am also grateful to the faculty, staff, and especially to Dr. Betterton for creating a cooperative and interdisciplinary working environment at the Atmospheric Sciences Department.

Finally, thanks to my dedicated wife, Erika, my daughters Paula and Claudia, and especially my brothers and sisters in my homeland of Peru for your love and unending support.

DEDICATION

To my parents: Jose Antonio Carrillo Carmelo and Florencia Cruz Garcia for their love and every day of care and happiness.

TABLE OF CONTENTS

ABSTRACT	10
CHAPTER 1: INTRODUCTION	12
1.1 Background	12
1.2 Tree-ring chronologies and low-frequency variability of the North American monsoon	13
1.3 Future climate projections of the North American monsoon	15
1.4 Low-frequency climate variability of the North American monsoon in a modeling framework	17
1.5 Purpose.....	19
CHAPTER 2: PRESENT STUDY	21
2.1 Appendix A: Low frequency variability of the North American monsoon as diagnosed through earlywood and latewood tree-ring chronologies in the southwestern U.S.	21
2.2 Appendix B: Pacific SST-related teleconnective influences on North American monsoon precipitation within North American Regional Climate Change Assessment Program (NARCCAP) models	22
2.3 Appendix C: Low frequency climate variability in western North America as diagnosed in a dynamically downscaled twentieth century reanalysis	24
REFERENCES	26
APPENDIX A: LOW FREQUENCY VARIABILITY OF THE NORTH AMERICAN MONSOON AS DIAGNOSED THROUGH EARLYWOOD AND LATEWOOD TREE-RING CHRONOLOGIES IN THE SOUTHWESTERN U.S.	31
Abstract	32
1. Introduction	33

2. Data Sources	37
a. Tree-ring chronology data	37
b. Precipitation data and Standardized Precipitation Index (SPI)	38
c. Sea surface temperature and geopotential height data	39
3. Statistical Analysis Methodologies	39
a. Empirical Orthogonal Functions (EOF)/PC analysis and Multiple Taper Method (MTM) spectrum	39
b. Canonical correlation analysis (CCA)	40
c. Principal component correlation analysis on large-scale teleconnection patterns	41
d. MTM-SVD analysis	42
4. Tree-ring chronologies as proxy for precipitation in the NAM region	43
a. Patterns of observed gridded precipitation	43
b. Analysis of tree-ring chronologies	45
5. Linkages between SST forcing and atmospheric teleconnection responses reflected by dominant EW and LWadj modes	47
6. Low-frequency climate variability as revealed by tree-ring network	50
a. Spatial variability of long-term drought	50
b. Mega droughts during the past four centuries	51
7. Summary	52
Acknowledgments	55
References	55
Tables	60
Figure Captions	60

APPENDIX B: PACIFIC SST-RELATED TELECONNECTIVE INFLUENCES ON NORTH AMERICAN MONSOON PRECIPITATION WITHIN NORTH AMERICAN

REGIONAL CLIMATE CHANGE ASSESSMENT PROGRAM (NARCCAP)

MODELS	83
Abstract	84
1. Introduction	85
2. Methodology and datasets	88
2.1 NARCCAP models	88
2.2 NARCCAP warm season precipitation	90
2.3 Dominant spatial modes of variability	91
3. Review of climatological behavior of NARCCAP models during the warm season	93
4. Warm season SST variability in NARCCAP AOGCMs	97
5. Impact of spectral nudging in representing ENSO-PDV warm season precipitation response in Phase I NARCCAP models	101
6. ENSO-PDV warm season precipitation response in Phase II NARCCAP RCMs.....	103
7. Concluding points and discussion	105
Acknowledgments	109
References	109
Tables	113
Figure Captions	114

APPENDIX C: LOW FREQUENCY CLIMATE VARIABILITY IN WESTERN NORTH AMERICA AS DIAGNOSED IN A DYNAMICALLY DOWNSCALED TWENTIETH CENTURY REANALYSIS	131
Abstract	132
1. Introduction	133
2. Data	137
a. Twentieth-century reanalysis	137
b. Sea surface temperature and geopotential height data	138
c. Dynamical downscaling of 20CR with WRF	138
d. Precipitation data	139

3. Statistical Analysis Methodologies	139
a. Moisture flux convergence and water vapor budget analysis	139
b. Standardized Precipitation Index (SPI)	140
c. MTM-SVD analysis	141
d. Correlation, local significance, and field significance	142
4. Results	142
a. Evidence of the dominant low-frequency drought mode as diagnosed by moisture flux convergence	143
b. Assessment of statistically significant low-frequency variability in 20CR MFC using MTM-SVD	146
c. Precipitation annual cycle in WRF DD-20CR	147
d. The low-frequency variability in the DD-20CR	148
e. Associated sea surface temperature anomalies and atmospheric teleconnections	150
5. Concluding points	152
Acknowledgments	155
References	155
Figure Captions	160

ABSTRACT

In the southwestern United States, the North American monsoon (NAM) is the main driver of severe weather and accounts for nearly half the annual precipitation. How the monsoon has behaved in the past and how it will change in the future is a question of major importance for natural resource management and infrastructural planning. In this dissertation, I present the results of three studies that have investigated North American monsoon variability and change from the perspective of paleoclimate records, future climate change projections, and simulation of the low-frequency variability with the longest retrospective atmospheric reanalysis.

In the first study, a monsoon-sensitive network of tree-ring chronologies is evaluated within its ability to reproduce NAM variability during the past four centuries. Matrix methods are used to detect the low-frequency spatiotemporal variability. The tree-ring chronologies can reasonably characterize the dominant modes of NAM climate variability. The monsoon tree-ring network is able to reproduce the interannual variability of cool and warm season precipitation, in a manner similar to the period of the instrumental record. Earlywood and latewood adjusted chronologies reveal low-frequency climate variability at decadal and longer timescales that is beyond the ability of the instrumental record to temporally well resolve. This low-frequency climate variability seems to be part of a much larger cycle that coincides with the occurrence of multiyear persistent droughts.

In the second study, we consider the modes of natural climate variability identified in the previous study to objectively assess the degree of physical uncertainty in climate change projections for NAM from Regional Climate Models (RCMs) used in the North American Regional Climate Change Assessment Program (NARCCAP). Climate change projection models are evaluated mainly on their ability to represent warm season driven by quasi-stationary Rossby wave trains and El Niño Southern Oscillation – Pacific Decadal Variability (ENSO-PDV). It is concluded that use of the NARCCAP model ensemble mean for NAM climate projections is probably not suitable. NARCCAP RCMs

are largely a slave to their driving global models and their error in the specification of large-scale atmospheric circulation. Only one out of eight NARCCAP RCMs has a reasonable representation of the seasonal cycle of monsoon precipitation and ENSO-driven interannual variability in both the 20th and 21st centuries. No decadal variability was observed in any of the NARCCAP RCMs.

In the third study, the low-frequency drought signal found with tree-ring chronologies is further explored within the framework of a regional climate modeling. Version 2 of the Twentieth-Century Reanalysis (DD-20CR) is dynamically downscaled over a contiguous U.S.-Mexico domain. Statistic analysis of the DD-20CR suggests that the low-frequency drought signal in the Southwest is driven by atmospheric circulation changes on global to continental scales that affect precipitation in Central American as well. DD-20CR reproduces the spatial patterns of precipitation associated with climate variability at decadal and longer timescales in a manner that compares well with observational records and tree-ring chronologies. Low-frequency climate variability is therefore likely responsible for the multiyear persistent droughts in the last four centuries, as independently evaluated from the tree-ring monsoon-sensitive network.

CHAPTER 1: INTRODUCTION

1.1 Background

Climate variability of the southwestern U.S. is a key and important aspect of water resources management in the region. Annual precipitation over the southwestern U.S. shows two maxima, one during the summer monsoon season and one during the winter season. Winter precipitation in the southwestern U.S. provides 30% of the annual precipitation (Sheppard et al., 2002), and it is mainly driven by mid-latitude cyclonic systems. Summer precipitation in the Southwest is produced by convective storms as part of the seasonal march of the North American monsoon (NAM) system. The variability of precipitation in both seasons plays an important role in the sustainability of ecosystems in the region, which compete for water with a rapidly growing population. Understanding the physical drivers of climate variability is therefore a critical part in evaluating water resources availability necessary to sustain diverse activities such as urban water supply, agriculture, and ecosystems.

Interannual variability of cool season precipitation over the Southwest is driven by El Niño Southern Oscillation (ENSO) and the Pacific Decadal Variability (PDV), which can be identified in sea surface temperature (SST) records (McCabe and Dettinger, 1999; Higgins and Shi, 2000; Ropelewski and Halpert, 1986; Ropelewski and Halpert, 1987). Pacific SST variability impacts the convection in the tropics and alters large-scale atmospheric patterns over North America via quasi-stationary atmospheric wave trains, or Rossby wave teleconnections (Wallace and Gutzler, 1981; Horel and Wallace, 1981). Wet and dry conditions over the Southwest during the cool season are linked primarily to the Pacific North America (PNA) pattern. The PNA wave trains of troughs and ridges is a continental scale pattern system with center of action in central north Pacific, northwestern United State, and western Canada. During El Niño years the PNA is typically in a positive phase and produces wet and cold winter seasons in the Southwest (Douglas and Englehart, 1981). A positive PNA pattern enhances the subtropical jet over southern U.S., favoring an increased frequency and intensity of mid-latitude cyclones

reaching the Southwest. During La Niña years the PNA tends to be in a negative phase, so drier and warmer winters are observed in the Southwest (Kiladis and Diaz, 1989). The rainfall regime in the Southwest is also modulated by the PDV, and constructively interferes with the ENSO. Therefore, wet (dry) seasons are observed when El Niño (La Niña) and the positive (negative) phase of the PDV are in-phase (Gershunov and Barnett, 1998).

NAM early summer precipitation is inversely related to the precipitation in central U.S., so a wet (dry) late spring precipitation in central U.S. is associated with a dry (wet) early summer in the Southwest. This antiphase relationship in early warm season precipitation between central U.S. and the Southwest is strongly related to the position and strength of the mid-level subtropical ridge. When the subtropical ridge is located north of its climatological position, the Southwest tends to have a wet early monsoon season and the opposite when it is located south (Carleton et al., 1990). NAM precipitation has a statistical weak relationship with ENSO in comparison to the cool season (Higgins et al., 1999). However, the constructively interaction of ENSO and PDV do explain interannual variability of NAM to an extent (Castro et al., 2001). A dry NAM is expected during positive ENSO and positive PDV phases, and a wet NAM in a reversal manner. As in the cool season, variation in the tropical Pacific sea surface temperature driven by ENSO-PDV causes Rossby train-wave teleconnection patterns (Castro et al., 2001). The northward displacement of the monsoon ridge allows the transport of moisture from the Gulf of Mexico above approximately 700 mb (Schmitz and Mullen, 1996). The northward displacement of the subtropical monsoon ridge is the main climatic driver of the monsoon onset (Douglas et al., 1993). The ridge displacement allows a change in direction of middle-level winds from westerly to easterly which facilitates moisture transport from the Gulf of Mexico. As the Sierra Madre mountains block the potential transport of moisture below 700 mb (Douglas et al., 1993), tropical moisture is transported through the Gulf of California via gulf surges, enhancing the convective outbreaks (Douglas and Leal, 2003).

1.2 Tree-ring chronologies and low-frequency variability of the North American monsoon

Natural variability of droughts is a big concern in light of increased demand of water in major cities in southwestern U.S. (Liverman and Merideth, 2002). Precipitation over the NAM region is highly related to large-scale variations of the climate system, such as the ENSO and PDV. Current persistent drought conditions in the southwestern U.S. could be driven by both interannual and low-frequency (decadal to multi-decadal scale) variability. Long-term drought or pluvial conditions, as well as the modulation of the inter-annual rainfall variability by low-frequency regimes are not yet well understood (Woodhouse and Overpeck, 1998). To understand drought variability, long records of climate parameters are needed. Analyzing low-frequency variability of the NAM requires long records, as instrumental records extend only about 100 years; thus, we can only observe frequencies of 50 years or less. This disadvantage can be overcome by using proxies of the climate variability. Recently, the Laboratory of Tree Ring Research at the University of Arizona has finished the dating and preparation of tree-ring chronology time series for analysis of NAM variations. With about 470-year length record, they are the most suitable information for a spatiotemporal variability analysis (Griffin et al., 2011; Griffin et al., 2013; Ciancarelli et al., 2013; Woodhouse et al. 2013; Leavitt et al., 2011). The first dense tree-ring chronology network sensitive to summer precipitation variations provides long-term records which could be used as proxies for rainfall that represents both cool and warm season precipitation.

Annual rings on most conifers in southwestern U.S. show two ring-bands: earlywood-width and latewood-width. Earlywood-width and latewood-width both have different physical characteristics. The earlywood width has large cells, thin walls, lower density and lighter wood. In contrast, the latewood width has small cells, thick walls, higher density, and darker wood. These differences are the indication of response to seasonal climate variability (Meko and Baisan, 2001).

Earlywood chronologies show a very robust ability to record the interannual variation of winter precipitation and have been used to reconstruct climatic parameters in the Southwest. Using a network located in southern Arizona and southern New Mexico, Woodhouse and Meko (1997) found that total tree-ring chronologies are able to explain 71% of the variance for the number of precipitation days during the winter wet season, November through March. In their analysis, using the reconstruction of precipitation-day

frequency for 300 years, they demonstrated that chronologies also can retain information for low and high frequency variability. They found two peaks, 4-year and 21-year, as important temporal modes of variation, which is consistent with the analysis on reconstructed streamflow for the Salt and Verde rivers (Smith and Stockton, 1981).

Summer precipitation signals influenced by the NAM system (NAMS) are strong in latewood width. However, latewood width shows a dependence on earlywood width. Meko and Baisan (2001) demonstrated that latewood width, which is the portion of the tree-ring width that grows late in the tree growing season, are able to record the interannual climate variability of the NAMS. Using a network of five *Pseudotsuga menziesii* chronologies, they found strong summer precipitation signals in latewood chronologies. This relationship is enhanced when the remaining earlywood signal existent in latewood chronologies is removed using an adjustment method. The correlation found in the NAM region between the latewood adjusted enhanced chronology and observed precipitation is about 0.6 (Meko and Baisan, 2001). This result is critically important because it settled the basis for large scale application of a dense network of tree-ring sites to reconstruct the NAM climate variability (Griffin et al., 2011; Griffin et al., 2013; Ciancarelli et al., 2013; Woodhouse et al., 2013; and Leavitt et al., 2011).

1.3 Future climate projections of the North American monsoon

Since the first assessment report issue by the Intergovernmental Panel on Climate Change (IPCC), evidences of global climate change have been confirmed with the use of dynamical modeling techniques. In arid regions like southwestern North America, climate models agree that the region will dry by the 21st Century (Seager et al., 2007; Cook and Seager, 2013). How well do Global Climate Models (GCM) simulate the NAM climate variability? From a GCM perspective, reproducing the NAM annual cycle is challenge. For instance, in a seasonal-interannual model evaluation, only one out of 17 GCMs was able to reproduce the NAM annual cycle (Liang et al., 2008).

Regional climate models (RCMs), alternatively, may be used to dynamically downscale IPCC GCMs to generate NAMS climate change projections. The principal advantage to the use of a RCM, at the scale of tens of kilometers, is the value added in

the representation of terrain-forced monsoon thunderstorms (Gutzler et al., 2009; Castro et al., 2007 and 2012), as this process is not physically represented well within a GCM. Castro et al. (2012) concluded that physical processes related to the development of thunderstorms, such as the diurnal cycle of convection, can be more realistically represented using regional climate models. To better capture monsoon thunderstorms, regional climate models (RCM) are considered. Even with the enhanced spatial resolution and model physics more appropriate for the mesoscale, RCMs are still challenged to physically represent the organized monsoon convection that accounts for more of the precipitation away from the mountains (e.g. Castro et al. 2012).

Climate model simulations generated as part of the North American Regional Climate Change Assessment Program (NARCCAP; Mearns et al., 2012) reflect the most comprehensive community research effort to date to generate dynamically downscaled climate projections using multiple global and regional atmospheric models. This effort was preceded by an early first initiative in North America (Project to Intercompare Regional Climate Simulations, PIRCS) to compare the performance of regional climate simulations (Takle et al., 1999). Phase I NARCCAP simulations force six RCMs with NCEP-NCAR Reanalysis 2 (Kanamitsu et al. 2002) boundary conditions during the historical period 1979-2003 to assess RCM sensitivity with “perfect” observed analysis conditions. Phase II simulations use boundary conditions from four different fully coupled atmosphere-ocean global climate models (AOGCMs) from the Coupled Model Intercomparison Project (CMIP3) that consider the A2 greenhouse gas emission scenario (Community Climate System Model [CCSM], Third Generation Coupled Global Climate Model [CGCM], Geophysical Fluid Dynamics Laboratory GCM [GFDL], and Hadley Centre Coupled Model version 3 [HadCM3]).

Similar to the aforementioned studies, Bukovsky et al. (2013) recently showed that when the NARCCAP RCMs were forced with lateral boundary forcing from an atmospheric reanalysis, the climatological evolution of the NAMS is improved. They also considered the NARCCAP RCMs that dynamically downscaled CMIP3 data to evaluate future changes in mean NAMS precipitation. Consistent with Cook and Seager (2013), they found that ensemble mean NAMS precipitation is projected to decrease, but that the decrease was not statistically significant due to the wide spread in model

solutions. Though the NARCCAP RCMs are forced with CMIP3 GCMs, to date their projections still represent the highest spatial resolution information generated by dynamical modeling.

At least for NARCCAP RCMs, a traditional climate projection approach that equally weights all the models to generate an ensemble mean change suggests that NAM precipitation will not substantially change in the future. Such approach implicitly favors statistical confidence based on the level of multi-model agreement, over physically-based metrics of model performance of the individual contributing models. What has been absent in the discussion of NAMS climate projections thus far is how the contributing models, whether they be GCMs or RCMs, represent known sources of natural climate variability. Should this also be considered as a physically-based metric to evaluate model quality? How would such information bear on the projected changes in NAMS precipitation? Consideration of natural climate variability is extremely important for real-time resource decision making at seasonal timescales and for worst-case scenarios, for example long-term drought.

1.4 Low-frequency climate variability of the North American monsoon in a modeling framework

Understanding past long-term climate variability is critically important as a benchmark by climate projections produced by dynamical modeling. There are hundreds of studies that have been done with climate data proxies such as tree-rings (e.g., Grissino-Mayer, 1996; Meko et al., 2007; Cook et al., 1999; Meko, 1992; Stahle and Cleaveland, 1988). In the southwestern U.S., Meko et al. (2007) reconstructed a millennium of annual flow of the upper Colorado River basin, to investigate extreme low-frequency droughts during the Medieval Climate Anomaly. They found a series of multi-year dry pulses of 62-year period. Grissino-Mayer (1996) reconstructed over 2000 years of annual precipitation at El Malpais National Monument in New Mexico, and were able to reproduce the low-frequency trends in the Four Corners region. However, a comprehensive understanding of low-frequency climate variability requires resolving the temporal and spatial variability.

Using a millennium record of reconstructed Palmer Drought Severity Index (PDSI), Herweijer et al., (2007), have shown a potential existence of a centennial drought signal. In their analysis, the centennial signal exists for the Medieval Climate Anomaly (1000-1450), but it vanishes for the Modern Era (1851-2010). This misrepresentation of the centennial drought during the Modern Era might be due to the misevaluation of the low-frequency summer season as suggested by Griffin et al. (2013). In the southwestern United States, we have identified a low-frequency drought signal obtained by tree-ring chronologies (Carrillo et al., 2014a; in preparation). We used the first monsoon-sensitive tree-ring network of earlywood (EW) and latewood adjusted (EW_{adj}) chronologies over the NAM region. This low-frequency scale signal, on the order of 50 to 100 years, seems to modulate the major droughts of the last 400 years. By analyzing the low-frequency variability for summer (LW_{adj}) and winter (EW), the temporal component of this drought signal shows a strong covariability between both seasons. Griffin et al. (2013) proposed three potential sources of this low-frequency covariability between seasons, with one of the sources due potentially to a climatic signal in the low-frequency regime; however, they did not explore further this possibility. Carrillo et al., (2014a, in preparation) provided additional evidence on the possibility of the existence of this drought climatic signal. By using a sophisticated and robust spatiotemporal statistic technique, they isolated this drought signal, which is statistically significant and also the spatial pattern is coherent in the Southwest. In addition, a seesaw pattern between the southwestern and central U.S. is associated with the centennial signal during the observational era; however, the significance of the results on precipitation could not be assessed because the short length of observed precipitation, and exploring the spatiotemporal pattern of the centennial signal only with tree-rings is a challenge.

Herweijer et al. (2007) argue that the potential forcing of this centennial drought is associated with a persistent La Niña-like mode in SST. This same argument has been claimed by Coats et al. (2013), when using a millennium of fully coupled ocean-atmosphere model. However, recent studies have shown the inability of fully coupled models to simulate low-frequency modes of variability (Ault et al., 2013). In recent evaluation of CMIP5, ENSO is generally well reproduced but teleconnections with North American climate varies among the fully-coupled models (Sheffield et al., 2013).

Another alternative to explore how the low-frequency variability works in a large-scale modeling framework is using the twentieth-century reanalysis (Compo et al., 2011; 20CR). The version 2 of the NCEP-NCAR Twentieth Century Reanalysis (20CR) project dataset, which is an international effort to produce retrospective analysis from global observed datasets from 1871 to the present at 6 hour and 2° degree resolutions (Compo et al., 2011). The 20CR is the first longest reanalysis currently available, which makes it the best candidate suitable to explore long-term climate variations. For instance, in its early version (version 1), it has been used to investigate the U.S. Dust Bowl impact (Cook et al., 2010). The 20CR employs an Ensemble Kalman Filter data assimilation (Whitaker and Hamill, 2002) to ingest observations of surface pressure from the International Surface Pressure Databank, and monthly sea surface temperature and sea-ice concentration as boundary conditions from the Hadley Centre Sea Ice and SST dataset (Rayner et al., 2003).

Although, 20CR is limited to about 140 years of length, it might be enough to capture one complete cycle of the centennial drought signal. Individual drought events have already been identified with 20CR (Cook et al., 2010); however, the implications of the periodic cycles as we described with tree-ring chronologies is not well understood. A major issue of using 20CR is that 20CR precipitation is not suitable reliable to be used directly into analysis to characterize precipitation in the Southwest. However, dynamically downscaled precipitation from atmospheric reanalyses has shown good results and is comparable with observed precipitation (NARR; Mesinger et al., 2006). For example, Bukovsky et al. (2013) and Mearns et al. (2012) have shown, that suite of several dynamically downscaled RCM precipitation with a “perfect” imposed reanalysis boundary conditions can simulate well the current climate of the Southwest. In addition, Carrillo et al., (2014b, in preparation) have shown that the same NARCCAP phase I simulations can retain the ENSO and PDV variability, which is not possible with NARCCAP phase II (fully coupled GCM cases).

1.5 Purpose

The scientific objective of this investigation is to characterize how natural climate variability and climate change affects North American monsoon precipitation in the

southwestern U.S. Consistent with emerging work that has characterized recent observational changes in monsoon precipitation globally, it is hypothesized that anthropogenic climate change is synergistically interacting with natural climate variability to intensify extreme climate events—that may push the already vulnerable human and natural systems in the southwestern U.S. to a fail point. In that respect, assessing how the North American monsoon will change in the future is a pressing and important research priority. Climate model projections must be considered within the scope of the existing observational and paleoclimate records to assess their uncertainty and credibility, both within the scientific community and by natural resource stakeholders.

In this dissertation, the NAM is considered as a unified framework from paleoclimate to future climate change projections. In that context, I am proposing the following three studies that are the main structure of the dissertation. In the first study, we identify the natural variability on observed precipitation and tree-rings with the intension of exploring low-frequency climate variability in the NAM region (Appendix A). In the second study, we explore the modes of climate variability, identified in the first study, on a set of high spatial resolution climate change projections existing at the moment of presenting this investigation (Appendix B). In the third study, we explore the limitation of a regional climate model to explicitly simulate the low-frequency regime on the southwestern United States (Appendix C).

CHAPTER 2: PRESENT STUDY

The methods, results, and conclusions of this investigation are presented in three manuscripts formatted for submission and appended in this dissertation. The following is a summary of the most relevant findings.

2.1 Appendix A: Low frequency variability of the North American monsoon as diagnosed through earlywood and latewood tree-ring chronologies in the southwestern U.S.

In the first study, the research question is to evaluate if tree-ring chronologies can record the low-frequency variability of the NAM climate region. Interannual variation of the winter and summer precipitation over the NAM region is well represented by earlywood and latewood, consistent with previous studies (e.g. Meko and Basin, 2001; Griffin et al., 2013; Stahle et al., 2009; Woodhouse et al., 2013). Our analysis with this tree-ring network shows the well-known teleconnection patterns with SST and geopotential height for both seasons (Castro et al., 2001; Ciancarelli et al., 2013). For winter, the positive anomaly rainfall over the NAM is associated with a positive phase of the ENSO-PDV (McCabe and Dettinger, 1999). For summer, the negative phase of the ENSO-PDV is found to enhance monsoon precipitation (Castro et al., 2001). The effect of the SST interannual variability on the distribution of the Southwest precipitation through quasi-stationary Rossby wave teleconnection responses is very well portrayed by using earlywood and latewood chronologies. Our analysis shows that the tree-ring network is able to reproduce the spatiotemporal interannual variability for summer and winter over the Southwest.

We have been able to isolate the low and high frequency variability in tree-ring chronologies as well as in precipitation records on the instrumental era. We also identified that the decadal modes for winter and summer have specific spectral signatures. The spectral signature for winter is in the range of 25-50 years and 10-15 years for summer. The significance of the spectral peaks is better resolved in tree-ring

chronologies datasets than in precipitation. This also has been pointed out by Ciancarelli et al. (2013) by using rotated Empirical Orthogonal Function/Principal Component (EOF/PC) analysis with high resolution precipitation (PRISM, 2004).

Using a longer tree-ring time record (400 years), we identified how persistent droughts in the past 400 years are strongly influenced by very low-frequency climate variability in the range of 50-100 years. As in recent studies (e.g. Griffin et al., 2013; Stahle et al., 2009), the variability of the 50-100 years climate regime represents the major southwest droughts: the Plueban drought in the 1670s, the 1770s and 1820s droughts, the late 1890s drought, and the 1950s drought (Griffin et al., 2013; Stahle et al. 2009). All the above mentioned droughts have been identified in previous studies (e.g. Griffin et al., 2013) except for the very pronounced 1740s drought, which was documented by Hubert H. Bancroft in his *Arizona and New Mexico History of Pacific States*, as a two-year drought in the Yuma area (Bancroft, 1889).

2.2 Appendix B: Pacific SST-related teleconnective influences on North American monsoon precipitation within North American Regional Climate Change Assessment Program (NARCCAP) models

In the second study, we evaluate NARCCAP data to assess the uncertainty of NAM future climate projections. We proposed metrics to objectively identify the signature of ENSO-PDV climate variability in sea surface temperature of the driving GCMs and precipitation patterns of the RCMs. This work logically follows from the recent study of Bukovsky et al. (2013), which considered the climatological performance of the NARCCAP models in representing the NAM. They found that RCMs forced with Reanalysis, in the Phase I NARCCAP experiments, performed generally well over Mexico and the southwestern U.S. An important question not addressed in Bukovsky et al (2013) is what is the role of natural climate variability in assessing the added value of the NARCCAP RCM projections?

NARCCAP provides a unique source of numerical experiments to assess the uncertainty of IPCC CMIP3 scenarios. Precipitation is highly dependent on regionalized meteorological processes and natural climate variability. Therefore consideration of just GCM-based ensemble model climate projections might not be an optimal way to proceed.

More physically robust results for projection of future NAM precipitation may be obtained by considering “well performing” dynamically downscaled GCMs that have a reasonable representation of NAM precipitation climatology and year-to-year precipitation variability. Even in the NARCCAP RCMs, not all models are able to reproduce a proper annual cycle of precipitation. For example, the NARCCAP RCMs forced with the CMIP3 GFDL GCM show an erroneous monsoon precipitation peak in September, which corresponds with the period of monsoon retreat. Though RCMs can improve the climatological representation of precipitation during the monsoon, the year-to-year variability in RCM-simulated precipitation is still very dependent on the driving GCM. For example, July-August precipitation anomalies in multiple NARCCAP RCMs are quite statistically similar, given boundary forcing from a single GCM. If the driving GCM does not reasonably represent the observed large-scale atmospheric teleconnections during the warm season driven by ENSO-PDV, this error will adversely affect the ability of the RCM to represent year-to-year precipitation variability. Aside of the lateral boundary forcing provided by the GCM, the RCM configuration also plays an important role in the ability of the RCM to represent warm season atmospheric teleconnections and their associated precipitation responses. Better performing NARCCAP RCMs incorporate spectral nudging in the interior of the domain, as this helps retain the large-scale atmospheric circulation patterns that exist in the driving GCM.

We considered the future change in NAM precipitation in the NARCCAP models. The ensemble-mean difference in July-August precipitation in the Southwest from the historical to future projected period would indicate a statistically insignificant decrease. However the individual best performing model, in term of representation of NAM climatology and natural climate variability (HRM3-HadCM3), shows a larger precipitation decrease than the NARCCAP ensemble mean. This is the most physically confident precipitation projection for the NAM from the NARCCAP models, and should be more heavily weighted for potential impacts assessment purposes. However, GCMs still are quite challenged to represent natural climate variability driven by ENSO-PDV. Considering the dominant spatiotemporal modes of SSTs in these GCMs, for historical and future projected periods, only two of the four GCMs can capture ENSO with a

correct 3-7 year cycle of variability in both the past and future (HadCM3 and GFDL). None of the models has a reasonable representation of PDV, beyond a 10 year timescale.

2.3 Appendix C: Low frequency climate variability in western North America as diagnosed in a dynamically downscaled twentieth century reanalysis

In the third study, we have investigated the low-frequency climate variability of the NAM in the version 2 of the Twentieth-Century Reanalysis (20CR). As 20CR has limitations to represent NAM precipitation, we have dynamically downscaled the 20CR using the Weather Research and Forecasting (WRF) model with the purpose of incorporating the best representation of the terrain-forced summer monsoonal precipitation highly dependent on the mesoscale and large-scale teleconnections.

We have hypothesized that 20CR contains low-frequency variability in a similar way obtained with tree-ring chronologies. Using the moist flux convergence (MFC), we were able to show that 20CR contains low-frequency climate variability. This is fundamentally important because RCMs cannot be able to generate this variability as part of its internal dynamics. Our major research question is whether the major Southwest droughts are driven by very low-frequency climate variability. Using enhanced monsoonal precipitation by the dynamically downscaled RCM on 20CR (DD-20CR), we show a potential existence of the low-frequency variability modulating the American Southwest drought. Our evaluation shows that the DD-20CR can generally reproduce the annual cycle and cool and winter interannual variability of precipitation. It is therefore possible to use of DD-20CR to explore the NAM climate variability at low-frequency. Persistent droughts in North America are driven by large-scale atmospheric circulation and droughts and pluvials in the Southwest are inversely related to Central America.

From a seasonal perspective, DD-20CR precipitation confirms the coherent summer and winter co-variability of precipitation at decadal and longer timescales. It was found that this dual-season low-frequency variation in precipitation can be responsible for multiyear persistent droughts in the Southwest. The modeling approach provides additional support to confirm the existence of this dual-season covariability. The drought/pluvial temporal phases and spatial patterns over the Southwest and central U.S. are observed at multidecadal timescales. However, the spectral 50-100 year signature is

not completely resolved In addition, the atmospheric teleconnection show a CGT type of Rossby wave trains as in Ding et al. (2011) and in Ciancarelli et al. (2013).

REFERENCES

- Ault TR, JE Cole, JT Overpeck, GT Pederson, SST George, B Otto-Bliesner, CA Woodhouse, C Deser. 2013. The Continuum of Hydroclimate Variability in Western North America during the Last Millennium. *Journal of Climate* **26**: 5863-5878.
- Bukovsky MS, DJ Gochis, LO Mearns. 2013. Towards assessing narccap regional climate model credibility for the north american monsoon: current climate simulations. *Journal of Climate* **26**: 8802-8826.
- Carleton AM, DA Carpenter, PJ Wever. 1990. Mechanisms of interannual variability of the southwest United States summer rainfall maxima. *Journal of Climate* **3**: 999-1015.
- Carrillo CM, Castro CL, Woodhouse CA, Griffin D. 2014a: Low frequency variability of the North American Monsoon as diagnosed through earlywood and latewood tree-ring chronologies in the Southwest U.S. *International Journal of Climatology*. To be submitted.
- Carrillo CM, Castro CL, Garfin G, Chang H-I, Bukovsky MS. 2014b: Pacific SST-related teleconnective influences on North American monsoon precipitation within North American Regional Climate Change Assessment Program (NARCCAP) models. *International Journal of Climatology*. To be submitted.
- Castro LC, TB McKee, RA Pielke. 2001. The relationship of the North American monsoon to tropical and north pacific sea surface temperature as revealed by observational analysis. *Journal of Climate* **14**: 4449-4473.
- Castro CL, RA Pielke Sr, JO Adegoke, SD Schubert, PJ Pegion. 2007. Investigation of the Summer Climate of the Contiguous U.S. and Mexico Using the Regional Atmospheric Modeling System (RAMS). Part II: Model Climate Variability. *Journal of Climate* **20**: 3866-3887.
- Castro CL, H Chang, F Dominguez, C Carrillo, J Kyung-Schemm, HH-M Juang. 2012. Can a regional climate model improve warm season forecasts in North America? *Journal of Climate* **25**: 8212-8237.
- Ciancarelli B, CL Castro, C Woodhouse, F Dominguez, H Chang, C Carrillo, D Griffin. 2013. Dominant pattern of U.S. warm season precipitation variability in a fine resolution observational record with focus on the southwest. *International Journal of Climatology*. doi:10.1002/joc.3716.
- Coats S, JE Smerdon, R Seager, BI Cook, JF Gonzalez-Rouco. 2013. Megadroughts in Southwestern North America in ECHO-G Millennial Simulations and Their Comparison to Proxy Drought Reconstructions. *Journal of Climate* **26**: 7635-7649.

Compo GP, JS Whitaker, PD Sardeshmukh, N Matsui, RJ Allan, X Yin, BE Gleason, RS Vose, G Rutledge, P Bessemoulin, S Brönnimann, M Brunet, RI Crouthamel, AN Grant, PY Groisman, PD Jones, M Kruk, AC Kruger, GJ Marshall, M Maugeri, HY Mok, Ø Nordli, TF Ross, RM Trigo, XL Wang, SD Woodruff, SJ Worley. 2011. The Twentieth Century Reanalysis Project. *Quarterly Journal of the Royal Meteorological Society* **137**: 1-28. doi: 10.1002/qj.776

Cook ER, Meko DM, Stahle DW, Cleaveland MK. 1999. Drought reconstructions for the continental United States. *Journal of Climate* **12(4)**: 1145-1162

Cook BI, R Seager. 2013. The response of the North American Monsoon to increased greenhouse gas forcing. *Journal of Geophysical Research*. **118(4)**: 1690-1699. DOI:10.1002/jgrd.50111.

Cook BI, Seager R, Miller RL. 2010. Atmospheric circulation anomalies during two persistent North American droughts: 1932-1939 and 1948-1957. *Climate Dynamics* **36(11)**: 2339-2355. DOI:10.1007/s00382-010-0808-1.

Ding Q, Wang B, Wallace JM, Branstator G. 2011. Tropical-extratropical teleconnections in boreal summer: observed interannual variability. *Journal of Climate* **24**: 1878-1896.

Douglas AV, PJ Englehart. 1981. On a statistical relationship between autumn rainfall in the central equatorial pacific and subsequent winter precipitation in Florida. *Monthly Weather Review* **109**: 2377-2382.

Douglas MW, RA Maddox, K Howard, S Reyes. 1993. The Mexican monsoon. *Journal of Climate* **6**: 1665-1677.

Douglas MW, JC Leal. 2003. Summer time surges over the gulf of California: aspect of their climatology, mean structure, and evolution from radiosonde, NCEP reanalysis, and rainfall data. *Weather and Forecasting* **18**: 55-74.

Gershunov A, TP Barnett. 1998. ENSO influence on intraseasonal extreme rainfall and temperature frequencies in the contiguous United States: observation and model results. *Journal of Climate* **11**: 1575-1586.

Griffin D, DM Meko, R Touchan, S Leavitt, CA Woodhouse. 2011. Latewood chronology development for summer-moisture reconstruction in the US Southwest. *Tree-ring Research* **67(2)**: 87-11.

Griffin D, CA Woodhouse, DM Meko, DW Stable, HL Faulstich, C Carrillo, R Touchan, CL Castro, SW Leavitt. 2013. North American monsoon precipitation reconstructed from tree-ring latewood. *Geophysical Research Letters*. doi:10.1002/grl.50184.

Grissino-Mayer HD. 1996. A 2129-year reconstruction of precipitation for northwestern New Mexico, USA. *Tree Rings, Environment and Humanity, Radiocarbon*, Tucson, AZ, 191-204.

Gutzler DS, LN Long, J Schemm, SB Roy, M Bosilovich, JC Collier, M Kanamitsu, P Kelly, D Lawrence, M-I Lee, RL Sánchez, B Mapes, K Mo, A Nunes, EA Ritchie, J Roads, S Schubert, H Wei, GJ Zhang. 2009. Simulations of the 2004 North American Monsoon: NAMAP2. *Journal of Climate* **22**: 6716–6740.

Herweijer C, R Seager, ER Cook, J Emile-Geay. 2007. North American droughts of the last millenium from a gridded network of tree-ring data. *Journal of Climate* **20**: 1353-1376.

Higgins RW, Y Chen, AV Douglas. 1999. Interannual variability of the North American warm season precipitation regime. *Journal of Climate* **12**: 653-680.

Higgins RW, Shi W. 2000. Intercomparison of the principal modes of interannual and intraseasonal variability of the North American Monsoon system. *Journal of Climate* **14**: 403-417.

Horel JD, JM Wallace. 1981. Planetary-scale atmospheric phenomena associated with the Southern Oscillation. *Monthly Weather Review* **109**: 813-829.

Kanamitsu M, A Kumar, H-M H Juang, JK Schemm, W Wang, F Yang, S-Y Hong, P Peng, W Chen, S Moorthi, M Ji. 2002. NCEP dynamical seasonal forecast system 2000. *Bulletin of the American Meteorological Society* **83**: 1019–1037.

Kiladis GN, HF Diaz. 1989. Global climate anomalies associated with extremes of the Southern Oscillation. *Journal of Climate* **2**: 1069-1090.

Leavitt SW, CA Woodhouse, CL Castro, WE Wriugh, DM Meko, R Touchan, D Griffin, B Ciancarelli. 2011. The North American monsoon in the U.S Southwest: potential for investigation with tree-ring carbon isotopes. *Quaternary International* **235**: 101-107.

Liang X-L, J Zhu, KE Kunkel, M Ting, JXL Wang. 2008. Do CGCMs Simulate the North American Monsoon Precipitaiton Seasonal Interannual Variability? *Journal of Climate* **21**: 4424-4448.

Liverman DM, Merideth. 2002. Climate and society in the US Southwest: the context for a regional assessment. *Climate Research* **21**: 199-218.

McCabe GJ, Dettinger MD. 1999. Decadal variations in the strength of ENSO teleconnections with precipitation in the western United States. *International Journal of Climatology* **19**: 1399-1410.

Mearns LO, coauthors. 2012. The North American Regional Climate Change Assessment Program: overview of phase I results. *Bulletin of the American Meteorological Society* **93**:1337-1362.

Meko DM. 1992. Dendroclimatic evidence from the Great Plains of the United States. In *Climate Since A.D. 1500*. RS Bradley and PD Jones Editors. Routledge: 312-330.

Meko DM, CA Woodhouse, CA Baisan, T Knight, JJ Lukas, MK Hughes, MW Salzer. 2007. Medieval drought in the upper Colorado River Basin. *Journal of Geophysical Research* **34**: 1-5. L10705, doi:10.1029/2007GL029988.

Meko DM, CH Baisan. 2001. Pilot study of latewood-width of conifers as an indicator of variability of summer rainfall in the North American monsoon region. *International Journal of Climatology* **12**: 697-708.

Mesinger F, G DiMego, E Kalnay, K Mitchell, PC Shafran, W Ebisuzaki, D Jović, J Woollen, E Rogers, EH Berbery, MB Ek, Y Fan, R Grumbine, W Higgins, H Li, Y Lin, G Manikin, D Parrish, W Shi. 2006. North American Regional Reanalysis. *Bulletin of the American Meteorological Society* **87**: 343–360. doi: <http://dx.doi.org/10.1175/BAMS-87-3-343>

PRISM Climate Group. 2004. Parameter-elevation Regressions on Independent Slopes Model monthly precipitation grid. *Oregon State University*. <http://www.prism.oregonstate.edu>.

Rayner NA, Parker DE, Horton EB, Folland CK, Alexander LV, Rowell DP, Kent EC, Kaplan A. 2003. Global Analyses of sea surface temperature, sea ice, and night marine air temperature since the late nineteenth century. *Journal of Geophysical Research* **108**(D14): 4407. DOI:10.1029/2002JD002670.

Ropelewski CF, MS Halpert. 1986. North American precipitation and temperature associated with El Niño/Southern Oscillation (ENSO). *Monthly Weather Review* **114**: 2352-2363.

Ropelewski CF, MS Halpert. 1987. Global and regional scale precipitation patterns associated with El Niño/Southern Oscillation (ENSO). *Monthly Weather Review* **115**: 1606-1626.

Schmitz JT, Mullen S. 1996. Water vapor transport associated with the summertime North American monsoon as depicted by ECMWF analyses. *Journal of Climate* **9**: 1621-1632.

Seager R, Coauthors. 2007. Model projection of an imminent transition to a more arid climate in southwestern North America. *Science* **316**: 1181-1184.

Sheffield J, SJ Camargo, R Fu, Q Hu, X Jiang, N Johnson, KB Karnauskas, ST Kim, J Kinter, S Kumar, B Langenbrunner, E Maloney, A Mariott, JE Meyerson, JD Neelin, S Nigam, Z Pan, A Ruiz-Barradas, R Seager, YL Serra, D-Z Sun, C Wang, S-P Xie, J-Y Yu, T Zhang, M Zhao. 2013. North American Climate in CMIP5 Experiments. Part II: Evaluation of Historical Simulations of Intraseasonal to Decadal Variability. *Journal of Climate* **26**: 9247-9290.

Sheppard PR, AC Comrie, GD Packin, K Argersbach, MK Hughes. 2002. The Climate of the Southwest. *Climate Research* **21**: 219-238.

Smith LP, CW Stockton. 1981. Reconstructed streamflow for the Salt and Verde rivers from three-ring data. *Water Resources Bulletin* **17**: 939-947.

Stahle DW, Cleaveland MK. 1988. Texas drought history reconstructed and analyzed from 1698 to 1980. *Journal of Climate* **1**:59–74

Stahle DW, MK Cleaveland, HD Grissino-Mayer, RD Griffin, FK Fye, MD Therrell, DJ Burnette, DM Meko, JV Diaz. 2009. Cool- and warm-season precipitation reconstructions over western New Mexico. *Journal of Climate* **22**: 3729-3750.

Takle ES, coauthors. 1999. Project to Intercompare Regional Climate Simulations (PIRCS): description and initial results. *Journal of Geophysical Research* **104**: 19443-19462.

Wallace JM, DS Gutzler. 1981. Teleconnections in the geopotential height during the northern hemisphere winter. *Monthly Weather Review* **109**: 784-812.

Whitaker JS, Hamill TM. 2002. Ensemble data assimilation without perturbed observations. *Monthly Weather Review* **130**: 1913-1924.

Woodhouse CA, DM Meko. 1997. Number of winter precipitation days reconstructed from southwestern tree-rings. *Journal of Climate* **10**: 2663-2669.

Woodhouse CA, DM Meko, D Griffin, CL Castro. 2013. Tree-rings and multiseason drought variability in the lower Rio Grand basin, U.S.A., *Water Resources Research* **49**: doi:10.1002/wrcr.20098.

Woodhouse CA, JT Overpeck. 1998. 2000 Years of Drought Variability in the Central United States. *Bulletin of the American Meteorological Society* **79**: 2693-2714.

**APPENDIX A: LOW FREQUENCY VARIABILITY OF THE NORTH
AMERICAN MONSOON AS DIAGNOSED THROUGH
EARLYWOOD AND LATEWOOD TREE-RING CHRONOLOGIES
IN THE SOUTHWESTERN U.S.**

Carlos M. Carrillo¹, Christopher L. Castro¹, Connie A. Woodhouse^{2,3}, and Daniel Griffin²

¹Department of Atmospheric Sciences, ²Laboratory for Tree Ring Research, and ³School of Geography and Development
University of Arizona, Tucson, Arizona, USA

To be submitted to *International Journal of Climatology*

Version December 7, 2014

Corresponding author address: Carlos M. Carrillo, Department of Atmospheric Sciences, University of Arizona, Physics and Atmospheric Sciences Building, Rm. 536, 1118 East Fourth Street, Tucson, Arizona 85721. E-mail: carloscc@email.arizona.edu, phone: (520) 626-6329, fax: (520) 621-6833.

Abstract

Understanding low-frequency climate variability over the North American monsoon (NAM) region is challenging to assess by using only observational records. In this study, we have analyzed the climate variability of the NAM region cool and warm seasons through tree-ring chronologies. We have taken advantage of the first systematic monsoon-sensitive network of tree-ring chronologies for southwestern North America. Empirical Orthogonal Functions (EOF) and Multi-Taper-Method Singular Value Decomposition (MTM-SVD) analyses were applied on earlywood (EW) and latewood adjusted (LW_{adj}) chronologies to determine the spatiotemporal dominant modes of variability as well as large-scale controlling mechanism as diagnosed with sea surface temperature and geopotential height at 500 mb. We present evidence of the capability of tree-ring chronologies to characterize the dominant modes of NAM climate variability in the interannual, decadal, and longer scales. In the instrumental era, the southwest tree-ring network is able to describe the climate variability similar to that in the observed precipitation. This in-depth evaluation provides the necessary confidence to use this dataset for a long-term climate analysis in the low-frequency regime. Using the complete four century-long dataset, EW and LW_{adj} chronologies reveal a low-frequency climate variability in the 50-100 year band that seems to be related to the occurrence of megadroughts.

1. Introduction

The arid southwest of the United States is arguably one of the regions most sensitive to climate variability and change. As summarized in a recent comprehensive regional climate change assessment report, the complex water delivery infrastructure and natural ecosystems have been taxed by sustained long-term heat and drought since the beginning of the twenty-first century, threatening Colorado River water supply and causing devastating wildfires (Garfin et al., 2013). Developing improved capability to both diagnose the causes of climate variability in the past and project how climate will behave in the future is essential for formulating resilient climate adaptation strategies. In this work we focus our attention on the past climate, specifically investigating the commonalities in the statistical characteristics of climate variability between gridded precipitation products based on gauge observations and precipitation proxy data from tree rings, and then using the tree-ring data to examine the period of time prior to instrumental records.

The characteristics of southwest U.S. climate variability during the period of the instrumental record are fairly well known. There are distinct climatological differences between cool and warm season precipitation, with the former associated with the passage of synoptic-scale mid-latitude cyclones and the latter with convective storms during the North American monsoon (Douglas and Englehart, 1981; Gershunov and Barnett, 1988; Carleton et al., 1990; Adams and Comrie, 1997). For the cool season, it is has been firmly established, that the combination of the El Niño Southern Oscillation and Pacific Decadal Variability (henceforth ENSO-PDV) facilitate large-scale atmospheric teleconnection patterns, principally the Pacific North America (PNA) pattern and

displacement of the winter storm track (Wallace and Gutzler, 1981; Ropelewski and Halpert, 1986 and 1987; Gershunov and Barnett, 1988; Trenberth, 1990). Wet (dry) cool seasons are therefore statistically significantly related to El Niño, and positive PDV (La Niña, negative PDV) (McCabe and Dettinger, 1999; Higgins and Shi, 2000; Gutzler et al., 2002). During the warm season, monsoon precipitation is strongly related to the positioning of the North American monsoon ridge. When the monsoon ridge is strong and displaced north of its mean climatological position in the Southwest, a wet and early monsoon occurs; dry, late monsoons correspond to a weak ridge, displaced to the south (Carleton et al., 1990). Previous work has described the nature of the warm season atmospheric teleconnection responses associated with ENSO-PDV, as quasi-stationary Rossby wave trains emanating from the western tropical Pacific (Castro et al., 2001 and 2007; Ciancarelli et al., 2013). The warm season teleconnection response modulates the strength and positioning of the monsoon ridge in early summer, such that a wet and early (dry and late) monsoon tends to occur during the negative (positive) phase of ENSO-PDV. Likely because of the changes in the ENSO-PDV atmospheric teleconnection responses between the cool and warm seasons, it has been generally observed during the late 20th century that a wet (dry) cool season is followed by a dry and late (wet and early) monsoon, providing some seasonal buffering capacity to the development of intense drought. However, the length of the instrumental record limits an assessment of this relationship over longer time scales. Consequently, we do not have a complete understanding of low-frequency climate variability (decadal to multidecadal timescales) in the Southwest, how such variability affects cool and warm season precipitation, and in

particular the occurrence of sustained dry conditions in both cool and warm seasons (i.e., dual-season droughts) which would profoundly impact human and natural systems.

Tree-ring chronologies in the Southwest can provide a robust proxy for both cool and warm season precipitation over past centuries (e.g., Ni et al. 2002, Meko and Baisan, 2001; Stahle et al., 2009; Faulstich et al. 2012, Griffin et al., 2013; Woodhouse et al., 2013). Conifers in the Southwest generally exhibit annual growth rings that can be divided into two intra-annual growth increments. The earlywood (EW) band reflects tree growth during the cool season, with relatively larger cells, lower density, and lighter wood; the latewood (LW) band more reflects tree growth during the warm season and has smaller cells, higher density, and darker wood. Although EW chronologies are quite reliable proxies for cool season precipitation, LW widths, reflecting warm season precipitation, are not totally independent of the EW. To obtain the best possible relationship with warm season precipitation, the LW is adjusted (LW_{adj}) by removing the variance explained by EW (Meko and Baisan 2001; Griffin et al, 2011). In this study, tree-ring data from a recently generated network of EW and LW_{adj} chronologies (henceforth SW tree-ring network), updated to 2008, were used. These included tree ring sites located in monsoon region of the U.S., Arizona, New Mexico, Colorado, Utah, Texas, and Baja California Norte, Mexico, with an average record length of 400 years (Griffin et al., 2013) (Fig. 1).

Previous studies using this monsoon region network of tree-ring data indicate the period of instrumental record may not fully represent the range of variability over longer time scales. Griffin et al. (2013) established that the late twentieth century is relatively unique with respect to the predominant inverse relationship between precipitation

anomaly in the cool and warm seasons over a large portion of the southwestern U.S. in the context of the past 400 years. Cool and warm season precipitation reconstructions for this region also document the occurrence of dual season wetness or drought. Notably, warm season droughts were found to occur during many of the previously documented cool season droughts (e.g., Stahle et al., 2009; Griffin et al., 2013).

Other work has investigated the relationships between monsoon precipitation in the Southwest and ocean/atmospheric circulation, and the manifestation of this relationship in a preliminary version of the monsoon tree-ring network. Ciancarelli et al. (2013) identified several distinct warm season atmospheric teleconnection responses (quasi-stationary Rossby wave trains) that control the continental-scale spatial variability of U.S. warm season precipitation. The most predominant of these is the aforementioned ENSO-PDV response in early summer that accounts for the anti-phase relationship in warm season precipitation anomalies between the central U.S. and the Southwest (Higgins et al., 1997 and 1998; Barlow et al., 1998; Castro et al., 2001, 2007, 2009, and 2012; Ciancarelli et al., 2013). It was additionally found that this same teleconnection exists in later summer but is more related to Indian monsoon convection. A preliminary analysis of LW_{adj} tree-ring data from a subset of the southwestern tree-ring network showed a clear relationship to the known ENSO-PDV signal consistent with the instrumental record.

The present study addresses three main questions that directly follow from Griffin et al. (2013) and Ciancarelli et al. (2013). First, considering the southwest tree-ring network, do the dominant spatiotemporal modes of variability in EW and LW_{adj} tree-ring chronologies reflect equivalent modes of precipitation variability? If so, then the tree-ring

chronologies within the network could be a suitable proxy to characterize regional-scale patterns of cool and warm season precipitation variability. Second, besides assessing the statistical relations between tree-ring chronologies and precipitation, do these spatiotemporal relationships in EW and LW_{adj} correspond to controlling mechanism (such as ENSO-PDV) as portrayed in the atmospheric and oceanic circulation? Third, given the advantage of extending these proxies several centuries back in time, does the phenomenon of dual season wet and dry period reflect statistically significant very low-frequency climate variability that cannot be resolved in the comparatively short period of the instrumental record?

This paper is organized as follows. Data sources and statistical analysis methodologies are described in sections 2 and 3. An evaluative comparison between tree-ring chronologies and precipitation interannual variability is presented in section 4. The linkages of tree-ring data and associated large-scale teleconnection patterns are explained in section 5. The low-frequency variability as revealed in the southwest tree-ring network is explored in section 6. A summary of relevant points is presented in sections 7.

2. Data Sources

a. Tree-ring chronology data

The southwest tree-ring network described in Griffin et al. 2013 is used to describe the spatial patterns of tree growth as a proxy for precipitation, and to analyze the low frequency characteristics of the reconstructed cool and warm season precipitation. Although the full network includes 53 chronologies (Griffin et al. 2013), 39 were used in this study as many of the analyses were undertaken before the completion of the network. Site tree-ring chronologies were developed from primarily ponderosa pine (*Pinus*

ponderosa) and Douglas-fir (*Pseudotsuga menzeisii*). Samples were processed, and earlywood and latewood widths were measured to develop site chronologies with the protocol described in Griffin et al. (2011). Locations are shown in Figure 1. The common period of time covered by all chronologies is from 1550 to 2008.

b. Precipitation data and Standardized Precipitation Index (SPI)

Monthly total precipitation data are from a new 0.5° by 0.5° gridded National Oceanic and Atmospheric Administration (NOAA) product (P-NOAA), provided by Drs. Russ Vose and Richard Heim. P-NOAA incorporates a terrain correction interpolation function, similar to the Parameter-elevation Regressions on Independent Slopes Model (PRISM) product (Daly et al., 1994), beneficial for the complex terrain of the Southwest. As we documented in Castro et al. (2012), P-NOAA appears to perform better in Mexico than the Climate Prediction Center (CPC) precipitation product (Higgins et al., 1997). The original dataset extends from 1895 to 2010 and covers the entire North America; however, we used the continental region from 15° to 50° N and 125° to 80°W.

The gridded precipitation data were used to generate the standardized precipitation index (SPI) to specify precipitation anomalies during the period 1895 to 2008. Cool season SPI is defined by the months November to April and warm season SPI from July to August. Note that June is not considered in our definition of the warm season because the onset of the monsoon in the NAM 2 region in the Southwest occurs climatologically in early July (Higgins et al., 1999), and in this region, JA precipitation accounts for 92% of the JJA season. Our analysis shows the low-frequency climate variability is insensitive to the selection of JA or JJA as monsoon season. SPI has been used to monitor short and long term droughts in the United States (Heim, 2002) and its

main advantage is the ability to identify spatial patterns of precipitation variability at regional and continental scales (Castro et al., 2009). We used the same methodology to compute SPI as in Castro et al. (2009) and Ciancarelli et al. (2013).

c. Sea surface temperature and geopotential height data

Global 2° by 2° gridded sea surface temperature (SST) from NOAA is averaged for the periods June-July (JJ) and November to April (Nov-Apr) during 1854 to 2010 (citation). SST is used to characterize the teleconnections between regional precipitation and remote SST forcing. Here, the period of early summer (JJ) is used instead of JJA because the influence of ENSO-PDV on monsoon precipitation in the Southwest is most statistically significant in June and early July and diminishes in late summer (Castro et al. 2001, their Fig. 3). Similarly, the atmospheric response to SST forcing is analyzed using summer (JA, July-August) and winter (Nov-Apr) geopotential height anomalies (GPHA) at 500 mb from the NCEP-NCAR reanalysis dataset for the years 1948-present (Kalnay et al., 1996).

3. Statistical Analysis Methodologies

a. Empirical Orthogonal Functions (EOF)/PC analysis and Multiple Taper Method (MTM) spectrum

Empirical Orthogonal Function/Principal Component (EOF/PC) analysis is used to determine the dominant mode of spatial variability in SPI and tree-ring chronologies (e.g. Wilks, 2006). For all cases, the EOF domain is from 20°N to 40°N and 120°W to 100°W as in Fig. 2a. The EOF maps show the pattern of spatial loading of leading modes of SPI. We show spatial loading maps only for SPI. For tree-ring chronologies, correlation maps between associated tree-ring PCs and gridded SPI are used to show

patterns corresponding to the pattern of spatial loading of SPI. The first dominant EOF mode is shown to demonstrate the effectiveness of the method, and the other modes are then considered by comparison with the prior REOF analysis with PRISM from Ciancarelli et al. (2013) and with canonical correlation analysis.

The multi taper method (MTM) is used to evaluate the spectral signature of the temporal mode of variability (PCs) and to show clearly the associated temporal variability related to ENSO-PDV. The MTM for spectral analysis results in a better trade-off between spectral resolution and statistical variance (Lees and Park, 1995). A Slepian taper is implemented in the MTM to minimize spectral leakage, where the choice of order for the taper represents a compromise between spectral resolution and variance and improves the efficiency of the signal detection (Mann and Lees, 1996). The MTM power spectrum is computed for the time series of the dominant mode, or first PC, for both the SPI and the tree-ring chronologies (MTM analysis tools were taken from <http://www.atmos.ucla.edu/tcd/ssa/>).

b. Canonical correlation analysis (CCA)

We use canonical correlation analysis (CCA) to evaluate the covariability between the tree-ring chronologies and SPI, and to characterize higher modes of variability. Once the dominant modes of SPI and tree-ring chronology are identified with EOF/PC analysis, their covariability is assessed using CCA, which is used to explicitly quantify the spatiotemporal similarity between the SPI and tree-ring chronologies. For each mode, CCA produces one singular vector for each field variable (e.g., cool season SPI and EW). CCA results are presented as homogeneous and heterogeneous correlation maps, as defined in Wallace et al. (1992). The SPI homogeneous map is obtained by

correlating the singular vector of SPI with the original SPI. The SPI heterogeneous map is generated by correlating the singular vector of SPI with EW or LW_{adj} data, and similarly for EW. Although only the homogeneous correlation map is enough to describe similarities, the EW or LW_{adj} heterogeneous correlation maps are needed to fully describe the spatial variability outside of the tree-ring site locations. The method used to compute CCA is the same as in Castro et al. (2009) and Ciancarelli et al. (2013), which are based on Professor Dennis Hartmann's online notes at the University of Washington. Before constructing the covariance matrix for CCA, fifteen modes were retained from the independent EOF/PC analysis on SPI and tree-ring chronologies. That number was selected based on the relatively invariant behavior of the homogeneous and heterogeneous maps of the CCA dominant mode when a greater number of modes were retained.

c. Principal component correlation analysis on large-scale teleconnection patterns

To explore the linkage between EW and LW_{adj} tree-ring chronologies during the instrumental period and the large-scale circulation, the Pearson correlation between the leading mode of temporal variability (PC1) and SST and 500-mb geopotential height anomalies (GPHA) fields is computed. We use these spatial correlation maps to determine the spatial pattern of SST forcing and its relation to atmospheric teleconnection patterns, as in our previous work (Ciancarelli et al., 2013). In addition, a bandpass filter treatment is applied on EW and LW_{adj} to evaluate a specific contribution or the variability related to the ENSO, PDV, and the combined ENSO-PDV mode. Local and field significance are respectively assessed with a t-statistic and the method of Livezey and Chen (1983), using a Monte Carlo technique with 500 iterations.

d. MTM-SVD analysis

Multi-Taper-Method Singular Value Decomposition (MTM-SVD, Mann and Park, 1994 and 1996; Mann and Lees, 1996; Rajagopalan et al., 1998) is used to determine the dominant spatiotemporal variability of tree-ring chronologies and SPI. We use MTM-SVD for two reasons: 1) to specifically examine low-frequency temporal variability longer than the decadal timescale, and 2) to determine the spatial pattern with significant temporal variability. We consider the Local Fractional Variance (LFV) spectrum and reconstructed spatial pattern (Mann and Park, 1996). The LFV is a form of a power spectrum where the temporal and spatial variation is accounted for simultaneously. Statistically significant spectral peaks in the LFV spectrum are identified by including statistical significance intervals determined by bootstrap resampling. The reconstructed spatial pattern represents the spatial variability associated with a specific spectral band, or temporal frequency. For our analyses, we always consider the reconstructed spatial pattern for spectral bands that are statistically significant at the 90% level or above. The reconstructed patterns are plotted as vectors, where the vector length indicates the amplitude of the signal and the direction shows the phase in relation to a user-specified reference point in the domain. The difference in angle between the vector at a given point in the domain relative to the reference point gives a sense of the temporal phasing of precipitation variability. If the vector at a given point is pointing towards the east (west), precipitation variability is completely in-phase (out of phase) with the reference point. If the given vector is pointing north or south precipitation variability is 90 degrees out of phase with the reference point. The reference point for both datasets analyzed is located at the center of the North American Monsoon Experiment (NAME)

region 2 (32.75°N, 110.25°W) (Gochis et al., 2009). We use the same methodology to compute MTM-SVD as in Castro et al. (2009) and the codes obtained from the website of Professor Michael Mann at the Pennsylvania State University. The MTM-SVD technique and implementation is explained in further detail in Rajagolapan et al. (1998).

4. Tree-ring chronologies as proxy for precipitation in the NAM region

In this section, spatial and time domain characteristics are explored first for the instrumental data, and then using the tree-ring networks, to show the principal modes of seasonal precipitation variability, and their links to large-scale atmospheric teleconnection and SST forcing. Comparisons are made between the instrumental and tree-ring data to demonstrate the ability of the tree-ring network to capture features in the instrumental data over the modern period.

a. Patterns of observed gridded precipitation

In order to evaluate the spatial patterns in the instrumental data, we first consider dominant mode of variability (EOF 1) for the cool and warm season SPI in Fig. 2. The dominant cool and warm season SPI modes respectively explain 39% and 17% of the total variance. The spatial differences in these dominant EOFs reflect the nature of cool and warm season precipitation variability. The cold season EOF shows a broader homogeneous spatial pattern due to the favored track of synoptic-scale mid-latitude cyclones across the Southwest and then north and eastward into the Great Plains that would occur during the positive phase of the mode. The warm season EOF, in its positive phase, shows a more regionalized pattern that corresponds to monsoon convective activity driven by enhanced flow around the south and west side of the upper-level

monsoon ridge. The associated PC temporal components are correlated with SSTA for the corresponding season in Figs. 2c and 2d. The correlation maps show the well-known relationships pattern between the southwest precipitation and ENSO-PDV. The field significance is higher for winter (99%) than for summer (79%).

The power spectra of these dominant seasonal modes of precipitation (PC1) are shown (Fig. 3). For this study, spectral peaks at timescales more than 10 years are defined as low-frequency and spectral peaks at timescales less than 10 years are defined as high frequency. For the cool season, three spectral bands are highlighted in yellow shading. They correspond to interannual (4 year), quasi-decadal (6-10 year), and inter-decadal (25-50 year) climate signals. Only the interannual signal, corresponding to the ENSO band, is statistically significant at the 90% confidence level. The quasi-decadal signal (6-10 year) contains the cool season 9-year signal identified by Castro et al. (2009) on precipitation and modeled soil moisture. The inter-decadal signal (25-50 year) may be related to the influence of the decadal variability of SST on winter precipitation described by McCabe and Dettinger (1999). The importance of these spectral peaks confirms the strong relationship between southwest U.S. winter precipitation and tropical SST during cold and warm ENSO years (Ropelewski and Halpert, 1986 and 1987; Castro et al., 2001). For the warm season, three spectral bands are highlighted: 2-4 years, 6-8 years, and 12-25 years. The 2-4 and 6-8 year bands are statistically significant and similar to SPI modes identified by Castro et al. (2009). As shown in Castro et al. (2009), the 6-8 year band is related to the anti-phase relationship in summer precipitation between the Southwest and central U.S. and the onset of the monsoon. Note that in both seasons the low-frequency (multidecadal) spectral peaks are just below the 90% confidence level, so how tree-ring

data may help to possibly enhance this signal is of interest. Later, we show the spatial pattern for each spectral band obtained with MTM-SVD.

b. Analysis of tree-ring chronologies

In order to assess the ability of the tree-ring network to replicate the spatial patterns in the instrumental data, we apply EOF analysis to EW and LW_{adj} chronologies with the Southwest monsoon region tree-ring network. Because the domain of the tree-ring data is limited to compare the main mode of variability of the tree-ring data with that of the gridded precipitation data, we show the correlation map of the dominant tree-ring modes for both with the EW and LW_{adj} PCs and gridded SPI for the respective season (Figs. 4a-b). The patterns are similar to those for EOF 1 of SPI in Figures 2a and 2b, but as they are not directly comparable, we show also the same correlation analysis maps based on SPI PCs correlated with gridded SPI for the same domain (Figs. 4c-d). The spatial pattern of correlation with leading modes of tree-ring chronologies and SPI are broadly similar, especially in the area defined by the tree-ring network (Fig. 1) with relatively higher and locally significant positive correlation in the range of 0.5 to 0.7. Within the vicinity of the southwest tree ring network the correlation values are roughly comparable for both seasons. However, in areas further away from the network the magnitude of correlation, not surprisingly, decreases since the tree-ring data are restricted to the southwestern U.S. So patterns beyond the Southwest are due to spatial relationships between this region and adjacent areas. The continental-scale nature of the pattern in the dominant modes of EW and LW_{adj} is less obvious. For example, the antiphase relationship in the Southwest to central U.S. precipitation is clearly present in the dominant mode of JA SPI (Fig. 4d) but is diminished in the dominant mode of the

LW_{adj} chronology network (Fig. 4b). Performing the equivalent EOF analysis using SPI taken only from grid points at the tree-ring site locations in Fig. 1, actually yields a nearly identical result as the EW and LW_{adj} EOF analyses, as shown in Figs. 5a-b. Thus, accounting for the observational limitations in the southwest monsoon tree-ring network, EW and LW_{adj} capture the dominant modes of cool and warm season precipitation variability quite well.

To confirm the strong degree of similarity between the EW and LW_{adj} chronologies and the corresponding observed precipitation we show the time series (PCs) of the dominant modes for the cool and warm seasons (Figs. 5c and 5d, respectively). The Pearson correlation for the cool season is 0.81 and 0.66 for the warm season, both statistically significant at the 99% level. Previous work has demonstrated the skill of the tree-ring data in reconstructing cool and warm-season precipitation (Faulstich et al., 2012; Griffin et al., 2013; Woodhouse et al., 2013). Our present results show that the monsoon tree-ring network is also able to capture well the dominant modes of interannual variability of cool and warm season precipitation.

The MTM spectrums of the leading modes of EW and LW_{adj} for the period 1895-2008 are shown in Figure 6. As in the observational data in Fig. 3, the same statistically significant decadal scale bands are observed (25-50 years in winter and 9-15 years in summer) at the 90% level or above. There is also statistically significant variability at ENSO timescales as well for both the cool and warm season. Therefore, considering the dominant modes of EW and LW_{adj}, their time variability does generally reflect the same type of variability in the corresponding SPI. .

We used CCA to evaluate the covariability between EW and LW_{adj} tree-ring chronologies and the corresponding cool and warm season SPI. The first two leading CCA modes for cool season SPI and EW, with the homogeneous and heterogeneous maps for SPI and the homogeneous map for EW are shown in Figure 7. The first CCA mode matches the dominant cool season EOF associated with ENSO-PDV (Figs. 7a-c), with all the tree-ring sites showing the same sign of response. The second mode (Figs. 7d-f) shows maximum variability outside the monsoon tree-ring network, with a center of action in California and Nevada and another of opposite sign in Texas. The second mode still shows a coherent spatial gradient across the tree ring sites with this mode. The first two leading CCA modes for warm season SPI and LW_{adj} equivalent are shown in Figure 8. The dominant warm season mode also matches the warm season EOF associated with ENSO-PDV, and abruptly ends around the continental divide, very similar to the spatial pattern found by Castro et al. (2007). The strongest response in this first CCA mode of LW_{adj} is in southeast Arizona, and the second CCA mode keys on precipitation variability in New Mexico and west Texas, east of the continental divide.

5. Linkages between SST forcing and atmospheric teleconnection responses reflected by dominant EW and LW_{adj} modes

To establish the linkage between Pacific SST forcing and its atmospheric teleconnection response via the tree-ring network dominant modes of EW and LW_{adj} networks of tree-ring chronologies are correlated with the corresponding SSTA and 500-mb geopotential height anomalies. The relationships with EW tree-ring chronologies in Figs. 9a and 9b show a very clear winter ENSO-PDV signature, just as in Fig. 2b and in a similar analysis by Ciancarelli et al. (2013) Also, a well defined wave train from the

western Pacific into the southern hemisphere is observed. Similarly, the relationship with LW_{adj} tree-ring chronologies and these large-scale fields is shown in Figs. 9c and 9d. There are fewer areas of locally significant correlation and the field significance values are overall lower, in comparison to EW. However the LW_{adj} mode is still able to resolve the relationship between wet and early (dry and late) monsoons with negative (positive) phase of ENSO-PDV and the associated west Pacific quasi-stationary Rossby wave train response.

We have shown that main modes of variability in tree-ring networks and SPI are comparable during both seasons (winter and summer). However, the matrix methods cannot explicitly relate the dominant spatial patterns to specific temporal frequencies. For our purpose of characterizing the low-frequency temporal variability this presents a problem because similar spatial patterns can be associated with significant temporal variability at different frequencies. MTM-SVD has the advantage of identifying the spatial pattern of variability associated with low frequencies, important in considering the tree-ring chronology. In this section, we repeat the comparison analysis on the instrumental period but using MTM-SVD. Although applying EOF and MTM-SVD might be seen redundant, it is important to demonstrate the robustness of the technique and is relevant when analyzing the low-frequency regime in the next section.

LFV spectra for SPI and tree-ring data, during the period of observational record (1895-2008), are shown in Fig. 10. They are reasonably comparable and the dominant spectral bands that are comparable in some degree to Fig. 3 are highlighted. Considering cool season SPI and EW, both data show a significant ENSO-related signal, maximized around 4-5 years. As previously discussed, there is also significant variability in SPI at

the 9 year timescale, though this signal is not as strong in EW. In EW there is statistically significant variability in the 25-50 year (interdecadal) band that is stronger than SPI. For warm season SPI and LW_{adj} , there is significant variability generally at the ENSO timescales (3-5 years) and decadal timescales (6-20 years), though the exact locations of spectral peaks differ.

The reconstructed cool season SPI and EW patterns for the three identified spectral bands from the LFV analysis are shown in Fig. 11. The spatial patterns across the entire domain can be clearly noted in gridded SPI, whereas for EW it is just at the tree-ring sites. The patterns between the cool season SPI and EW are similar for all three significant spectral bands, with a coherent in-phase signal through the entire tree-ring network area in both sets of data. The correlation maps of the three spectral reconstructed EW time series correlated on SSTA are shown in Fig. 12. As expected, the interannual and quasi-decadal signals (3-6 and 6-12 years) are clearly related to ENSO-PDV, with no significant correlation outside of the Pacific basin. Multi-decadal variability (25-50 years) appears to be related to a PDV and AMO signal. Wet conditions in the cool season, as indicated by EW, occur in association with a positive phase of PDV and a negative phase of AMO, quite consistent with what has been already documented with analysis of observed precipitation data in the central and western United States (Hu and Feng, 2002 and 2008; Feng et al., 2011; Ciancarelli et al., 2013).

Similar analysis of the warm season for the reconstructed patterns are shown in Fig. 13 and correlation maps with reconstructed LW_{adj} time series with SSTA shown in Fig. 14. Reconstructed patterns of warm season SPI and LW_{adj} are generally in phase throughout the Southwest for all of the spectral bands. The anti-phase relationship with

precipitation in the central U.S. is clearly evident in the 12-20 year band of JA SPI.

Similar to what has already been shown in correlating the dominant mode of JA SPI and LW_{adj} to SSTA in Fig. 7. The 10-15 and 6-9 year bands in LW_{adj} appears to key most on the ENSO-PDV monsoon precipitation signal (Figs. 14b-c) and accounts for much of the spatial variability in the Pacific when considering all the significant spectral bands (Fig. 14d). However, SSTA patterns associated with these bands are not a spatially coherent and are less statistically significant than they are in the winter season.

6. Low-frequency climate variability as revealed by tree-ring network

a. Spatial variability of long-term drought

We have already demonstrated that EW and LW_{adj} networks of tree-ring chronologies are able to capture the associated precipitation responses of cool and warm season atmospheric teleconnections within the instrumental period. Given this good result, what insight do EW and LW_{adj} provide for understanding the low-frequency NAM climate variability? The LFV spectrum for both EW and LW_{adj} for the entire tree-ring chronology time series during the period 1650-2005 is shown in Figure 15. As our focus in this part is on the low-frequency climate variability, the LFV spectrum is shown only for periods longer than 10 years. Significant peaks that appeared in the previous analyses of EW and LW_{adj} during the period 1895-2008 are for the most part retained for periods shorter than 15 years. The MTM-SVD spectrum reveals the existence of a statistically significant very low-frequency variability in both EW and LW_{adj} , especially in the 50-100 year band.

Spatial patterns for the three EW spectral bands identified with LFV (Fig. 15) are shown in Fig. 16. They are spatial correlation maps for three spectral-band EW

reconstructed time series: 10-15, 15-25, and 50-100 years. The left panel shows correlation maps between each band-pass reconstructed EW and gridded JA SPI during the period of instrumental record. The right panel shows the same information, but with band-pass filtered EW and unfiltered EW for the entire tree ring record, shown as superimposed triangles at the tree ring sites. Irrespective of the spectral band, the variation in EW is of the same phase throughout the Southwest, so wet or dry conditions would occur throughout the entire region as a superposition of these modes of spatiotemporal variability. The spatial correlation pattern of EW with cool season SPI in the 50-100 year band strongly resembles the ENSO-PDV signal on winter precipitation, with an out-of-phase relationship between the Southwest and the Pacific Northwest.

An identical analysis is performed during the warm season for LW_{adj} and these results are shown in Fig. 17. The 10-15 year band reflects the anti-phase relationship between North American monsoon precipitation and precipitation in the central U.S., as shown in Fig. 13. Of relevance here is the precipitation variability in the 50-100 year band, with an out-of-phase relationship between the Southwest (positive) and central U.S. (negative), which is observed in the correlation map with JA SPI (left panel) for the observational period (1895-2005). Using the complete LW_{adj} time series (right panel), the positive phase of this pattern is still observed at the tree-ring sites (triangle).

b. Megadroughts during the past four centuries

The EW and LW_{adj} time series of the decadal (10-15 year) and interdecadal (15-25 and 50-100 years) modes identified with MTM-SVD are shown in Figure 18. These time series were used for constructing correlation maps in Figs. 16 and 17. The anti-phasing of EW and LW_{adj} that would be expected associated with ENSO-PDV tends to

occur more in the 10-15 year band. This is particularly the case after 1950, the period over which this relationship has been established in the prior literature mentioned in the Introduction, but prior to 1950 the same time series reveals a transitional behavior from an in-phase to out-of-phase behavior which we are not able to explain. In the interdecadal band, the variation of the 50-100 year band in EW and LW_{adj} are in-phase. This in-phase relationship is consistent with the low-frequency covariability between reconstructed summer and winter precipitation over the NAM 2 region (Griffin et al., 2013). Thus, the temporal variation of this time series and its associated spatial pattern strongly suggest that this mode represents the spatiotemporal variation of the droughts in the Southwest. This is better clarified by arrows located at the coincident local minima in EW and LW_{adj} (Figure 18), which correspond to the following documented major droughts in the Southwest during the past four centuries (Woodhouse and Overpeck, 1998; Seager et al. 2009; Stahle et al. 2009; Griffin et al., 2013;).

7. Summary

This work has considered dominant spatiotemporal modes of EW and LW_{adj} variability using data from a southwestern U.S., monsoon region, tree-ring network. We address three questions by this analysis: 1) do the dominant spatiotemporal modes of variability in EW and LW_{adj} tree-ring chronologies reflect equivalent modes of precipitation variability?; 2) do these spatiotemporal relationships in EW and LW_{adj} correspond to large-scale forcing (such as ENSO-PDV) as portrayed in the atmospheric and oceanic circulation?; and 3) does the phenomenon of dual season wet and dry period reflect statistically significant very low-frequency climate variability that cannot be resolved in the comparatively short period of the instrumental record?

We assessed the first question by using EOF and CCA to present evidence that the monsoon region tree-ring network is able to reasonably represent the interannual variability of cool and warm season precipitation, during the period of recent instrumental record. At a continental scale, EW is able to resolve features better than LW_{adj} , due to the more heterogenous nature of the monsoon precipitation, compared to cool season precipitation. This result is consistent with previous studies (e.g. Meko and Baisan, 2001; Stahle et al. 2009; Griffin et al. 2013).

The dominant mode of EW and LW_{adj} unquestionably captures ENSO-PDV forcing on cool and warm season precipitation in the Southwest during the past 100 years, which affirmatively answers the second question. The dominant mode of EW is related to quasi-stationary Rossby wave trains emanating from the west tropical Pacific, resembling the positive phase of the PNA pattern, and a split jet stream with an enhanced cool season storm track into the Southwest U.S. The dominant mode of LW_{adj} is also related to the ENSO-PDV warm season teleconnection response that governs monsoon ridge position in early summer and the anti-phase relationship in precipitation the southwestern U.S. and central U.S. MTM-SVD confirms the distinct influences of ENSO-PDV on EW and cool season SPI and LW_{adj} and warm season SPI at their expected temporal scale of variability.

We answer the third question by using MTM-SVD and the complete 400-year record of tree-ring chronologies. Our analysis reveals a very low-frequency (50-100 year) mode of climate variability, which may be a factor in synchronizing many of the major cool and monsoon season droughts over the last four centuries, as documented by Griffin et al. (2013). The synchronous very low-frequency climate variability has been the

orchestrator of all the documented major long-term droughts in the Southwest. EW in the centennial spectral band resembles the ENSO-PDV signal on winter precipitation, as can be inferred from the out-of-phase spatial pattern between the Southwest and the Pacific Northwest. This result is entirely consistent with Herweijer et al. (2007) which suggested that persistent La Niña-like conditions is a likely influence on major cool season droughts in the western and central United States during the Medieval Climate Anomaly, Little Ice Age, and Modern eras. LW_{adj} variability in the 50-100 year band, however, seems to more resemble the one phase of the Circumglobal Teleconnection (CGT) that the Southwest tree-ring network is able to detect and not the early warm season ENSO-PDV precipitation pattern. This is shown in Table 1 by comparing these spatial pattern modes with the CGT modes described in Ciancarelli et al. (2013), and further supported by Tables 2 and 3 (Also Fig. 19 shows the summer spatial patterns used to compute correlations in Tables 1 and 2).

This finding is important given that the CGT likely arises as internal mode of variability in the warm season, to the best of current physical understanding (Ding and Wang, 2005; Ding et al., 2011). Is there some plausible physical mechanism that would cause the CGT to vary significantly on centennial timescales? Consistent with current suggested ideas as described in Ding and Wang (2005) and Ding et al., (2011) two possibilities could be Indian monsoon variability and/or variation of the jet stream in the North Atlantic. Considering the dual influences of cool and warm season precipitation, long-term megadrought conditions, from this analysis, would appear to derive 1) from persistent La Niña, low PDV conditions that would tend to decrease winter precipitation and 2) from the persistent recurrence of the phase of the CGT pattern that would tend to

decrease monsoon precipitation in the intermountain west, while increasing precipitation in the central U.S. We propose that this very low-frequency mode is the mostly related to the occurrence of megadroughts, as supported by evidence showed in this study which cannot be resolved with observational record. We suggest that future research should be directed toward examining these hypothesized physical mechanisms in the context of long-term global climate model integrations on a millennial timescale.

Acknowledgments

This research was funded by the National Science Foundation under grants ATM-0813656. Additional funding was provided by the Water Sustainability Graduate Student Fellowship Program at the University of Arizona. We are grateful to Russ Vose and Richard Heim for access to the gridded precipitation data.

References

- Adams DK, Comrie AC. 1997. The North American Monsoon. *Bulletin of the American Meteorological Society* **10**: 2197-2213.
- Barlow M, Nigam S, Berbery EH. 1998. Evolution of the North American Monsoon system. *Journal of Climate* **11**: 2238-2257.
- Carleton AM, Carpenter DA, Wever PJ. 1990. Mechanisms of interannual variability of the southwest United States summer rainfall maxima. *Journal of Climate* **3**: 999-1015.
- Castro CL, McKee TB, Pielke RA. 2001. The relationship of the North American monsoon to tropical and north pacific sea surface temperature as revealed by observational analysis. *Journal of Climate* **14**: 4449-4473.
- Castro CL, Pielke Sr. RA, Adegoke JO, Schubert SD, Pegion PJ. 2007. Investigation of the summer climate of the contiguous United States and Mexico using Regional Atmospheric Modeling System (RAMS). Part II: Model climate variability. *Journal of Climate* **20**: 3866-3887.

- Castro CL, Beltrán-Prezekurat AB, Pielke Sr. RA. 2009. Spatiotemporal variability of precipitation, modeled soil moisture, and vegetation greenness in North America within the recent observational record. *Journal of Hydrometeorology* **10**: 1355-1378. DOI: 10.1175/2009JHM1123.1.
- Castro CL, Chang H, Dominguez F, Carrillo C, Kyung-Schemm J, Juang H. 2012. Can a regional climate model improve warm season forecasts in North America? *Journal of Climate* **25**: 8212-8237.
- Ciancarelli B, Castro CL, Woodhouse C, Dominguez F, Chang H, Carrillo C, Griffin D. 2013. Dominant pattern of U.S. warm season precipitation variability in a fine resolution observational record with focus on the southwest. *International Journal of Climatology*. DOI:10.1002/joc.3716.
- Daly C, Neilson RP, Phillips DL. 1994. A statistical topographic model for mapping climatological precipitation over mountains terrain. *Journal of Applied Meteorology* **33**: 140-158.
- Ding Q, Wang B. 2005. Circumglobal teleconnection in the Northern Hemisphere summer. *Journal of Climate* **18**: 3483-3505.
- Ding Q, Wang B, Wallace JM, Branstator G. 2011. Tropical-extratropical teleconnections in boreal summer: observed interannual variability. *Journal of Climate* **24**: 1878-1896.
- Douglas AV, Englehart PJ. 1981. On a statistical relationship between autumn rainfall in the central equatorial pacific and subsequent winter precipitation in Florida. *Monthly Weather Review* **109**: 2377-2382.
- Faulstich HL, Woodhouse CA, Griffin G. 2012. Reconstructed cool- and warm-season precipitation over for the tribal lands of northeast Arizona. *Climatic Change* **118**:457–468.
- Feng S, Hu Q, Oglesby RJ. 2011. Influence of Atlantic sea surface temperatures on persistent drought in North America. *Climate Dynamics* **37**: 569-586.
- Garfin, G, Jardine A, Merideth R, Black M, Leroy S, eds. 2013. *Assessment of Climate Change in the Southwest United States: A Report Prepared for the National Climate Assessment*. A report by the Southwest Climate Alliance. Washington, DC: Island Press.
- Gershunov A, Barnett TP. 1998. ENSO influence on intraseasonal extreme rainfall and temperature frequencies in the contiguous United States: observation and model results. *Journal of Climate* **11**: 1575-1586.
- Gochis D, Schemm J, Shi W, Long L, Higgins W, Douglas A. 2009. A Forum for Evaluating Forecasts of the North American Monsoon. *EOS Transactions American Geophysical Union* **90**(29): 249. DOI:10.1029/2009EO290002.

- Griffin D, Meko DM, Touchan R, Leavitt S, Woodhouse CA. 2011. Latewood chronology development for summer-moisture reconstruction in the US Southwest. *Tree-ring Research* **67**(2): 87-11.
- Griffin D, Woodhouse CA, Meko DM, Stable DW, Faulstich HL, Carrillo C, Touchan R, Castro CL, Leavitt SW. 2013. North American monsoon precipitation reconstructed from tree-ring latewood. *Geophysical Research Letters*. DOI:10.1002/grl.50184.
- Gutzler DS, Kann DM, Thornbrugh C. 2002. Modulation of ENSO-based long-lead outlooks of southwestern U.S. winter precipitation by the Pacific Decadal Oscillation. *Weather and Forecasting* **17**: 1163-1172. DOI: 10.1175/1520-0434.
- Heim RR. 2002. A review of Twentieth-Century Drought Indices Used in the United States. *Bulletin of the American Meteorological Society* **83**: 1149-1165.
- Herweijer C, Seager R, Cook ER, Emile-Geay J. 2007. North American droughts of the last millenium from a gridded network of tree-ring data. *Journal of Climate* **20**: 1353-1376.
- Higgins RW, Yao Y, Wang XL. 1997. Influence of the North American Monsoon System on the U.S. summer precipitation regime. *Journal of Climate* **10**: 2600-2622. DOI: 10.1175/1520-0442.
- Higgins RW, Chen Y, Douglas AV. 1999. Interannual variability of the North American warm season precipitation regime. *Journal of Climate* **12**: 653-680.
- Higgins RW, Shi W. 2000. Intercomparison of the principal modes of interannual and intraseasonal variability of the North American Monsoon system. *Journal of Climate* **14**: 403-417.
- Hu Q, Feng S. 2002. Interannual rainfall variations in the North American Monsoon region: 1900-98. *Journal of Climate* **15**: 1189-1202.
- Hu Q, Feng S. 2008. Variation of North American summer monsoon regimes and the Atlantic multidecadal oscillation. *Journal of Climate* **21**: 2373-2383.
- Kalnay E, Kanamitsu M, Kistler R, Collins W, Deaven D, Gandin L, Iredell M, Saha S, White G, Woollen J, Zhu Y, Chelliah M, Ebisuzaki W, Higgins W, Janowiak J, Mo KC, Ropelewski C, Wang J, Leetmaa A, Reynolds R, Jenne R, Joseph D. 1996. The NCEP/NCAR 40-year Reanalysis Project. *Bulletin of the American Meteorological Society* **77**: 437-471.
- Kiladis GN, Diaz HF. 1989. Global climate anomalies associated with extremes of the Southern Oscillation. *Journal of Climate* **2**: 1069-1090.

Latif M, Barnett TP. 1994. Causes of Decadal Climate Variability over the North Pacific and North America. *Science* **266**: 634-637.

Leavit, SW, Woodhouse CA, Castro CL, Wrigth WE, Meko DM, Touchan R, Griffin D, Ciancarelli B. 2011. The North American monsoon in the U.S Southwest: potential for investigation with tree-ring carbon isotopes. *Quaternary International* **235**: 101-107.

Lees JM, Park JM. 1995. Multi-Taper Spectral Analysis: A Stand-Alone C-subroutine. *Computer and Geology* **21**: 199-236.

Livezey RE, Chen WY. 1983. Statistical Field Significance and its Determination by Monte Carlo Techniques. *Monthly Weather Review* **111**: 46-59.

Livezey RE, Mo KC. 1987. Tropical-extratropical teleconnections during the Northern Hemisphere winter. Part II: Relationships between monthly mean Northern Hemisphere circulation patterns and proxies for tropical convection. *Monthly Weather Review* **115**: 3115-3132.

Mann ME, Lees JM. 1996. Robust Estimation of background noise and signal detection in climatic time series. *Climate Change* **33**: 409-445.

Mann ME, Park J. 1994. Global-scale modes of surface temperature variability on interannual to centennial timescales. *Journal of Geophysical Research* **99**: 1055-1058.

Mann ME, Park J. 1996. Joint spatiotemporal modes of surface temperature and sea level pressure variability in the Northern Hemisphere during the last century. *Journal of Climate* **9**: 2137-2162.

McCabe GJ, Dettinger MD. 1999. Decadal variations in the strength of ENSO teleconnections with precipitation in the western United States. *International Journal of Climatology* **19**: 1399-1410.

McKee TB, Doesken NJ, Kleist J. 1993. The relationship of drought frequency and duration to time scales. *Eight Conference on Applied Climatology*. 17-22 January. Anaheim, California.

Meko DM, Baisan CH. 2001. Pilot study of latewood-width of conifers as an indicator of variability of summer rainfall in the North American monsoon region. *International Journal of Climatology* **12**: 697-708.

Ni F, Cavazos T, Hughes MK, Comrie AC, Funkhouser G. 2002. Cool-season precipitation in the southwestern USA since A.D. 1000: comparison of linear and nonlinear techniques for reconstruction. *International Journal of Climatology* **22**: 1645-1662.

- Parks JA, Dean JS, Betancourt JL. 2006. Tree rings, drought, and the pueblo abandonment of south- central New Mexico in the 1670s. In: Doyel DE, Dean JS (eds) Environmental change and human adaptation in the ancient American southwest. University of Utah Press. Salt Lake City. 214-227.
- Rajagolapan B, Mann ME, Lall U. 1998. A multivariate frequency-domain approach to long-lead climatic forecasting. *Weather and Forecasting* **13**: 58-74.
- Ropelewski CF, Halpert MS. 1986. North American precipitation and temperature associated with El Niño/Southern Oscillation (ENSO). *Monthly Weather Review* **114**: 2352-2363.
- Ropelewski CF, Halpert MS. 1987. Global and regional scale precipitation patterns associated with El Niño/Southern Oscillation (ENSO). *Monthly Weather Review* **115**: 1606-1626.
- Seager R, Ting M, Davis M, Cane M, Naik N, Nakamura J, Li C, Cook E, Stahle DW, 2009: Mexican drought: an observational modeling and tree ring study of variability and climate change, *Atmósfera* **22**: 1–31.
- Stahle DW, Cleaveland MK, Grissino-Mayer HD, Griffin RD, Fye FK, Therrell MD, Burnette DJ, Meko DM, Villanueva Diaz J, 2009: Cool- and warm-season precipitation reconstructions over western New Mexico. *Journal of Climate* **22**: 3729-3750.
- Trenberth KE. 1990. Recent observed interdecadal climate changes in the Northern Hemisphere. *Bulletin of the American Meteorological Society* **71**: 988-993.
- Wallace JM, Gutzler DS. 1981. Teleconnections in the geopotential height during the northern hemisphere winter. *Monthly Weather Review* **109**: 784-812.
- Wallace JM, Smith C, Bretherton CS. 1992. Singular value decomposition of wintertime sea surface temperature and 500-mb height anomalies. *Journal of Climate* **5**: 561-576.
- Wilks DS. 2006. *Statistical Methods in the Atmospheric Sciences*. Elsevier: Burlington, MA.
- Woodhouse CA, Overpeck JT. 1998. 2000 Years of Drought Variability in the Central United States. *Bulletin of the American Meteorological Society* **79**: 2693-2714.
- Woodhouse CA, Meko DM, Griffin D, Castro CL, 2013. Tree-rings and multiseason drought variability in the lower Rio Grand basin, U.S.A., *Water Resources Research* **49**. doi:10.1002/wrcr.20098.

Tables

	JJ PRISM EOF	Forcing Mechanism	JA P-NOAA CORR	Forcing Mechanism
EOF1	-0.09	ENSO/PDV	-0.16	ENSO/PDV
EOF2	-0.11	GCT1	0.40	GCT1
EOF3	-0.43	Climate Change?	-0.08	not shown in Fig. 19
EOF4	0.06	ENSO/PDV;AMO	-0.55	Climate Change?
EOF5	-0.20	CGT2	0.03	ENSO/PDV;AMO

Table 1: Spatial correlation between the LW_{adj} 50-100 mode and both JJ PRISM REOF and JA P-NOAA CORR patterns from Fig. 19.

	LW_{adj} EOFs					Forcing Mechanism	PRISM Exp.Var.
	EOF1	EOF2	EOF3	EOF4	EOF5		
JJ PRISM REOF1	0.51	0.32	-0.40	0.52	-0.12	ENSO-PDV	24%
JJ PRISM REOF2	-0.25	0.38	0.09	-0.23	0.15	CGT1	23%
JJ PRISM REOF3	0.03	-0.32	-0.07	0.49	0.32	Climate Change?	19%
JJ PRISM REOF4	0.10	0.26	0.13	-0.15	0.06	ENSO-PDV;AMO	17%
JJ PRISM REOF5	-0.47	0.46	-0.01	-0.01	-0.23	CGT2	16%
	36%	10%	7%	5%	4%	LW_{adj} EOF Exp. Var.	

Table 2: Spatial correlation of JJ PRISM REOFs PRISM versus LW_{adj} correlation. LW_{adj} correlation was obtained from correlation between LW_{adj} PCs against gridded JA SPI.

	JA PNOAA EOFs					Forcing Mechanism	PRISM Exp.Var.
	EOF1	EOF2	EOF3	EOF4	EOF5		
JJ PRISM REOF1	0.81	-0.04	-0.34	-0.08	-0.05	ENSO-PDV	24%
JJ PRISM REOF2	0.33	0.49	0.06	-0.21	0.03	CGT1	23%
JJ PRISM REOF3	0.19	-0.75	-0.10	0.48	0.12	Climate Change?	19%
JJ PRISM REOF4	-0.32	0.58	0.24	0.12	0.40	ENSO-PDV;AMO	17%
JJ PRISM REOF5	0.33	0.49	0.06	-0.21	0.03	CGT2	16%
	17%	14%	11%	6%	24%	JA EOF Exp. Var.	

Table 3: Spatial correlation of JJ PRISM REOFs versus JA SPI correlation. JA SPI correlation is obtained from correlation between JA SPI PCs against gridded JA SPI.

Figure Captions

Figure 1: Location of tree-ring sites are shown in triangles: blue and red are for ponderosa pine and Douglas-fir respectively. Other pine and fir in grey. Terrain elevation is shaded.

Figure 2: Leading mode of spatial variability of SPI, EOF1(SPI:NOAA) winter (a), November through April, and summer (b), July and August. Spatial correlation between the temporal dominant mode of SPI, PC1(SPI:NOAA) and sea surface temperature anomalies, ΔSST , for both winter (c) and summer (d). Local significance at the 90% level

is indicated in oblique lines and its field significance is shown in the lower left on each plot.

Figure 3: Power spectrum (Multiple Taper Method-MTM) of the temporal leading mode (PC1) of SPI obtained with EOF analysis for both winter (a) and summer (b).

Figure 4: Left panel: spatial correlation between the dominant mode of tree-ring chronologies, PC1(earlywood and latewood), and gridded SPI, for both winter (a), and summer (b) seasons. Right panel: spatial correlation between the dominant mode of SPI, PC1(winter and summer), and gridded SPI, for both winter (c), and summer (d).

Figure 5: Spatial correlation between the dominant mode of SPI at sites, PC1[site], and gridded SPI, SPI, for both winter (a) and summer (b) seasons. Time series of the leading mode for both earlywood index (blue) and superimposed with winter SPI (red) (c). Also similar as (c) but for latewood adjusted index and winter SPI (d).

Figure 6: Power spectrum (Multiple Taper Method-MTM) of the temporal leading mode (PC1) of tree ring chronologies obtained with EOF analysis for earlywood (a) and latewood (b).

Figure 7: Upper panel: Homogeneous correlation map of dominant NA SPI singular vector (a). Homogeneous correlation map of dominant Earlywood singular vector (b). Heterogeneous correlation map between Earlywood singular vector and NA SPI (c). Singular vectors were obtained from CCA analysis on NA SPI and Earlywood. Lower panel: as in upper panel but for second CCA mode.

Figure 8: Upper panel: Homogeneous correlation map of dominant JA SPI singular vector (a). Homogeneous correlation map of dominant Latewood singular vector (b). Heterogeneous correlation map between Latewood singular vector and JA SPI (c). Singular vectors were obtained from CCA analysis on JA SPI and Latewood. Lower panel: as in upper panel but for second CCA mode.

Figure 9: Spatial correlation maps between the temporal leading mode of EW chronologies and both winter sea surface temperature anomalies, Δ SST, [PC1(EW) versus Δ SST(N-A)], (a) and geopotential height anomalies, Δ GPH, [PC1(EW) versus Δ GPH(N-A)], (b). Also, spatial correlation maps between the temporal leading mode of LW_{adj} chronologies and both summer sea surface temperature anomalies, Δ SST, [PC1(LW_{adj}) versus Δ SST(JJ)], (c) and geopotential height anomalies, Δ GPH, [PC1(LW_{adj}) versus Δ GPH(JA)], (d). Local significance at the 90% level is indicated in oblique lines and its field significance is shown at lower left on each plot.

Figure 10: Left panel: Local Fractional Variance (LFV) spectrum of the SPI leading modes obtained by MTM-SVD analysis for both winter (a) and summer (b). Right panel: LFV spectrum of the tree-ring chronology leading modes obtained by MTM-SVD analysis for both earlywood (c) and latewood (d).

Figure 11: Upper panel: Reconstructed spatial pattern (U component in shade and total component in vector) of NA SPI as highlighted in Fig. 11 for three spectral bands: 3-6 year (a), 6-12 year, and 25-50 year (c). The reference point is located near the center of the NAME 2 zone (32.75°N; 110.25°W). Lower panel: as in upper panel but for Earlywood chronology.

Figure 12: Spatial correlation maps between the MTM-SVD reconstructed temporal pattern of Earlywood and winter sea surface temperature anomalies, N-A Δ SST, for the identified spectral bands: 3-6 year (a), 6-12 year (b), 25-50 year (c), and all modes (d). The Earlywood temporal pattern was reconstructed over a site near the center of the NAME 2 zone (32.75°N; 110.25°W). Local significance at the 90% level is indicated in oblique lines and its field significance is shown in the lower left on each plot.

Figure 13: Upper panel: Reconstructed spatial pattern (U component in shade and total component in vector) of JA SPI as highlighted in Fig. 12 for three spectral bands: 2-5 year (a), 6-9 year, and 10-15 year (c). The reference point is located near the center of the NAME 2 zone (32.75°N; 110.25°W). Lower panel: as in upper panel but for Latewood chronology.

Figure 14: Spatial correlation maps between the MTM-SVD reconstructed temporal pattern of Latewood and summer sea surface temperature anomalies, JJ Δ SST, for the identified spectral bands: 2-5 year (a), 6-9 year (b), 10-15 year (c), and all modes (d). The Latewood temporal pattern was reconstructed over a site near the center of the NAME 2 zone (32.75°N; 110.25°W). Local significance at the 90% level is indicated in oblique lines and its field significance is shown in the lower left on each plot.

Figure 15: Power spectrum (Local Fractional Variance-LFV) of the leading mode of tree-ring chronologies obtained with MTM-SVD analysis for both earlywood (a) and latewood (b). For a tree-ring record of 360 years.

Figure 16: Left panel: spatial correlation map for the historical period (1895-2005) between winter SPI and band-pass reconstructed EW for 10-15 year (top), 15-25 year (middle), and 50-100 year (bottom). Right panel: same as right panel but for EW and band-pass reconstructed EW (1650-2005) showed inside the triangles. Results from the left panel are superimposed in right panel.

Figure 17: Same as Fig. 16 but for summer SPI and LW chronologies.

Figure 18: Time series of MTM-SVD dominant reconstructed modes for both EW in red and LW in blue. For decadal (top: 10-15 year), inter-decadal (middle: 15-25 year [EW] and 25-50 year [LW]), and centennial (bottom: 50-100 year) modes. Blue arrows indicate extreme drought event in southwestern U.S.

Figure 19: Left panel: JJ PRISM SPI EOF modes as in Ciancarelli et al. (2013) with its mode name labeled for each EOF. Central panel: JA P-NOAA correlation pattern obtained by correlating JA SPI temporal PCs and its gridded JA SPI. Right panel: LW_{adj}

correlation pattern obtained by correlating LW_{adj} temporal PCs and gridded JA SPI. The EOF/PC explained variance for each case is indicated in blue, and the spatial correlation between PRISM EOF pattern and both P-NOAA and LW_{adj} correlation pattern for each case in magenta.

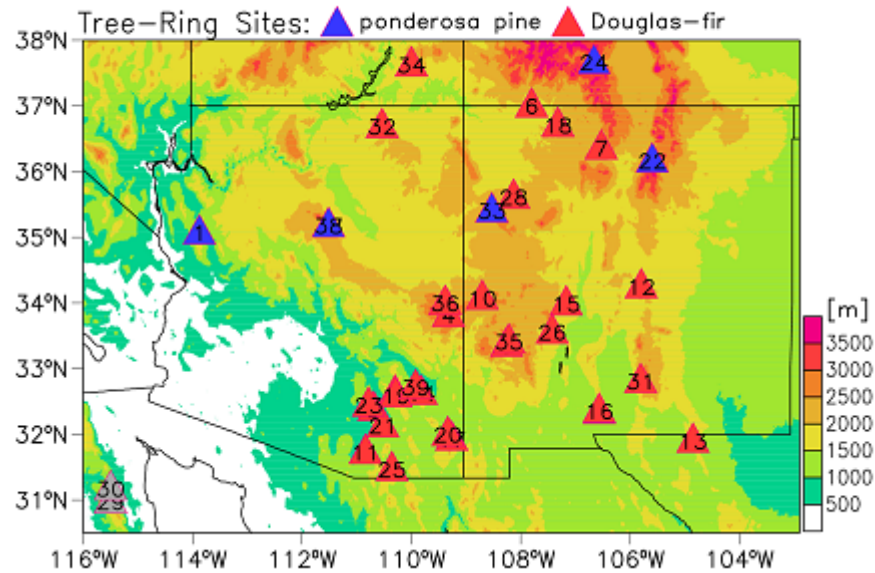


Figure 1: Location of tree-ring sites are shown in triangles: blue and red are for ponderosa pine and Douglas-fir respectively. Other pine and fir in grey. Terrain elevation is shaded.

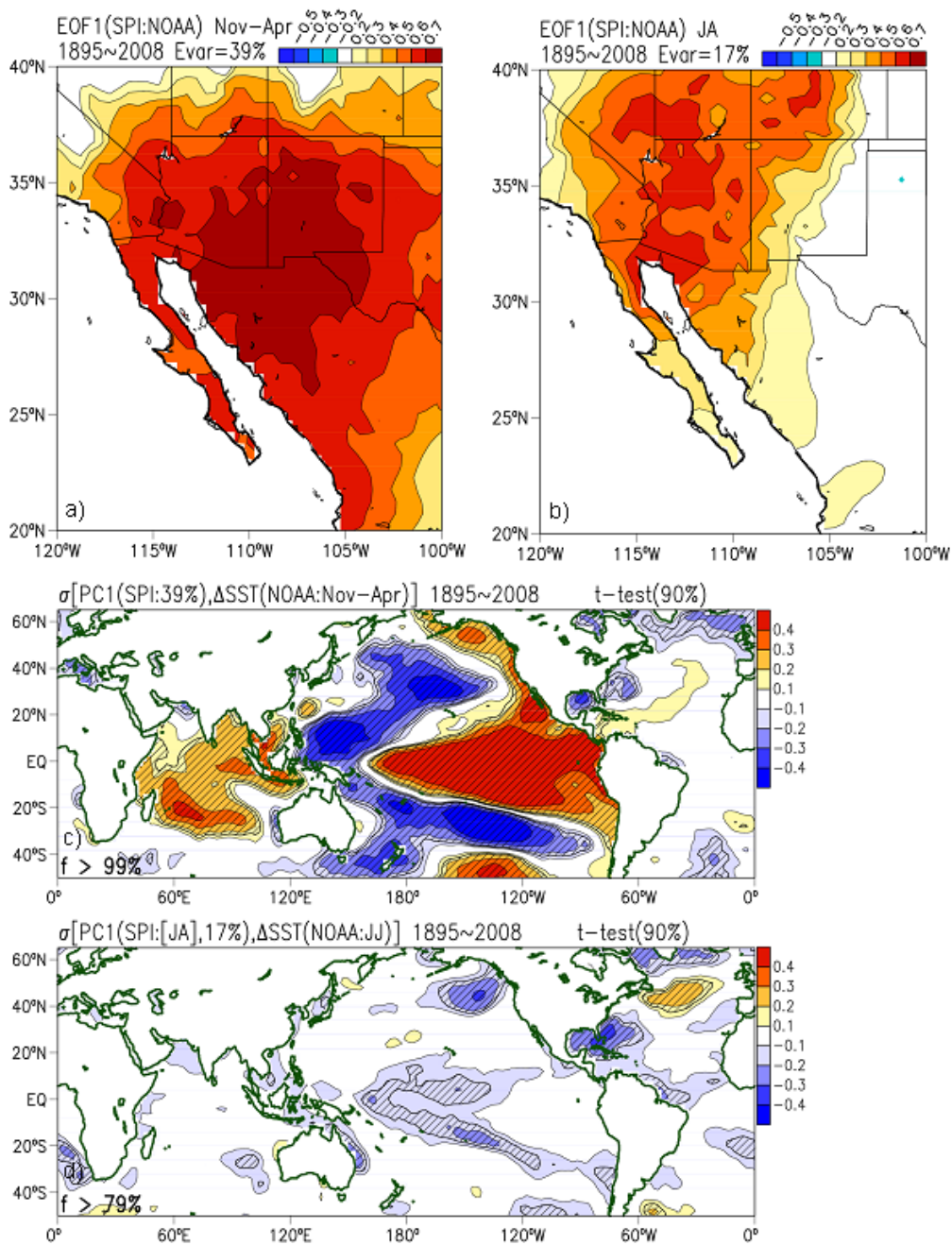


Figure 2: Leading mode of spatial variability of SPI, EOF1(SPI:NOAA) winter (a), November through April, and summer (b), July and August. Spatial correlation between the temporal dominant mode of SPI, PC1(SPI:NOAA) and sea surface temperature anomalies, Δ SST, for both winter (c) and summer (d). Local significance at the 90% level is indicated in oblique lines and its field significance is shown in the lower left on each plot.

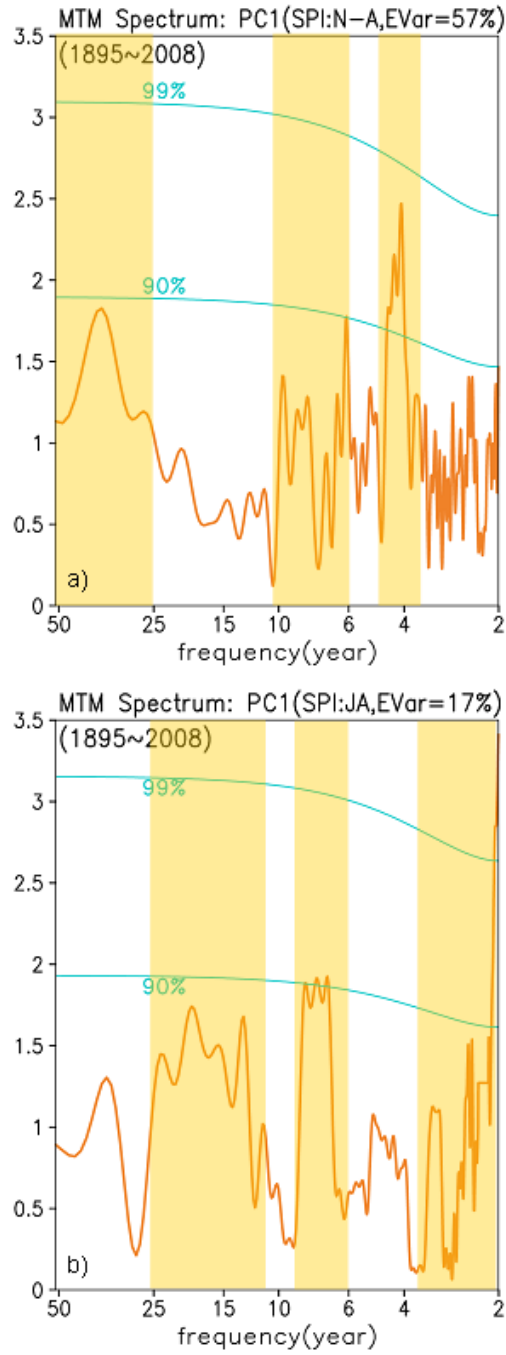


Figure 3: Power spectrum (Multiple Taper Method-MTM) of the temporal leading mode (PC1) of SPI obtained with EOF analysis for both winter (a) and summer (b).

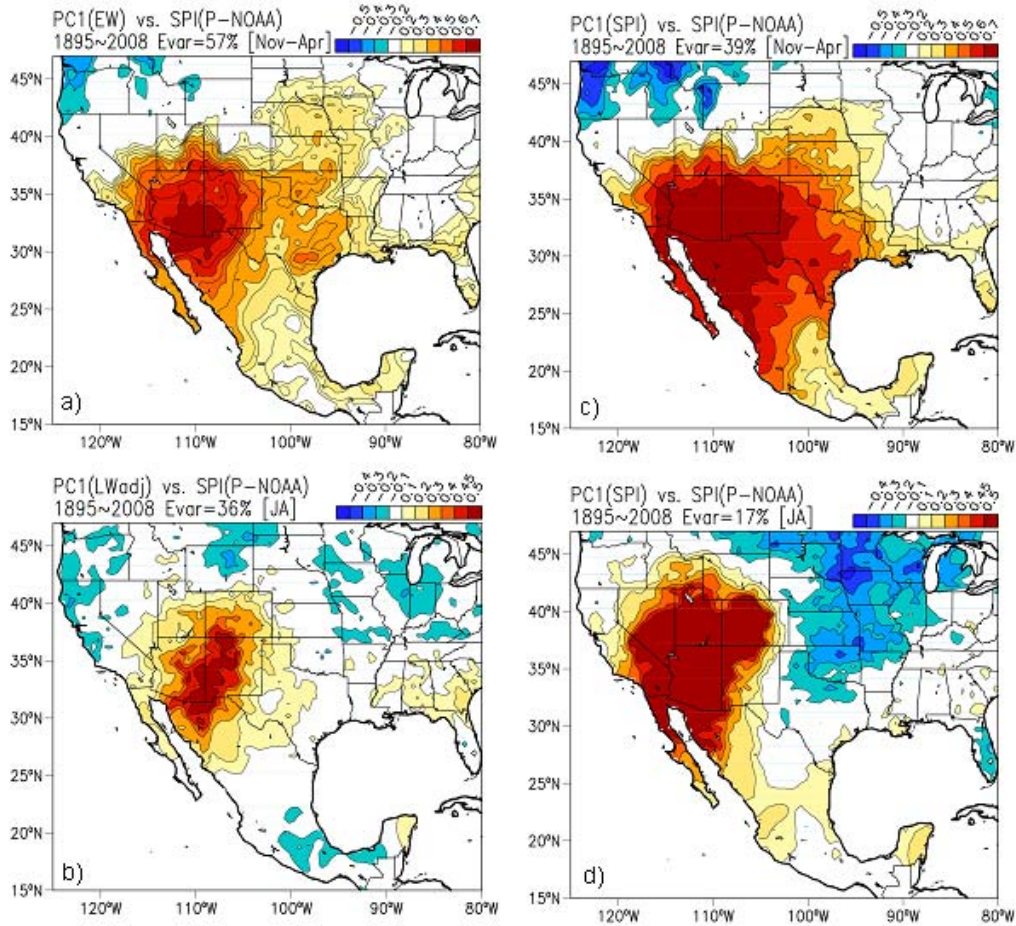


Figure 4: Left panel: spatial correlation between the dominant mode of tree-ring chronologies, PC1(earlywood and latewood), and gridded SPI, for both winter (a), and summer (b) seasons. Right panel: spatial correlation between the dominant mode of SPI, PC1(winter and summer), and gridded SPI, for both winter (c), and summer (d).

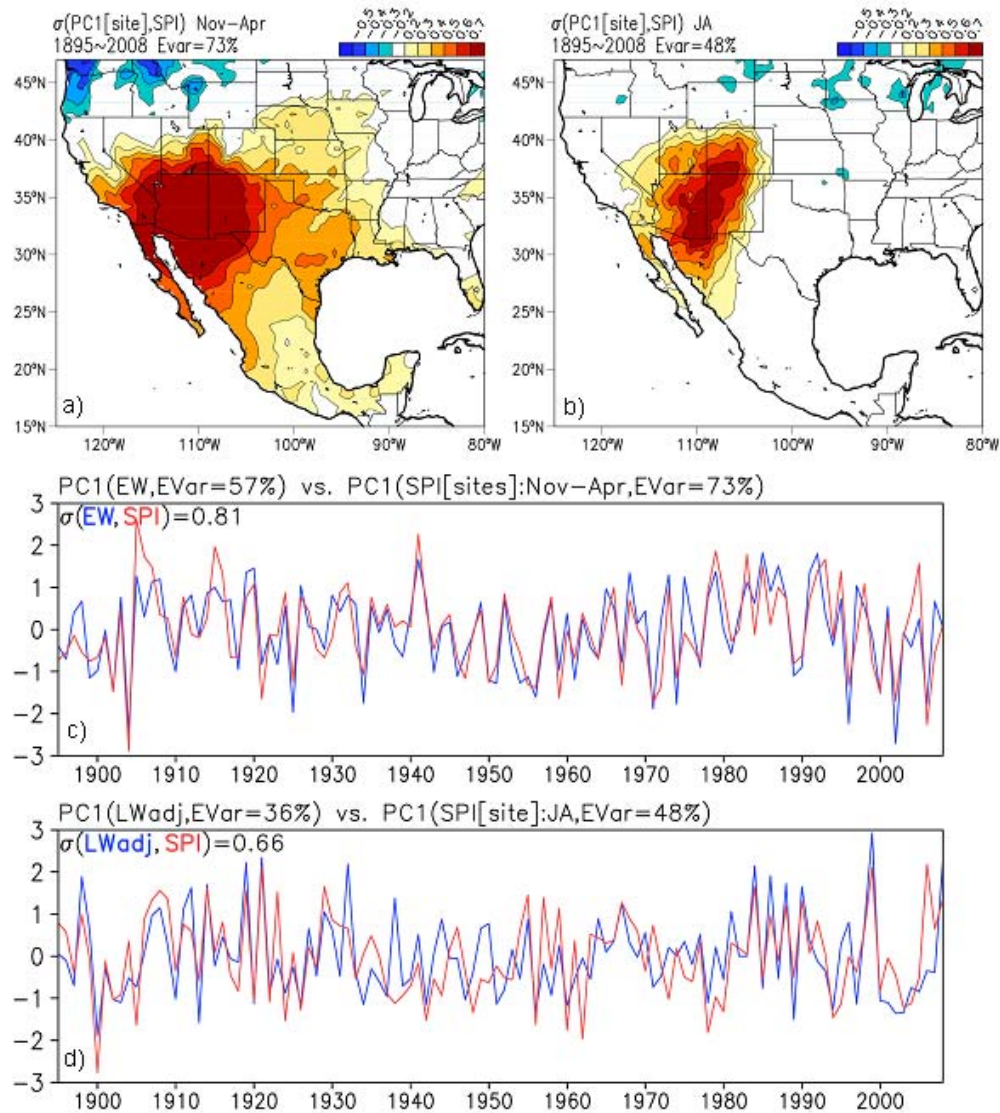


Figure 5: Spatial correlation between the dominant mode of SPI at sites, PC1[site], and gridded SPI, SPI, for both winter (a) and summer (b) seasons. Time series of the leading mode for both earlywood index (blue) and superimposed with winter SPI (red) (c). Also similar as (c) but for latewood adjusted index and winter SPI (d).

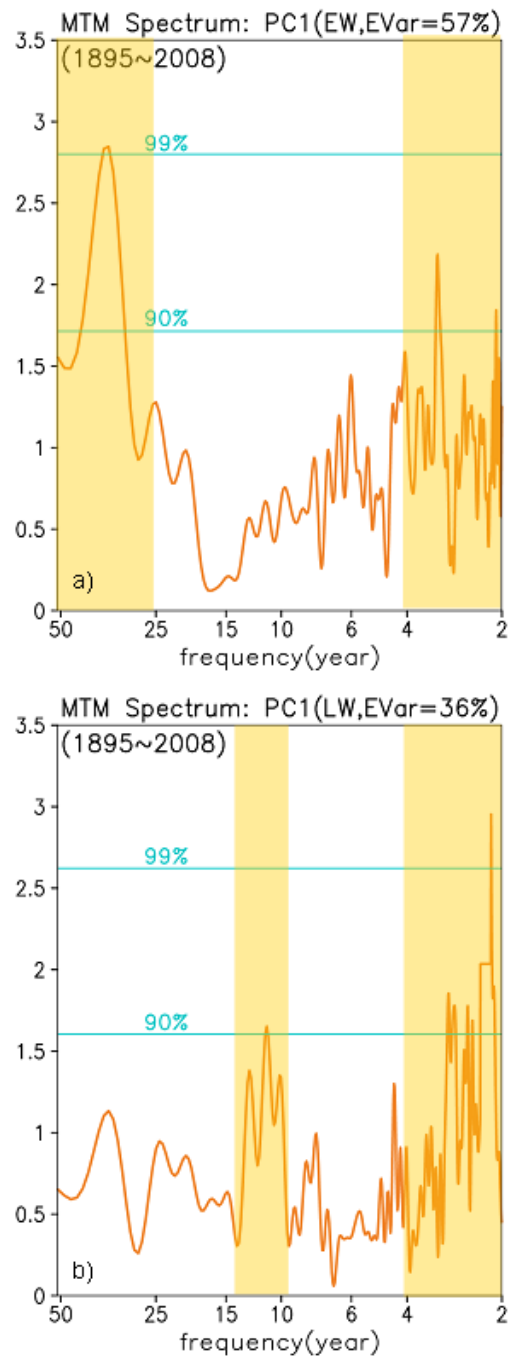


Figure 6: Power spectrum (Multiple Taper Method-MTM) of the temporal leading mode (PC1) of tree ring chronologies obtained with EOF analysis for earlywood (a) and latewood (b).

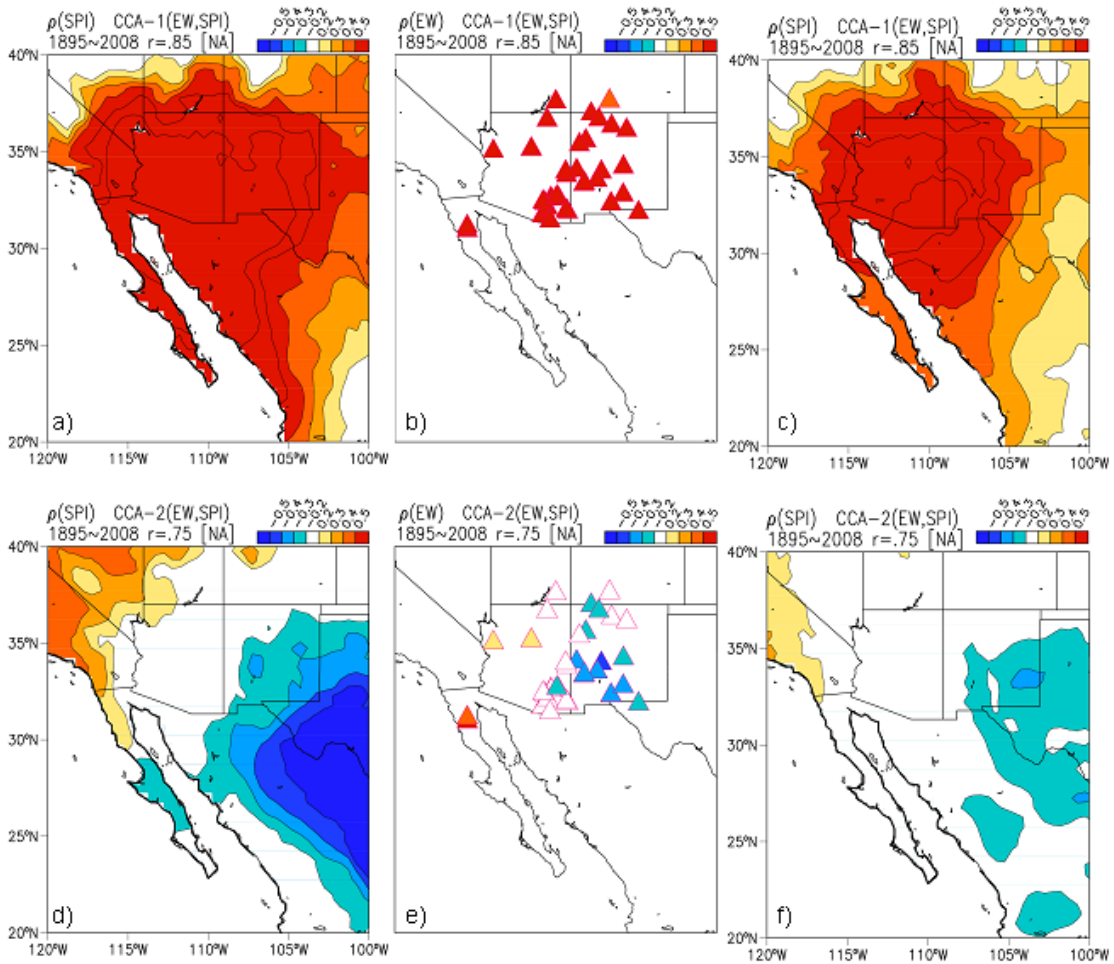


Figure 7: Upper panel: Homogeneous correlation map of dominant NA SPI singular vector (a). Homogeneous correlation map of dominant Earlywood singular vector (b). Heterogeneous correlation map between Earlywood singular vector and NA SPI (c). Singular vectors were obtained from CCA analysis on NA SPI and Earlywood. Lower panel: as in upper panel but for second CCA mode.

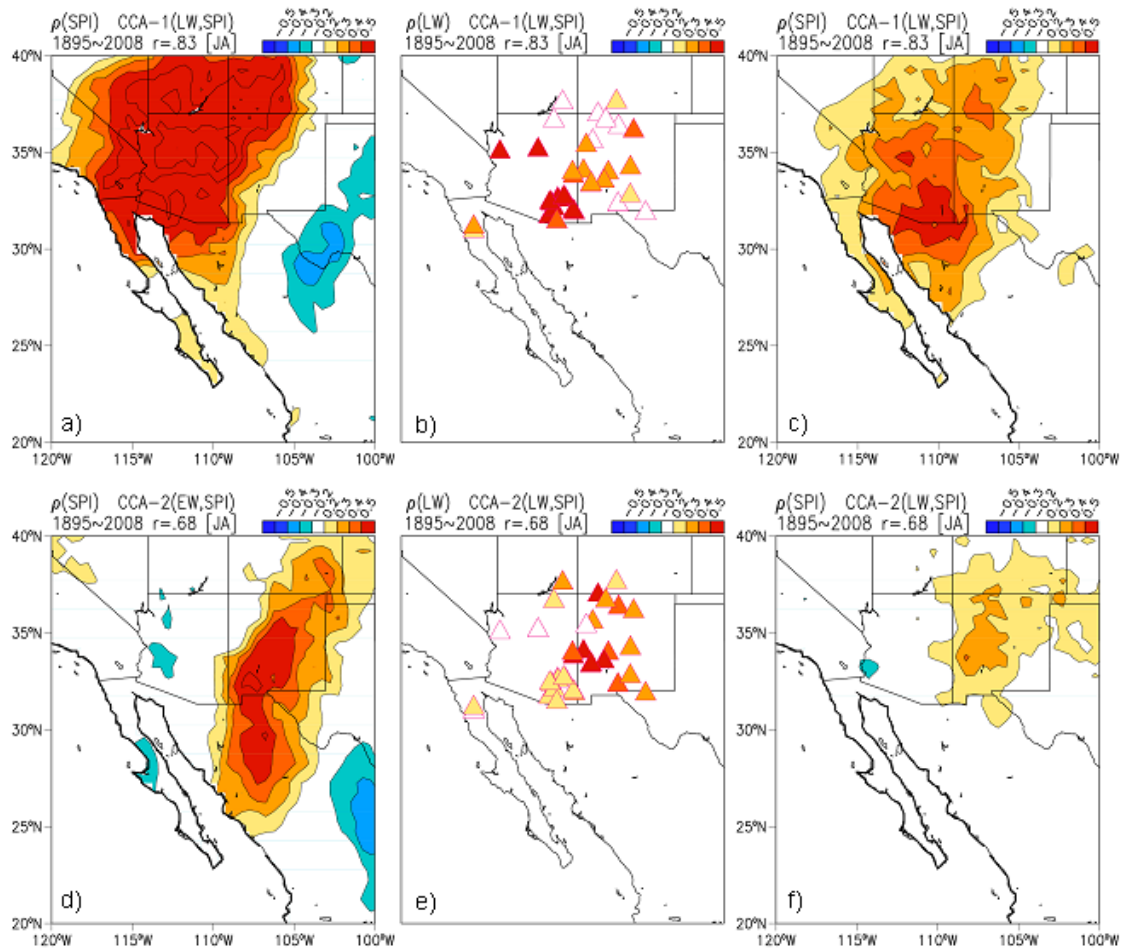


Figure 8: Upper panel: Homogeneous correlation map of dominant JA SPI singular vector (a). Homogeneous correlation map of dominant Latewood singular vector (b). Heterogeneous correlation map between Latewood singular vector and JA SPI (c). Singular vectors were obtained from CCA analysis on JA SPI and Latewood. Lower panel: as in upper panel but for second CCA mode.

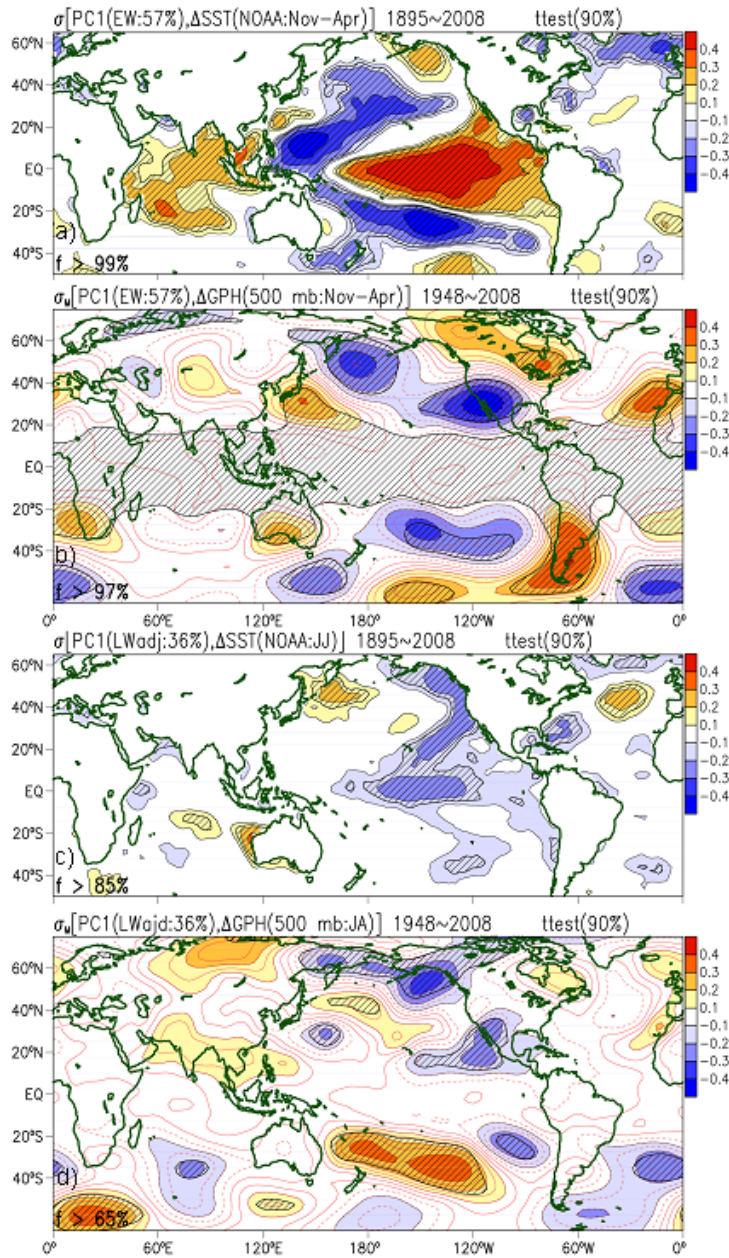


Figure 9: Spatial correlation maps between the temporal leading mode of EW chronologies and both winter sea surface temperature anomalies, ΔSST , [PC1(EW) versus $\Delta SST(N-A)$], (a) and geopotential height anomalies, ΔGPH , [PC1(EW) versus $\Delta GPH(N-A)$], (b). Also, spatial correlation maps between the temporal leading mode of LW_{adj} chronologies and both summer sea surface temperature anomalies, ΔSST , [PC1(LW_{adj}) versus $\Delta SST(JJ)$], (c) and geopotential height anomalies, ΔGPH , [PC1(LW_{adj}) versus $\Delta GPH(JA)$], (d). Local significance at the 90% level is indicated in oblique lines and its field significance is shown at lower left on each plot.

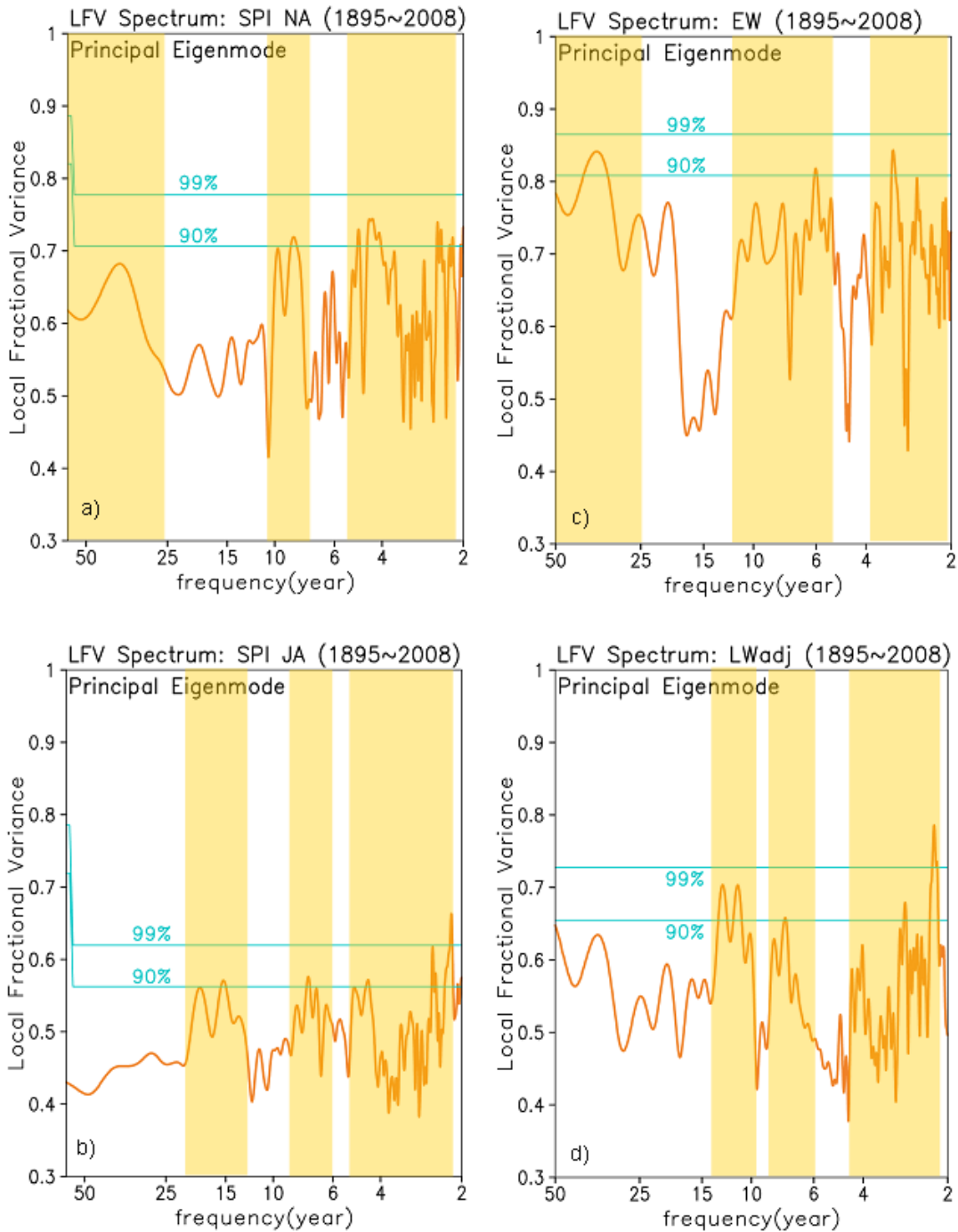


Figure 10: Left panel: Local Fractional Variance (LFV) spectrum of the SPI leading modes obtained by MTM-SVD analysis for both winter (a) and summer (b). Right panel: LFV spectrum of the tree-ring chronology leading modes obtained by MTM-SVD analysis for both earlywood (c) and latewood (d).

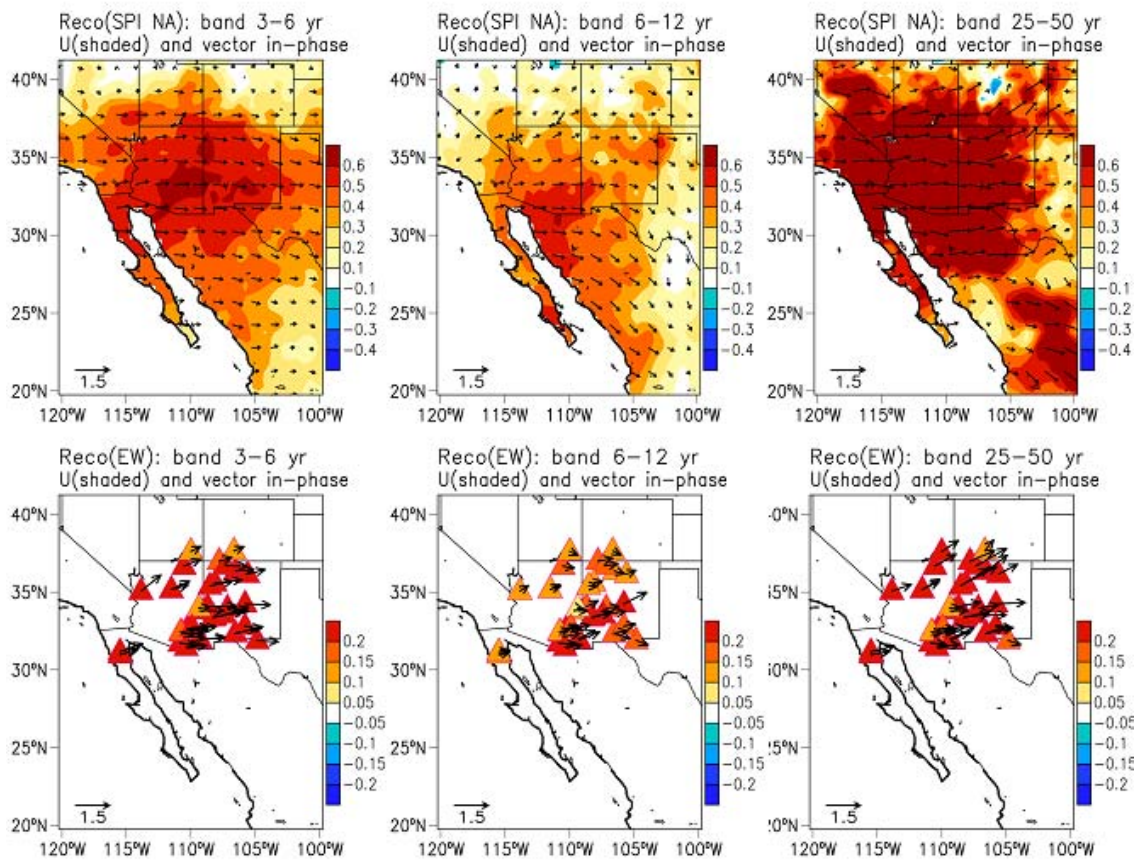


Figure 11: Upper panel: Reconstructed spatial pattern (U component in shade and total component in vector) of NA SPI as highlighted in Fig. 11 for three spectral bands: 3-6 year (a), 6-12 year, and 25-50 year (c). The reference point is located near the center of the NAME 2 zone (32.75°N; 110.25°W). Lower panel: as in upper panel but for Earlywood chronology.

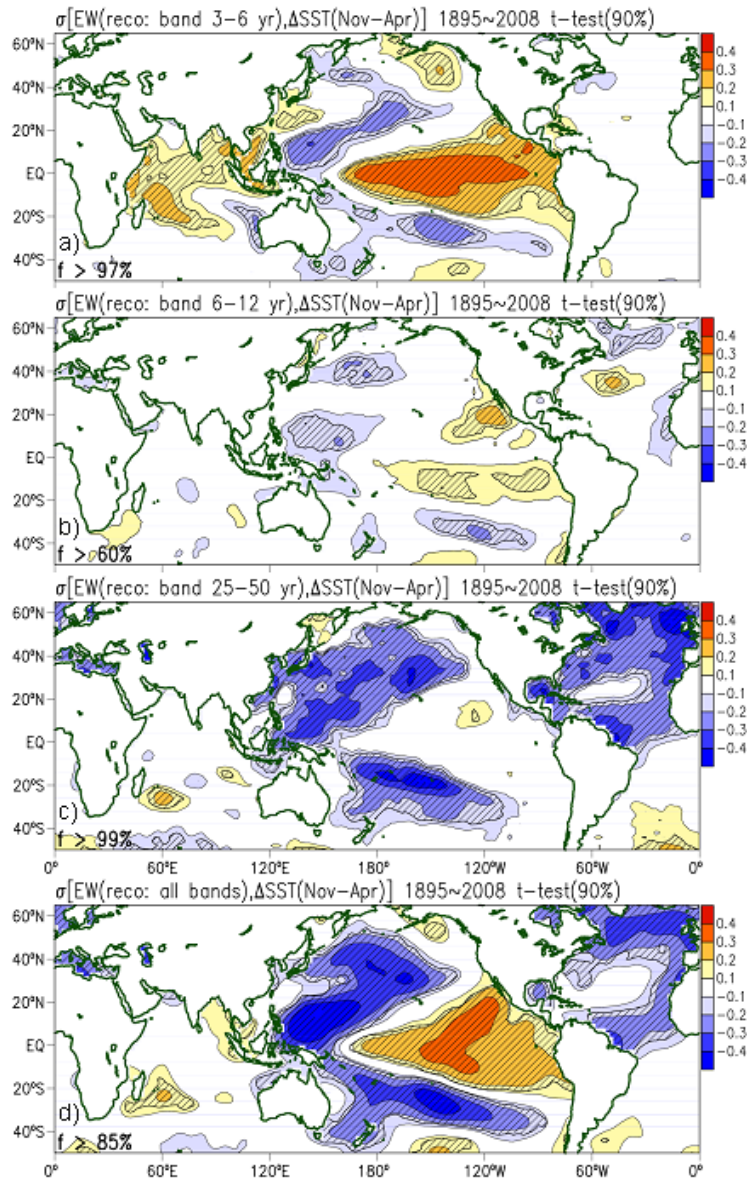


Figure 12: Spatial correlation maps between the MTM-SVD reconstructed temporal pattern of Earlywood and winter sea surface temperature anomalies, N-A ΔSST , for the identified spectral bands: 3-6 year (a), 6-12 year (b), 25-50 year (c), and all modes (d). The Earlywood temporal pattern was reconstructed over a site near the center of the NAME 2 zone (32.75°N; 110.25°W). Local significance at the 90% level is indicated in oblique lines and its field significance is shown in the lower left on each plot.

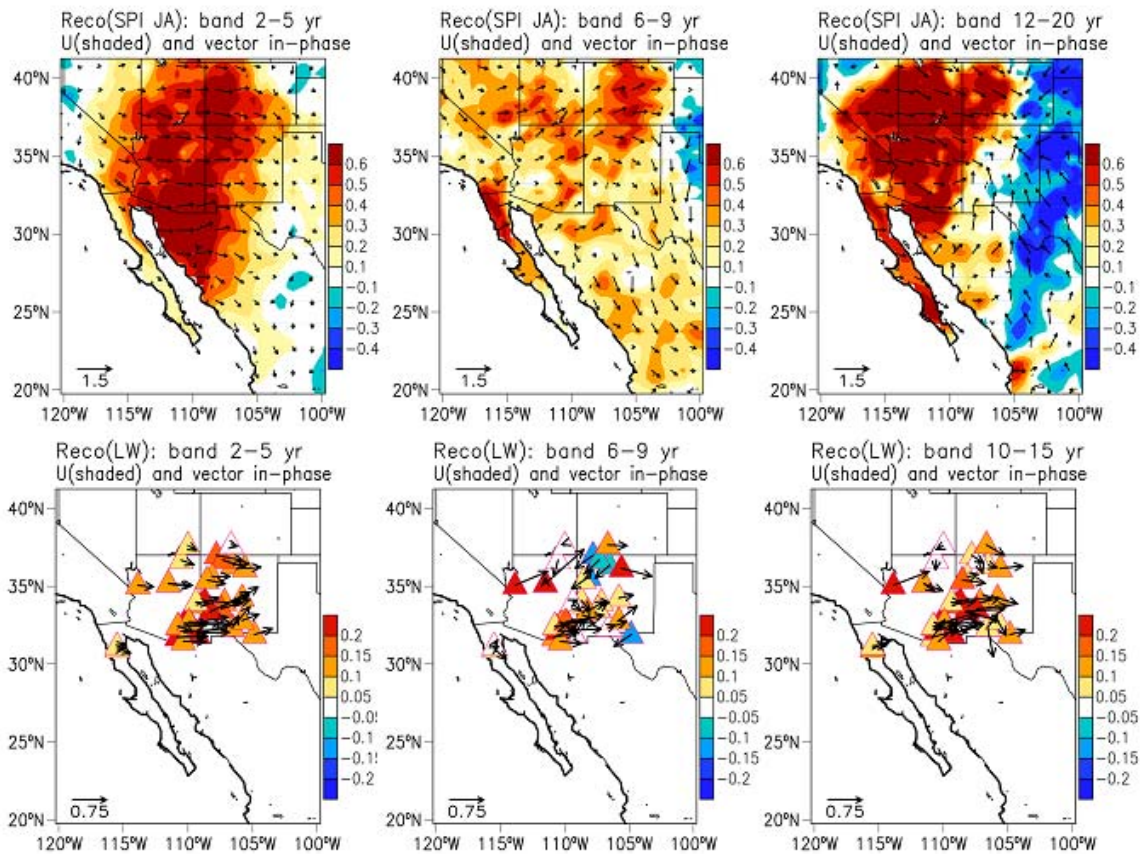


Figure 13: Upper panel: Reconstructed spatial pattern (U component in shade and total component in vector) of JA SPI as highlighted in Fig. 12 for three spectral bands: 2-5 year (a), 6-9 year, and 10-15 year (c). The reference point is located near the center of the NAME 2 zone (32.75°N; 110.25°W). Lower panel: as in upper panel but for Latewood chronology.

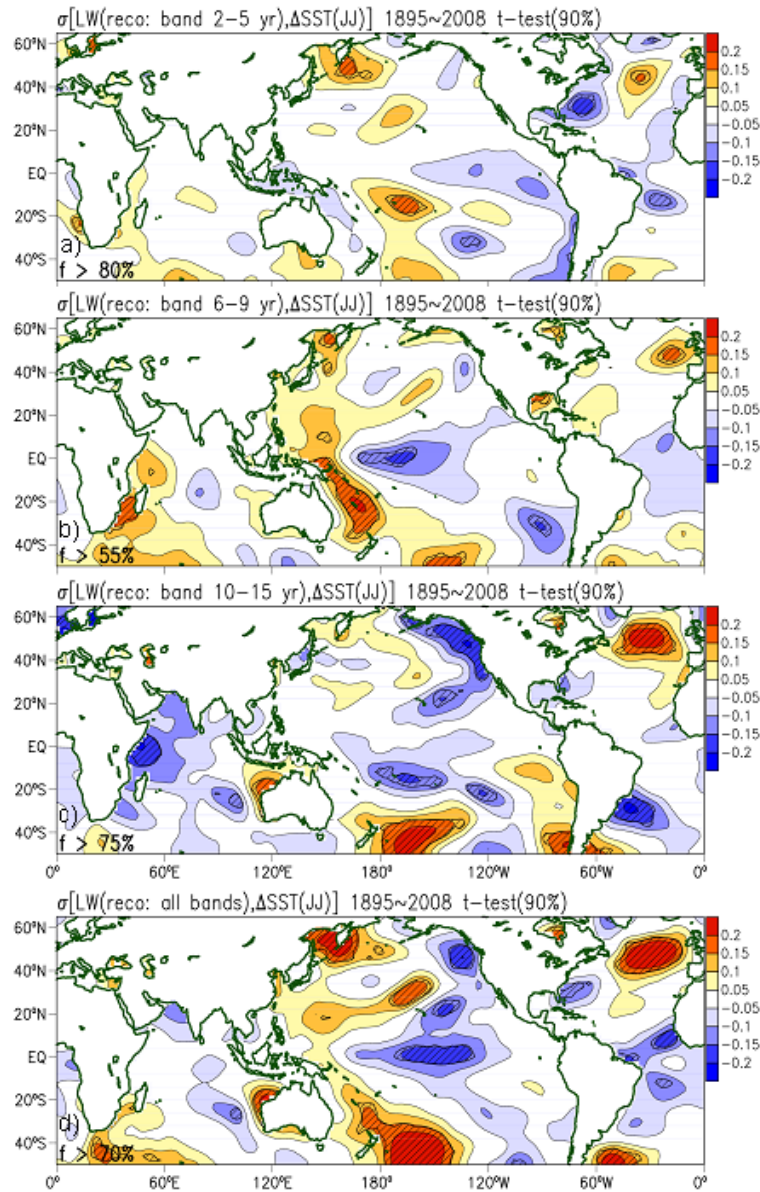


Figure 14: Spatial correlation maps between the MTM-SVD reconstructed temporal pattern of Latewood and summer sea surface temperature anomalies, JJ ΔSST , for the identified spectral bands: 2-5 year (a), 6-9 year (b), 10-15 year (c), and all modes (d). The Latewood temporal pattern was reconstructed over a site near the center of the NAME 2 zone (32.75°N; 110.25°W). Local significance at the 90% level is indicated in oblique lines and its field significance is shown in the lower left on each plot.

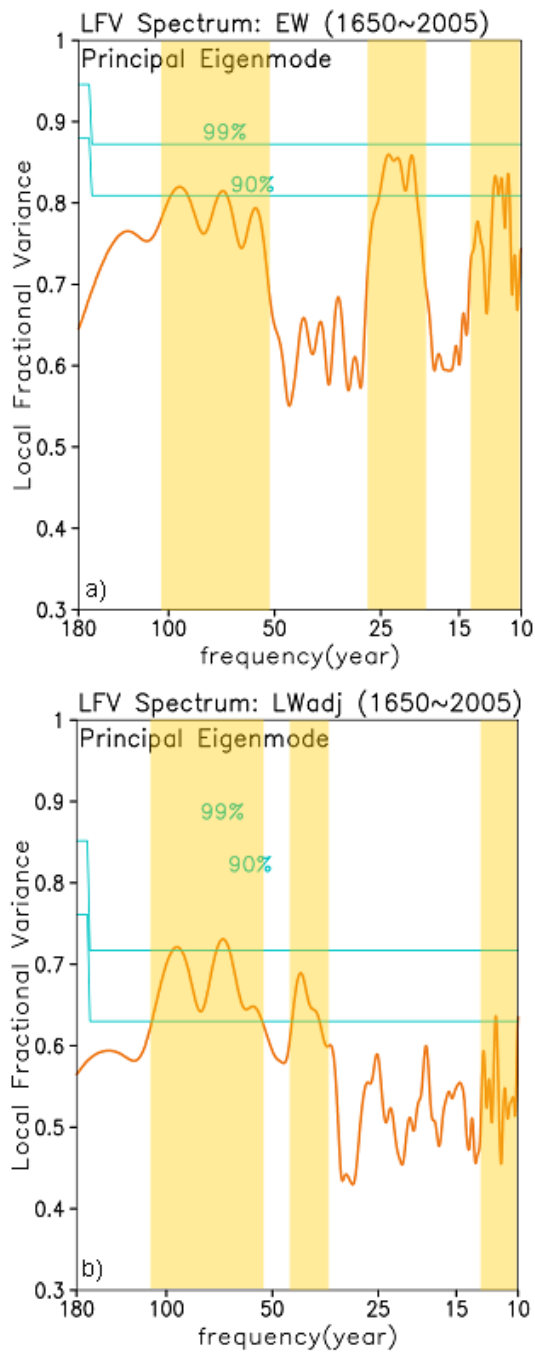


Figure 15: Power spectrum (Local Fractional Variance-LFV) of the leading mode of tree-ring chronologies obtained with MTM-SVD analysis for both earlywood (a) and latewood (b). For a tree-ring record of 360 years.

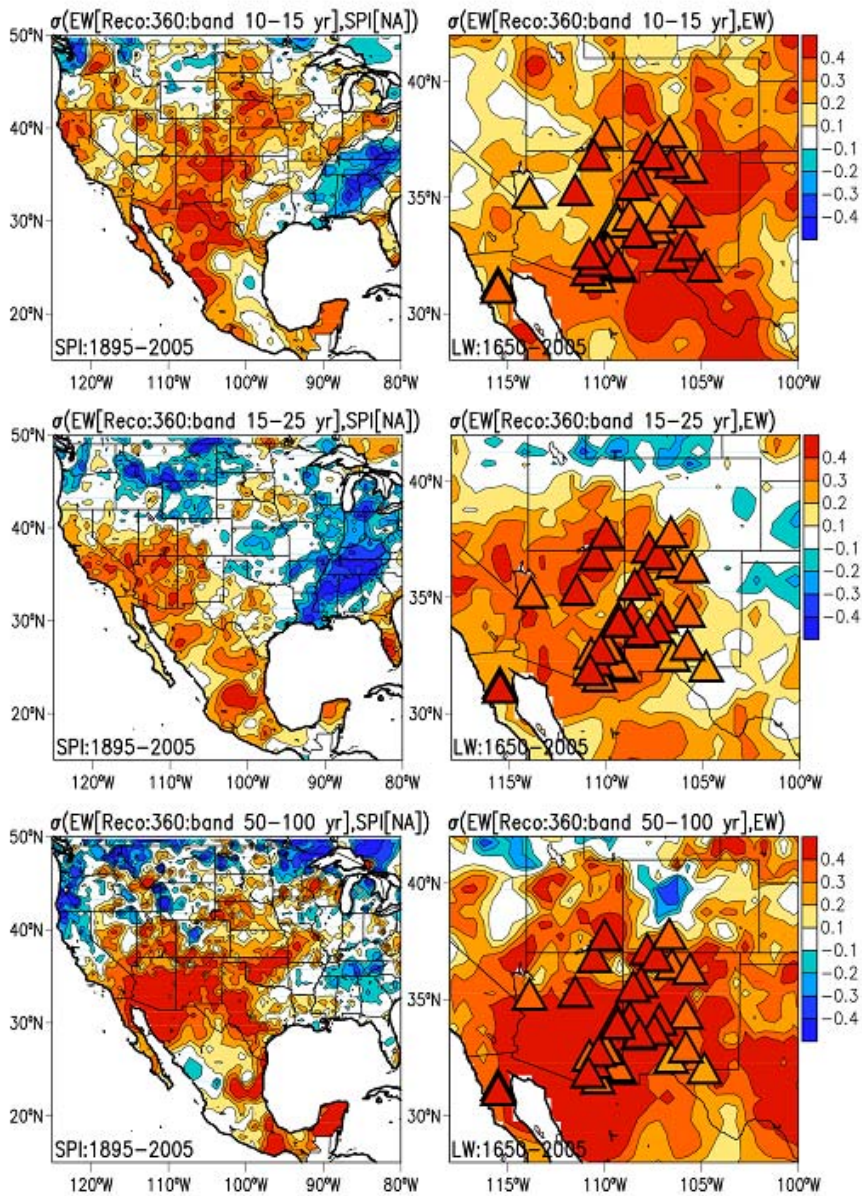


Figure 16: Left panel: spatial correlation map for the historical period (1895-2005) between winter SPI and band-pass reconstructed EW for 10-15 year (top), 15-25 year (middle), and 50-100 year (bottom). Right panel: same as right panel but for EW and band-pass reconstructed EW (1650-2005) showed inside the triangles. Results from the left panel are superimposed in right panel.

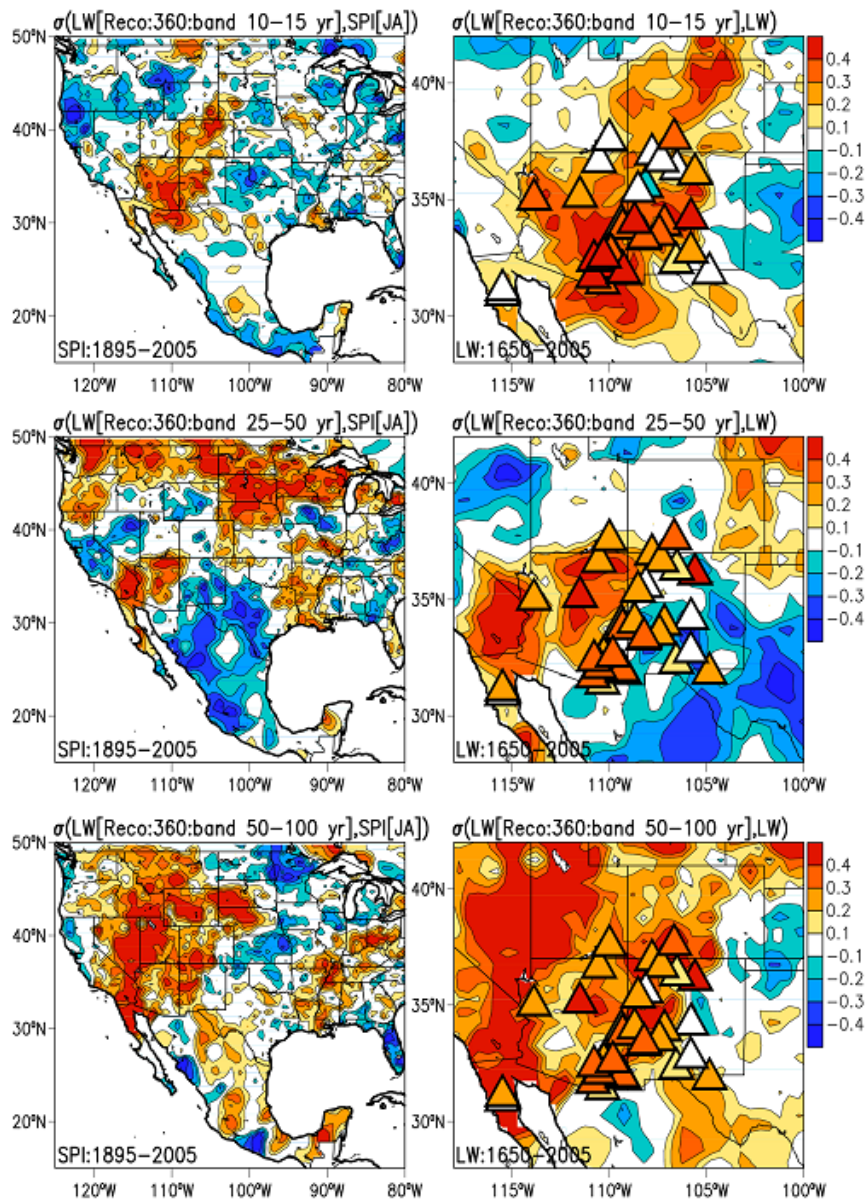


Figure 17: Same as Fig. 16 but for summer SPI and LW chronologies.

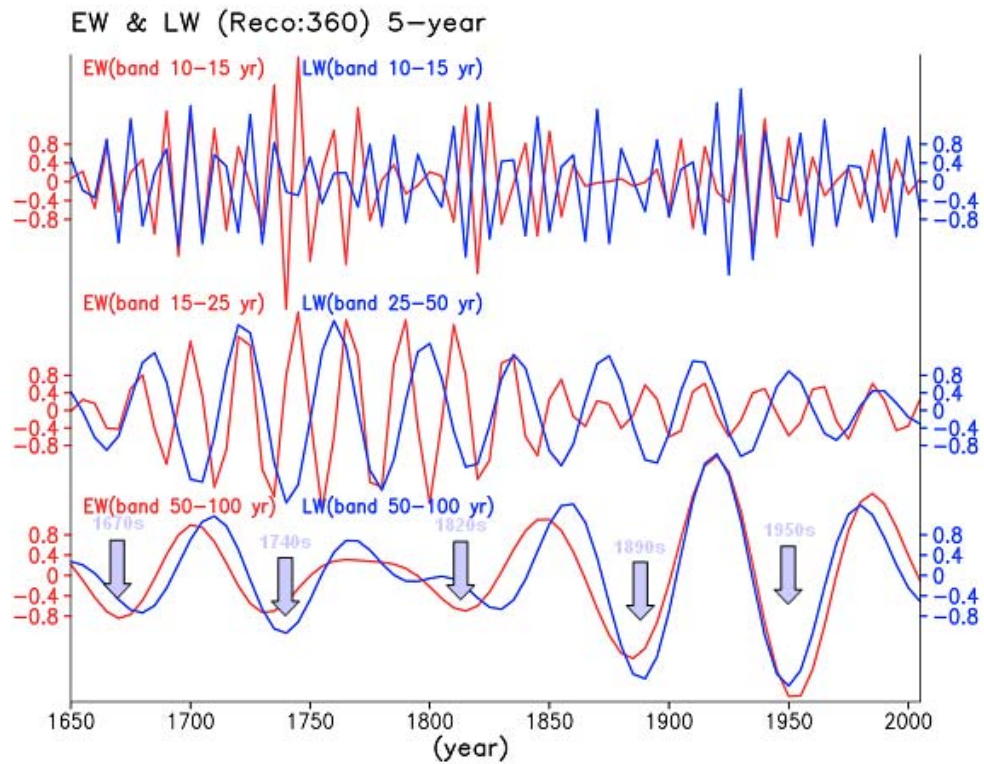


Figure 18: Time series of MTM-SVD dominant reconstructed modes for both EW in red and LW in blue. For decadal (top: 10-15 year), inter-decadal (middle: 15-25 year [EW] and 25-50 year [LW]), and centennial (bottom: 50-100 year) modes. Blue arrows indicate extreme drought event in southwestern U.S.

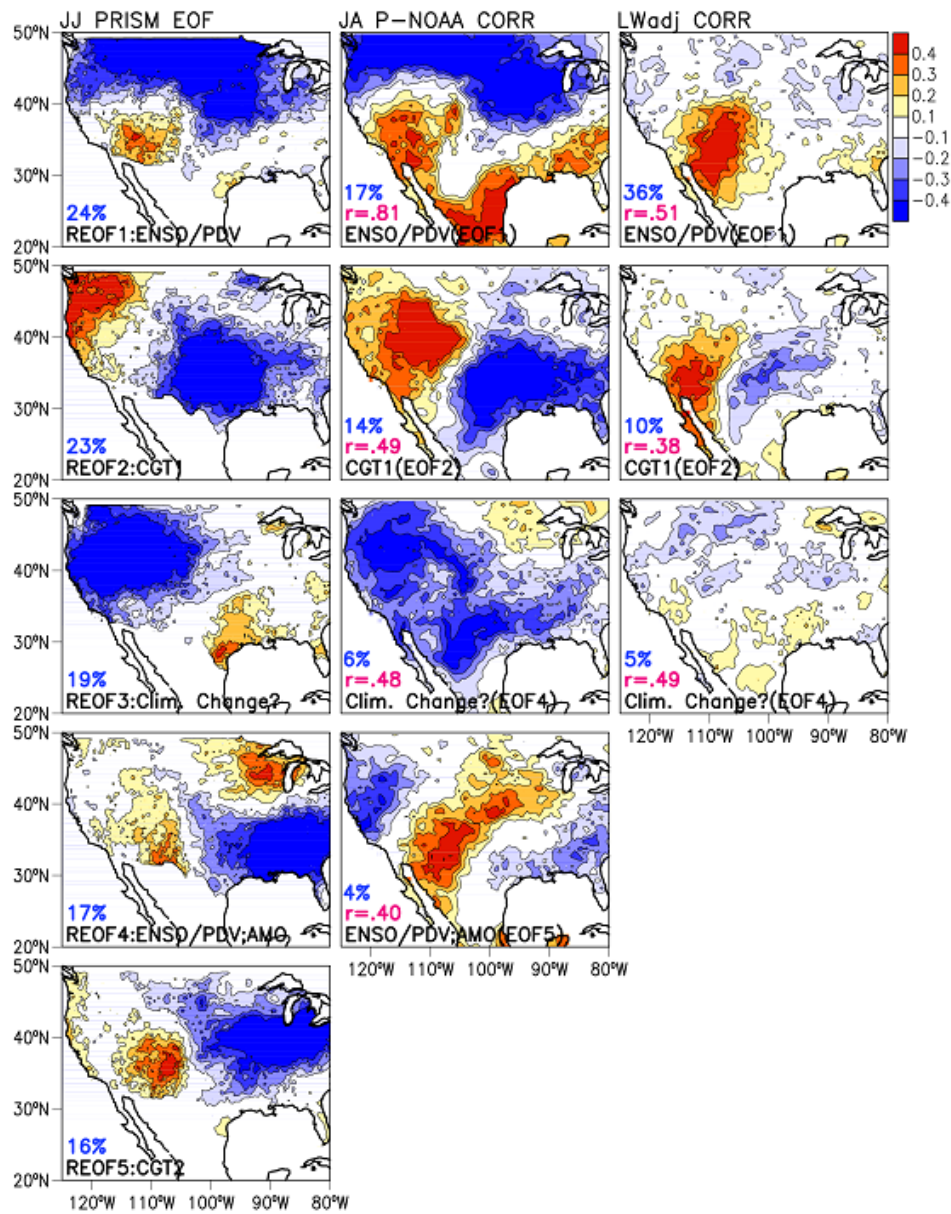


Figure 19: Left panel: JJ PRISM SPI EOF modes as in Ciancarelli et al. (2013) with its mode name labeled for each EOF. Central panel: JA P-NOAA correlation pattern obtained by correlating JA SPI temporal PCs and its gridded JA SPI. Right panel: LW_{adj} correlation pattern obtained by correlating LW_{adj} temporal PCs and gridded JA SPI. The EOF/PC explained variance for each case is indicated in blue, and the spatial correlation between PRISM EOF pattern and both P-NOAA and LW_{adj} correlation pattern for each case in magenta.

**APPENDIX B: PACIFIC SST-RELATED TELECONNECTIVE INFLUENCES
ON NORTH AMERICAN MONSOON PRECIPITATION WITHIN NORTH
AMERICAN REGIONAL CLIMATE CHANGE ASSESSMENT PROGRAM
(NARCCAP) MODELS**

Carlos M. Carrillo¹, Christopher L. Castro¹, Gregg Garfin², Hsin-I Chang¹, and Melissa S. Bukovsky³

¹ *Department of Atmospheric Sciences, the University of Arizona, Tucson, Arizona*

² *School of Natural Resources and the Environment / Institute of the Environment, the University of Arizona, Tucson, Arizona*

³ *National Center for Atmospheric Research, Boulder, Colorado*

To be submitted to *International Journal of Climatology*

Version December 7, 2014

Corresponding author address: Carlos M. Carrillo, Department of Atmospheric Sciences, University of Arizona, Physics and Atmospheric Sciences Building, Rm. 536, 1118 East Fourth Street, Tucson, Arizona 85721. E-mail: carlosc@email.arizona.edu, phone: (520) 626-6329, fax: (520) 621-6833.

Abstract

Natural climate variability over the North American monsoon (NAM) region is associated with El Niño Southern Oscillation (ENSO) and Pacific Decadal Variability (PDV). Wet and dry conditions over the southwestern U.S. are determined by atmospheric Rossby wave teleconnections driven by the ENSO-PDV, through modulation of the subtropical ridge position. Bukovsky et al. (2013) performed an in-depth analysis of the North American Regional Climate Change Assessment Program (NARCCAP) simulations over the NAM region. They found that NARCCAP regional climate models forced with reanalysis performed well but performance degrades with dynamically downscaled global climate model projections. However, the large-scale forcing mechanism was not evaluated in association with the future NAM precipitation change. This study evaluates the continental-scale patterns of warm season precipitation variability within the NARCCAP simulations. We investigated whether the known dominant mode of warm season precipitation is connected to ENSO-PDV and its associated Rossby wave teleconnection. Multivariate statistics analyses are applied on multiple sea surface temperature and precipitation datasets to determine the dominant modes of variability at a continental scale, with focus on the Southwest. Our analysis shows that NARCCAP simulations are able to portray the spatial pattern in a similar way to observations for the NARCCAP models forced by a reanalysis dataset. However, all simulations forced by fully coupled global climate models from CMIP3, except one, generally fail to reproduce this climate variability. An inevitable question that rises is how relevant is the use of the ensemble model mean. We suggest more physically-based metrics to evaluate model quality are needed in assessment of uncertainty of future climate change. Although including all possible NARCCAP model simulations increases the statistical degree of confidence, not necessary better physical reliability is achieved.

1. Introduction

How the North American monsoon System (NAMS) is going to change in the future is an important and pressing question because of its impact on severe weather and water resources (Garfin et al. 2013, Ray et al. 2007). Climate change projections, based on the global climate models (GCMs) used for the Coupled Model Intercomparison Project version 5 (CMIP5, Taylor et al. 2012), currently project a seasonal delay in NAMS. A more intense subtropical high, or monsoon ridge, leads to greater atmospheric stability and decreased precipitation in early summer (June-July). Increased precipitation in late summer occurs once the atmosphere becomes sufficiently unstable to support convection (Cook and Seager 2013). The CMIP5 NAMS projections conform to the broader paradigm of more abrupt transitions in monsoonal climates (Cook and Seager, 2013), with increased contrast between the dry and wet regimes. However, there are some caveats to this projection. It has been demonstrated that most CMIP models do not faithfully reproduce NAMS intraseasonal variability (Lin et al. 2008, Sheffield et al., 2013). Though CMIP5 models reasonably represent NAMS precipitation during the onset period in early summer, they generally overestimate precipitation during late summer (Geil et al. 2013), precisely the period that is projected to become wetter.

Regional climate models (RCMs), alternatively, may be used to dynamically downscale CMIP GCMs to generate NAMS climate change projections. The principal advantage to the use of a RCM at the scale of tens of kilometers is the value added in the representation of terrain-forced monsoon thunderstorms (Gutzler et al., 2005 and 2009; Castro et al., 2007 and 2012), as this process is not physically represented well within a GCM. Even with enhanced spatial resolution and model physics more appropriate for the

mesoscale, RCMs do not faithfully physically represent the organized propagating monsoon convection that accounts at a distance away from the mountains (e.g. Castro et al., 2012). This paper specifically considers RCM data generated as part of the North American Regional Climate Change Assessment Program (NARCCAP, Mearns et al., 2012), to be described in further detail later. Similar to the aforementioned studies, Bukovsky et al. (2013) showed that when the NARCCAP RCMs were forced with lateral boundary forcing from an atmospheric reanalysis, the climatological evolution of the NAMS is improved. Also Bukovsky et al. (2014) recently considered NARCCAP RCMs that dynamically downscaled CMIP3 data from the A2 emission scenario, to evaluate future changes in mean NAMS precipitation. Consistent with Cook and Seager (2013), they found that mean NAMS precipitation is projected to decrease, considering the ensemble of all NARCCAP RCM-GCM combinations, but that the decrease was not statistically significant. Though the NARCCAP RCMs are forced with CMIP3 GCMs, to date their projections still represent the highest spatial resolution information generated by dynamical modeling.

At least for NARCCAP RCMs, a traditional climate projection approach that equally weights all the models to generate an ensemble mean change suggests that NAM precipitation will not substantially change in the future. Such an approach implicitly favors statistical confidence based on the level of multi-model agreement, over physically-based metrics of model performance of the individual contributing models. What has been absent in the discussion of NAMS climate projections thus far is how the contributing models, whether they be GCMs or RCMs, represent known sources of natural climate variability. Should this also be considered as a physically-based metric to

evaluate model quality? How would such information bear on the projected changes in NAMS precipitation? As we have argued previously in Carrillo et al. (2014a, in preparation), consideration of natural climate variability is extremely important for real-time resource decision making at seasonal timescales and for worst-case scenarios, for example long-term drought.

Our prior work, along with others, has characterized NAMS climate variability in the context of observational analyses, and downscaled atmospheric reanalyses and a global seasonal forecast model (e.g. Castro et al., 2001; Castro et al., 2007; Castro et al., 2012; Bukovsky et al., 2013). In particular, Castro et al. (2012) showed that a downscaled global seasonal forecast model was able to statistically represent the dominant mode of early warm season precipitation in North America. This mode reflects the anti-phase relationship between precipitation in the southwestern U.S. and central U.S., related to an atmospheric teleconnection (quasi-stationary Rossby wave train) emanating from the western tropical Pacific. Variability in the El Niño Southern Oscillation and Pacific Decadal Variability (ENSO-PDV) govern the teleconnection response, such that a positive (negative) phase of ENSO-PDV during early summer is associated with wet (dry) conditions in the central U.S. and a dry and delayed (wet and early) North American monsoon. We assert that a “well performing” climate model should reasonably represent the spatial and temporal structure of this dominant mode of warm season climate variability, especially given that a very recent community assessment of CMIP5 models by Sheffield et al. (2013) has explicitly considered ENSO and PDV-driven winter precipitation variability in North America. They generally

conclude that only a relative few number of CMIP5 models are able to physically represent such variability.

This work evaluates the continental-scale patterns of warm season precipitation variability within the NARCCAP simulations, using similar objective analysis approaches that have been applied to observational data sources in our aforementioned work. Our main research question of interest is: Is the known dominant mode of early warm season climate variability, and its connection to ENSO-PDV, reasonably represented each component NARCCAP RCM? More broadly, is it appropriate to consider natural climate variability as an additional metric to assess physical uncertainty in NARCCAP model-generated climate projections?

This paper is organized as follows. The methodology and datasets are described in section 2. A review of the climatological behavior of NARCCAP simulation during the warm season is presented in section 3. The warm season SST variability in NARCCAP AOGCMs is described in section 4. The impact of spectral nudging in representing ENSO-PDV warm season precipitation in Phase I NARCCAP simulations is explained in section 5. The ENSO-PDV warm season precipitation response in Phase II NARCCAP RCMS is described in section 6. Concluding points and discussion are presented in section 7.

2. Methodology and datasets

2.1 NARCCAP models

We use regional climate model simulations generated as part of the North American Regional Climate Change Assessment Program (NARCCAP; Mearns et al., 2012), because these data reflect the most comprehensive research effort to date to

generate dynamically downscaled climate projections using multiple global and regional atmospheric models. A summary of NARCCAP model simulations used in this study is shown in Tables 1 and 2. Phase I NARCCAP simulations force six RCMs with NCEP-NCAR Reanalysis 2 (Kanamitsu et al. 2002) boundary conditions during the historical period 1979-2003 to assess RCM sensitivity with “perfect” observed analysis conditions. Phase II simulations use boundary conditions from four different fully coupled atmosphere-ocean global climate models (AOGCMs) from the Coupled Model Intercomparison Project (CMIP3) that are forced by the A2 greenhouse gas emission scenario (Community Climate System Model [CCSM], Third Generation Coupled Global Climate Model [CGCM], Geophysical Fluid Dynamics Laboratory GCM [GFDL], and Hadley Centre Coupled Model version 3 [HadCM3]). There are two periods of simulation, a twentieth century historical (1971-2000) and a twenty-first century climate change period (2038-2070). Eight of the twelve possible AOGCM-RCM combinations were generated (Table 3) with a grid spacing of 50 km. Additional NARCCAP experiments force some of the GCMs with observed sea surface temperatures, as described in Bukovsky et al. (2013), but are not considered here.

In considering how the NARCCAP models represent natural climate variability, it is important to note that two (CRCM and ECP2) of the participating RCMs utilize spectral nudging in both NARCCAP Phases I and II (Mearns et al., 2012). The spectral nudging approach may be advantageous because it preserves the properties of the synoptic-scale circulation of the driving atmospheric reanalysis or AOGCM (Castro et al., 2005 and 2012). When specifically considering NARCCAP Phase I experiments, the spectrally nudged RCMs generally outperform the non-spectrally nudged models with

respect to the representation of the mean climate (Mearns et al., 2012; Bukovsky et al., 2013).

2.2 NARCCAP warm season precipitation

This study considers NARCCAP RCM-generated precipitation during the period of July-August, as the majority of North American monsoon-related precipitation occurs during this time. Precipitation from each RCM is interpolated to a common grid of 0.5° because of the different model grid projections used (Mearns et al., 2012). To consider interannual variability, gridded JA precipitation is converted to a two-month standardized precipitation index (SPI; McKee et al. 1993), following the identical procedures we have used in prior analysis of gridded precipitation products in North America (Castro et al. 2009; Ciancarelli et al. 2013). The gamma distribution of precipitation for SPI computation of NARCCAP Phase II data is obtained independently for the twentieth and twenty-first centuries. Ciancarelli et al. (2013) showed that the dominant spatial modes of warm-season SPI in North America derived from PRISM precipitation data (PRISM Climate Group, 2004) are tied to distinct large-scale atmospheric teleconnections, or quasi-stationary Rossby wave trains. We consider equivalent observed precipitation obtained from a new NOAA precipitation (P-NOAA) product that covers the entire U.S. and Mexico, provided by Dr. Russ Vose. P-NOAA incorporates a terrain interpolation function similar to PRISM. We utilized the P-NOAA precipitation data previously in the evaluation of dynamically downscaled data from the Climate Forecast System (CFS) model, Version 1, reforecast (Castro et al. 2012).

Observed and GCM-derived sea surface temperature is considered only for the early summer (JJ). The main reason for the slight lead in time for SSTs is because of the

relative stronger influence of ENSO-PDV variability on North American warm season precipitation in early summer (Castro et al., 2001). Our guiding premise is that NARCCAP CMIP3 models may have a reasonable representation of the ENSO-PDV forced atmospheric teleconnection response, in reference to what we previously found considering a global atmospheric reanalysis (Ciancarelli et al. 2013). The level of correspondence in the warm season atmospheric teleconnection response may be used as a subjective physically-based measure of NARCCAP model quality. Observed SST is obtained from the two-degree NOAA Extended Reconstructed SST dataset (Smith et al., 2008)

2.3 Dominant spatial modes of variability

Dominant spatial modes of variability JA SPI and JJ SST are determined using two complementary statistical analysis tools. As in Ciancarelli et al. (2013), we apply empirical orthogonal function, principal component analysis (e.g. Wilks, 2006). The dominant principal component (PC) of SPI can be regressed onto 500-mb height and sea surface temperature anomalies, to reveal atmospheric teleconnection patterns and their relationship to SST. Where point source correlation is determined, local significance is determined by a t-test and field significance is determined by a Monte Carlo technique consistent with Livezey and Chen (1983) using 500 iterations. To isolate significant temporal variability in the dominant mode, we apply a multiple taper method (MTM) spectrum. MTM attempts to maximize both spectral resolution and variance by use of a Slepian taper to the data (Mann and Lees 1996). MTM toolkit for spectral analysis was taken from the Theoretical Climate Dynamic group at the University of California, Los

Angeles. The MTM toolkit is explained in further details in Ghil et al. (2002), and can be access at <http://web.atmos.ucla.edu/tcd//ssa/>.

Multi-taper method singular value decomposition (MTM-SVD) is a multivariate method that uses spectral and spatial disaggregation simultaneously. Low-frequency signals are enhanced by applying multiple Slepian data tapers. Conceptually, MTM-SVD first transforms time-space data to spectral domain and then finds dominant spatio-temporal variability by solving a complex eigenvalue problem. The three main outputs of MTM-SVD analysis are: 1) the local fractional variance (LFV) spectrum, similar to a power spectrum of a time series of point source data but applicable to the entire spatial domain, which statistical significance of spectral peaks are assessed by bootstrap resampling (Rajagopalan et al., 1998); 2) the reconstruction time series, determined typically for the specific spectral bands that are statistically significant; 3) the phase pattern map, which provides the phasing information for a spatial pattern in a given frequency band with respect to a designated reference point in the domain and can be shown as a vector plot. In Castro et al. (2009) we applied MTM-SVD in North America during the warm season to gridded observed precipitation (SPI), soil moisture (from National Land Data Assimilation System), and satellite derived normalized difference vegetation index (NDVI). Significant temporal variability in all of these fields was found at interannual to decadal timescales, corresponding to ENSO-PDV forced climate variability. Here, we essentially want to know if similar behavior exists within the NARCCAP AOGCMs and RCMs.

3. Review of climatological behavior of NARCCAP models during the warm season

The climatological behavior of Phase I and II NARCCAP models with respect to their representation of the NAMS during the warm season (JJAS) has been previously evaluated by Bukovsky et al. (2013). Considering the RCMs in the Phase I experiments, these generally showed a salient NAMS in the core region, with a rapid increase in precipitation in early summer and seasonal peak in rainfall in late July and August. However, Arizona was noted as a geographic area that exhibits a dry precipitation bias due to inadequate low-level moisture transport from the Gulf of California. The Phase II NARCCAP RCM simulations do not represent the NAMS well during the twentieth century historical period, in terms of the timing and amount of monsoon precipitation, and there is considerable variation in performance among the various RCM-GCM combinations. The most well-performing NARCCAP Phase II models, by the metrics of NAMS precipitation timing and amount, are CRCM[cgcm3], RCM3[cgcm3], WRF3[cgcm3], and HRM3[hadcm3]. The RCMs that utilized GFDL boundary forcing were by far the worst performing and comparatively a major outlier to other Phase II RCMs simulations, with summer monthly precipitation amounts exceeding observed values by a factor of two to three.

Before we consider the performance of the NARCCAP models with respect to their representation of year-to-year climate variability, we first briefly revisit some aspects of their climatological performance that augment what has already been done by Bukovsky et al. (2013). The most critical issue for the NAMS region is the representation of the annual cycle of precipitation, and this is also true when considering the CMIP3 and CMIP5 models directly (Geil et al., 2013). Figure 1 (left panels) shows the monthly

mean precipitation in the NAMS 2 region (Gochis et al., 2009) during the historical and climate change projection periods for all NARCCAP Phase II RCMs. Corresponding P-NOAA observations are shown in the light blue histogram on the top left panel. The observed precipitation shows an abrupt jump from 0.3 mm day^{-1} in June to 1.6 mm day^{-1} in July. Considering the ensemble mean of all NARCCAP Phase II RCMs (thick red line), this abrupt precipitation transition is absent. Removing the four NARCCAP RCMs that have the largest precipitation biases yields a more physically reasonable result, as shown on the right of Figure 1. The better performing NARCCAP RCMs are those forced by CGCM3 and HadCM3 while the poorer performing RCMs are those forced by GFDL and CCSM. This performance evaluation is in concurrence with Bukovsky et al. (2013). However, even the four better performing NARCCAP RCMs do not accurately represent monsoon onset and retreat. Only CRCM-CGCM3 and HRM3-HadCM3 are able to do this. The climatological performance of the NARCCAP RCMs also does not substantially change from the historical to future period (bottom panels of Figure 1). As previously stated, we use JA as our period of analysis for consideration of year-to-year climate variability in the following subsections because monsoon precipitation is maximized at this time and ENSO-PDV is known to significantly influence monsoon precipitation during the onset period in July. Our guiding supposition in the proceeding analyses is that the NARCCAP Phase II models which have the best representation of the NAMS climatology would also have the best representation of year-to-year climate variability.

The spatial distribution of JA precipitation for all eight Phase II NARCCAP models during the historical and future periods, along with the difference, is shown in

Figure 2. These precipitation maps confirm that there is a wide variation in the climatological representation of the NAMS in these RCMs, with some models generating little to no monsoon precipitation at all. As shown by Bukovsky et al. (2013), the ensemble mean difference of Phase II NARCCAP RCMs exhibits little to no change in NAMS precipitation with a low level of confidence due to the lack of model agreement. However, the NARCCAP RCMs that have the best NAMS precipitation climatology (CRCM-CGCM3 and HRM-HadCM3) also show the largest projected decreases in monsoon precipitation during JA. The results from these two particular NARCCAP models are actually the most consistent with recent NAMS projections from CMIP5 models (Cook and Seager, 2013), which as a whole improve the climatological representation of the NAMS in comparison to CMIP3 models.

To further illustrate the spread in NAMS precipitation projections in the NARCCAP models and the potential impact of distinguishing models by their physical performance, Figure 3 shows the JA mean precipitation for NAMS precipitation region 2 (Arizona) for the historical and future periods (yellow and red bars, respectively). The three models that project wetter conditions are highlighted in dark blue and the five models that project drier conditions are highlighted in light blue. Error bars at the top of the histogram are one standard deviation about the mean, as an indication of the degree of spread in the data. The models which project wetter conditions in the future are those with the least faithful climatological representation of the NAMS, forced by GFDL and CCSM. Inclusion of these models in the ensemble mean projection causes the NAMS precipitation change to be negligible. However, if just those models with the best climatological representation of the NAMS are considered (HRM3-HadCM3 and CRCM-

CGCM3), then there is a projected decrease in NAMS precipitation that exceeds one standard deviation in both models. Thus, applying some basic physical performance metrics of NAMS behavior to the NARCCAP models may have substantial bearing on the degree of statistical confidence of a projected climate change.

Dominance of boundary forcing on NARCCAP interannual climate variability

Bukovsky et al. (2013) also have previously noted that the sign of projected precipitation changes in the NARCCAP Phase II RCMs is largely consistent with that of the driving AOGCM. To further illustrate the influence of the driving AOGCM on the RCM solutions we consider the time evolution of the NARCCAP RCM simulated SPI for the historical and future periods in Figure 4 for the NAME 2 precipitation region. RCM SPI solutions are grouped according to their parent driving AOGCM. As these are each free running, coupled AOGCMs with their own unique representations of natural climate variability, we do not expect any deterministic correspondence of the SPI time series when comparing NARCCAP RCM simulations forced by different AOGCMs. When comparing RCMs driven by the same parent AOGCM, the SPI time series are always statistically significantly correlated at the 90% level or above in both periods (correlation coefficients shown on plot). The interannual variability of the NARCCAP RCM precipitation solution is largely a slave to the large-scale atmospheric circulation of the driving AOGCM. This is the case irrespective of whether or not spectral nudging is applied to the RCM. We submit that a “well performing” AOGCM-RCM system should reasonably represent the spatial structure of known atmospheric teleconnection patterns and their continental-scale precipitation responses. We reached basically the same

conclusion in our previous consideration of dynamically downscaled global seasonal forecast model data in Castro et al. (2012).

4. Warm season SST variability in NARCCAP AOGCMs

Given that interannual variability of NARCCAP RCM precipitation substantially depends on the imposed boundary forcing from a reanalysis or AOGCM, we consider how each of the four NARCCAP Phase II AOGCMs represent interannual variability in global SSTA in comparison to observations. Figure 5 shows the leading EOF of JJ SSTA (right) and the corresponding MTM spectrum of the principal component. The spatial pattern of the leading mode of observed JJ SSTA shows a clear ENSO-PDV signal (top of Fig. 5) with maxima in spatial loading in the eastern tropical Pacific and central North Pacific. This leading mode has statistically significant temporal variability at a typical ENSO timescale of 3-5 years. Additional, but not statistically significant peaks in the MTM spectrum occur between approximately 6-9 years and 12-16 years. All of the NARCCAP AOGCMs have at least some representation of ENSO variability in their corresponding dominant mode. HadCM3 and GFDL appear to have the better representations, with statistically significant peaks in their MTM spectra at a reasonable ENSO timescale of approximately 3-7 years. CCSM incorrectly represents ENSO as a biennial cycle, a problem that has been previously documented in the literature (Hu et al., 2012). CGCM3 has relatively low spatial loading in the eastern tropical Pacific, though the mode peaks at a timescale of 5 years.

A limitation of EOF analysis of global SSTA is that ENSO-PDV variability may be present in more than one dominant mode. We apply MTM-SVD to specifically isolate

ENSO and PDV-related signals at their known timescales of temporal variability. The MTM-SVD analysis of observed SSTA is shown in Fig. 6. Consistent with other analyses of observed global SSTA, statistically significant temporal variability is mostly present in two bands, an ENSO band (2-6 years) and a decadal band (greater than ten years), as highlighted on the LFV spectrum at the top of the figure. As the analysis period considered here is limited to fifty years, the lowest possible resolvable frequency is 25 years. Figs. 6c and 6d shown of both the SSTA patterns associated with these two frequency bands, reference to a grid point in the eastern tropical Pacific (center of the Niño 3.4 region). These reconstructed SSTA pattern maps show a clear distinction between ENSO and PDV signatures in the Pacific Ocean, as compared to just consideration of the dominant EOF in Fig. 5a. Also of note in the reconstructed decadal band is the presence of statistically significant variability in the Atlantic basin, which suggests the Atlantic Multidecadal Oscillation (AMO). The combination of both interannual and decadal SSTA bands is shown in Fig. 6a, revealing the combined ENSO-PDV SSTA signature similar to that of Castro et al. (2007), their Figure 4.

MTM-SVD analysis is similarly applied to global SSTA for the NARCCAP AOGCMs for the historical and future climate periods in Figs. 7 and 8. The number of years considered in these analyses is more than the period of simulation of the NARCCAP RCMs. We use 40-50 year periods as denoted on the figure to resolve any possible statistically significant decadal variability. None of these four AOGCMs have significant temporal variability in their LFV spectra, shown by the yellow bars, beyond a timescale of 10 years. Generally speaking, the only significant SSTA variability in these four CMIP3 models is associated with ENSO, similar to what has been found in prior

studies (Sheffield et al., 2013). For that reason, the figures of reconstructed SSTA patterns associated with significant temporal variability are not so substantially different from the EOF dominant modes presented earlier in Fig. 5. HadCM3 and GFDL both show significant temporal variability in JJ SSTA at an ENSO timescale. The reconstructed SSTA patterns in the 2-6 year bands for these models show a well-defined ENSO signal in the eastern equatorial Pacific. Though CGCM3 and CCSM also have ENSO signals, these occur at a higher frequency and the SSTA signature in the eastern equatorial Pacific is comparatively less extensive. CCSM incorrectly represents ENSO as a biennial oscillation, consistent with the EOF analysis, as has been previously documented (Hu et al., 2012). For the future period, only HadCM3 and GFDL retain significant ENSO-related SSTA variability. There is not statistically significant spatiotemporal variability in SSTA for CGCM3 and CCSM in the future period, though reconstructed SSTA is shown for the bands that were significant in the historical period. HadCM3 shifts ENSO variability to a slightly longer timescale (6-10 years). From these analyses, we conclude that only HadCM3 and GFDL models have reasonable representations of ENSO variability, in terms of frequency and spatial distributions of SSTA. These models also retain ENSO as a statistically identifiable feature proceeding into the future.

Warm season atmospheric teleconnections

The next step in assessment of NARCCAP AOGCMs with respect to their representation of warm season climate variability is the examination of atmospheric teleconnection patterns. Fig. 9 shows the regression of ENSO-PDV associated SSTA on JA 500-mb geopotential height anomalies in a band of 2-6 years and greater than 10

years, according to the significant bands in the LFV spectrum of observed SSTA. Consistent with our previous work (Castro et al. 2007; Ciancarelli et al. 2013) there is the signature of a quasi-stationary Rossby wave train emanating from the western tropical Pacific that affects the large-scale atmospheric circulation pattern over North America. The spatial structure of the teleconnection does not appear unique to either of significant temporal bands. The regressed patterns are field significant at the 95% level or above.

The equivalent results during the historical period for the four NARCCAP AOGCMs, for just the 2-6 year band, are shown in Fig. 10 and their pattern correlation with the observed map in Fig. 9 is shown in Table 4. Only two of the NARCCAP AOGCMs have field significant regression of 500-mb height anomalies that statistically compare well to observations. Not surprisingly, these two models are HadCM3 and GFDL, as these two models have the best representations of ENSO SST variability. CGCM3 and CCSM do not exhibit atmospheric teleconnective structures that are field significant. The future period yields similar results, as shown in Fig. 11 and Table 4. The teleconnection in HadCM3 tends to have a weaker statistical relationship to that of the atmospheric reanalysis as compared to GFDL, but is still statistically significant. It is worth noting that we are just considering the warm season atmospheric teleconnections that are associated with ENSO in these AOGCMs, since that is the dominant control on the year-to-year early warm season precipitation variability. We acknowledge that there are higher order warm season teleconnection responses, namely the Circumglobal Teleconnection (CGT; Ciancarelli et al. 2013, Ding and Wang, 2005; Ding et al., 2011), but these likely arise as free stochastic modes. Though these other modes are important as well, they are not considered in this work.

5. Impact of spectral nudging in representing ENSO-PDV warm season precipitation response in Phase I NARCCAP models.

The observed spatial structure of precipitation anomalies associated with ENSO-PDV is determined by regressing SSTA in the significant spectral bands from MTM-SVD analysis. The regressed patterns shown in Fig. 12 reveal the expected antiphase relationship between precipitation in the Southwest and the regions of the central U.S. and northern Rockies. There is also a statistically significant relationship to precipitation in the Southeast U.S. These precipitation patterns are very similar to the dominant mode of early warm season precipitation in the U.S. found by Ciancarelli et al. (2013), their Figures 2 and 3. Note that we choose to orient the maps to reflect a negative phase of ENSO-PDV, with positive precipitation anomalies in the Southwest.

A reasonable expectation would be that the Phase I NARCCAP RCMs are able to reasonably reproduce this dominant spatial pattern of precipitation variability, since they are forced with “perfect” boundary conditions from an atmospheric reanalysis. We have already demonstrated, by dynamically downscaling the NCEP-NCAR reanalysis with the Regional Atmospheric Modeling System (RAMS) for a 50-year period, that this mode can be well reproduced in a RCM simulation (Castro et al. 2007). Given the fact that our previous RAMS model simulations utilized internal nudging, as motivated by findings in Castro et al. (2005) and Rockel et al. (2008), it is also reasonable to assume that those NARCCAP phase I RCMs that incorporate spectral nudging would have the best representation of year-to-year precipitation variability. Mearns et al. (2012) reported that the spectrally nudged Phase I NARCCAP RCMs have the lowest root mean square error when compared with observed precipitation. The two NARCCAP RCMs that incorporate

spectral nudging are CRCM and ECP2. Fig. 13 shows the correlation maps between ENSO and PDV associated SST and RCM-generated JA SPI, in the identical manner as done for observed precipitation in Fig. 12. Results combining ENSO-PDV are shown in Fig. 14. The spatial correlation (r) from these model generated precipitation results to the corresponding observed precipitation result is included on each plot. A value of r that exceeds 0.3 is considered statistically significant at the 90% level or above, given the sample size of the data.

For the ENSO band, the spectrally nudged models yield the closest result to the observed precipitation pattern, with $r = 0.54$ for CRCM and $r = 0.36$ for ECP2. HRM3 ($r = 0.3$) also exhibits significant pattern correlation. For the PDV band, the pattern correlations in WRFG ($r = 0.33$) and CRCM ($r = 0.36$) are statistically significant, with ECP2 and MM5 being the next best ($r = 0.24$). There may be two reasons why the PDV-associated precipitation pattern has generally less of a correspondence with observations. The observed pattern has relatively high spatial loading in the Great Plains (Fig. 12b), and RCMs generally have a problem in representing organized, propagating convection there (Castro et al., 2012). The length of record considered also may not be long enough to robustly assess decadal variability. In any case, those models which are not spectrally nudged generally present a lower correspondence with observed precipitation patterns associated with ENSO-PDV variability in the warm season (combined mode shown in Fig. 14). If spectral nudging is not included, RCMs will not be able to reproduce as well the observed, continental-scale spatial patterns of precipitation variability that are driven by atmospheric teleconnection responses.

6. ENSO-PDV warm season precipitation response in Phase II NARCCAP RCMs

The relatively short period of the NARCCAP Phase II RCM data limits the range of observable frequencies when considering year-to-year precipitation variability. Decadal variability is not temporally well resolved in a thirty year period and none of the NARCCAP GCMs exhibited significant SST variability at the decadal timescale. For these two reasons, we only can consider the relationship of Phase II NARCCAP RCM-generated precipitation within the temporally significant ENSO-related band in the general range of 2-6 years (with some minor variation therein among the models). We repeat the same type of analysis as in the previous section, regressing Phase II NARCCAP model simulated JA SPI on ENSO-band associated SSTA from MTM-SVD analysis in Section 3.3. The regressed SPI patterns for all Phase II NARCCAP RCMs are shown in Fig. 15 along with the pattern correlation (r) with the equivalent observed precipitation pattern as shown in Fig. 12a. The pattern correlations for Phase II NARCCAP RCMs, overall, are generally lower than what we found for the Phase I RCMs, and this is to be expected since the Phase I RCMs utilize “perfect” reanalysis boundary forcing. Considering first the historical period, the best performing model by the metric of pattern correlation is HRM3-HadCM3 ($r = 0.38$), and this value of pattern correlation actually slightly exceeds the equivalent Phase I NARCCAP RCM ($r = 0.3$). This is the only exception to the aforementioned general behavior of the pattern correlation in Phase II NARCCAP results. All of the other NARCCAP Phase II models in the historical period are not able to reproduce the spatial pattern of JA precipitation anomalies associated with ENSO variability. RCM3-CGCM3 does capture the nature of the antiphase relationship in precipitation between the southwest U.S. and the regions of

the Great Plains and Northern Rockies, but incorrectly represent the phasing of the precipitation anomaly in the Southeast. The worst performing model by the pattern correlation metric is CRCM-CCSM ($r = -0.33$), which has totally opposite phase of precipitation anomalies to the observed pattern and therefore a statistically significant, but negative value.

We attribute the good performance of HRM-HadCM3 with respect to its representation of warm season precipitation variability the fact that: 1) the driving AOGCM HadCM3 has a reasonable representation of the ENSO warm season atmospheric teleconnection response and 2) HRM-HadCM3 has one of the best climatological representations of the NAMS. For the future period, recall that only two of the NARCCAP Phase II AOGCMs are able to simulate significant temporal variability SST at the ENSO timescale (HadCM3 and GFDL). If just the RCMs which utilize these two GCMs as boundary forcing are considered, HadCM3-HRM3 retains the highest pattern correlation ($r = 0.25$). Though the value of the pattern correlation exceeds 0.3 for CRCM-CGCM3 and RCM3-CGCM3, the driving CGCM3 AOGCM does not exhibit any significant ENSO-related SST variability and does not capture the associated warm season atmospheric teleconnection response. Though these two RCMs do capture the spatial pattern of the ENSO-related precipitation response at least from the standpoint of statistical correspondence, they do so with incorrect underlying physics that would cause the response, at least as we presently understand that within the observed instrumental record.

7. Concluding points and discussion

This work has evaluated whether or not NARCCAP models can reasonably represent the continental-scale pattern of North American monsoon precipitation variability associated with ENSO-PDV. Per previous studies of the observational record, this pattern is basically the anti-phase relationship in precipitation between the southwest U.S. and Central U.S. that is dominant in the early part of the warm season. NARCCAP Phase I models with imposed reanalysis boundary forcing can represent it in a manner that similar to observations, consistent with our previous findings considering a dynamically downscaled 50-year retrospective reanalysis (Castro et al. 2007). However, when Phase II NARCCAP models are considered with boundary forcing imposed from CMIP3 GCMs only one of them (HRM3-HadCM3) is able to satisfy this condition. This particular NARCCAP model simulation exhibits a correct pattern and phasing of precipitation anomalies and a statistically significant atmospheric teleconnection that has a clear tie to Pacific SST forcing, in both the historical climate and climate change projection periods. HRM3-HadCM3 is also one of the most well performing Phase II models with respect to the climatology of warm season precipitation, in accordance with our hypothesis posed in Section 2.

Generally speaking, NARCCAP Phase I models are able to better represent the influence of large-scale atmospheric teleconnections in the warm season when spectral nudging in the RCM is applied. The nudging ensures that the structure of the large-scale, or synoptic-scale, atmospheric circulation as it exists in the driving GCM is preserved, especially and including the teleconnective structures. It also ensures that there is still added value on mesoscale by a better representation of diurnally-generated convective

precipitation. Even if spectral nudging is applied for a Phase II model, if the known dominant atmospheric teleconnections that drive warm season precipitation are absent in that driving GCM, there would be absolutely no hope of representing the associated continental-scale precipitation response in any RCM. We basically came to the same conclusion in Castro et al. (2012) with respect to dynamically downscaled warm season seasonal forecasts from the Climate Forecast System model. Though we are considering free-running, fully coupled atmosphere-ocean global climate models in the case of CMIP3, the paradigm is essentially the same.

We have suggested in this work that an appropriate standard for a “well performing” NARCCAP Phase II model for North American monsoon is that the model simulations have a reasonable representation of warm season precipitation climatology and year-to-year variability driven by natural climate variability. Again, only HRM3-HadCM3 mostly satisfies these criteria by the analysis presented here. With respect to the latter criterion, let us presuppose that CMIP3 models should be expected to at least represent ENSO and its associated atmospheric teleconnection responses, but probably not the other coupled ocean-atmosphere modes that vary on decadal timescales (PDO, AMO). These expectations would conform to recent overviews of CMIP5 performance in North America (Sheffield et al. 2013). In our case, only two of the four NARCCAP CMIP3 GCMs meet this condition (GFDL and HadCM3). But the errors in the climatological representation of warm season precipitation in the Phase II NARCCAP RCMs with GFDL imposed boundary forcing are quite large relative to the NARCCAP RCMs forced with the other three GCMs and observations. In our own experience working with water resource providers in Arizona, we have concluded it is problematic to

use the GFDL-forced RCMs in a climate change impacts assessment, as they simulate more than twice the normal amount of monsoon precipitation and it erroneously occurs mostly during September (Shamir et al., 2014).

NARCCAP does provide a unique source of dynamically downscaled climate change projection data from an ensemble of models. As it represents the best presently available, community generated source of such information in North America, it has been employed to estimate changes in mean climate in North America in the context of regional climate change assessments (e.g. Garfin et al. 2013). We do not disagree with the well established paradigm that a multimodel ensemble approach is necessary to robustly characterize statistical uncertainty. However, we question the notion that adding more models to ensemble mean projections should be done because this helps “cancel out” the errors among models due to their varying representations of natural variability and parameterized physics (Pierce et al., 2009). If we do so, a more statistically confident climate change projection can be achieved, but it may not be based on models with robust physical performance. It is even more important to establish a well-defined standard of physical performance in dynamically downscaled climate change projections, since overarching purpose of the dynamical downscaling is to add value with respect to mesoscale meteorological processes that are more dependent on the surface boundary conditions, like convective precipitation. If RCM-GCM combinations are ultimately shown to be physically unreasonable, then why proceed with considering them as part of a model ensemble within climate change impacts assessment analyses? In the case of North American monsoon precipitation, Bukovsky et al. (2013) established that there is little statistical confidence in projected changes in North American monsoon

precipitation, based on the level of model agreement. We would add that from the work presented here that there is low physical confidence in these projected changes as well, because the wide variation in Phase II results is attributable in great part to an inadequate representation of the warm season precipitation climatology and natural climate variability (ENSO-PDV). We acknowledge that our conclusion is somewhat disconcerting from the perspective of climate change impacts assessment for the southwest U.S., given the pressing need for more confident North American monsoon climate projections. We also would emphasize it is not universally applicable across the entire NARCCAP simulation domain. Areas of the western United States that are not influenced by North American monsoon precipitation exhibit a much greater level of model agreement with respect to projected decreases in warm season precipitation.

It may be possible to differentially weight GCMs or RCMs, using physically based metrics, prior to constructing the ensemble mean climate projection. In the case of North American monsoon precipitation simulated by NARCCAP GCM-RCM model combinations, the historical performance of HRM-HadCM3 far exceeds that of the other NARCCAP combinations—which would limit the value of weighting. We hope that CMIP5 models are able to better physically represent natural climate variability during the warm season, and North American warm season precipitation; this would make constructing an ensemble mean climate projection that would include physically “well performing” GCMs, per the criteria established here, more practicable. The results of Cook and Seager (2013) and Geil et al. (2013) collectively suggest that the climatology of North American monsoon precipitation has been improved in CMIP5, especially in models with higher spatial resolution. It remains to be seen, though, if the CMIP5

models can reasonably represent warm season atmospheric circulation variability. We hope our work here provides guidance for future analysis of dynamically downscaled CMIP5 models from the North American Coordinated Regional Climate Downscaling Experiment (NA-CORDEX; Mearns et al., 2013), in a continuing effort for more statistically and physically confident projections of the North American monsoon in the future.

Acknowledgments

This research was funded by the City of Tucson Office of Conservation and Sustainable Development and the National Science Foundation (NSF). Additional funding was provided by both the Water Sustainability Graduate Student Fellowship Program and the Climate Assessment for the Southwest (CLIMAS) at the University of Arizona. We thank NARCCAP for providing the dataset. NARCCAP is funded by the NSF, the U.S. DOE, NOAA, and the U.S. EPA. We are grateful to Drs. Russ Vose and Richard Heim for access to the gridded precipitation dataset.

References

- Bukovsky MS, Gochis DJ, Mearns LO. 2013. Towards Assessing NARCCAP Regional Climate Model Credibility for the North American Monsoon: Current Climate Simulations. *Journal of Climate* **26**: 8802-8826. DOI: <http://dx.doi.org/10.1175/JCLI-D-12-00538.1>
- Bukovsky MS, Carrillo CM, Gochis DJ, Hammerling D, McCrary RR, Mearns LO. 2014. Towards Assessing NARCCAP Regional Climate Model Credibility for the North American Monsoon: Future Climate Simulations. *Journal of Climate*. Submitted.
- Carrillo CM, Castro CL, Woodhouse CA, Griffin D. 2014a: Low frequency variability of the North American Monsoon as diagnosed through earlywood and latewood tree-ring

chronologies in the Southwest U.S. *International Journal of Climatology*. To be submitted.

Castro CL, McKee TB, Pielke RA. 2001. The relationship of the North American monsoon to tropical and north pacific sea surface temperature as revealed by observational analysis. *Journal of Climate* **14**: 4449-4473.

Castro CL, Pielke RA, Leoncini G. 2005: Dynamical downscaling: assessment of value retained and added using the Regional Atmospheric Modeling System (RAMS). *Journal of Geophysical Research* **110**: No D5, D05108. DOI:10.1020/2004JD004721.

Castro CL, Pielke Sr. R, Adegoke JO. 2007. Investigation of the summer climate of the contiguous United States and Mexico using Regional Atmospheric Modeling System (RAMS). Part I: Model Climatology (1950-2002). *Journal of Climate* **20**: 3844-3865. DOI: 10.1175/JCLI4211.1.

Castro CL, Pielke Sr. RA, Adegoke JO, Schubert SD, Pegion PJ. 2007. Investigation of the summer climate of the contiguous United States and Mexico using Regional Atmospheric Modeling System (RAMS). Part II: Model climate variability. *Journal of Climate* **20**: 3866-3887.

Castro CL, Beltrán-Prezekurat AB, Pielke Sr. RA. 2009. Spatiotemporal variability of precipitation, modeled soil moisture, and vegetation greenness in North America within the recent observational record. *Journal of Hydrometeorology* **10**: 1355-1378. DOI: 10.1175/2009JHM1123.1.

Castro CL, Chang H, Dominguez F, Carrillo C, Kyung-Schemm J, Juang H. 2012. Can a regional climate model improve warm season forecasts in North America? *Journal of Climate* **25**: 8212-8237.

Ciancarelli B, Castro CL, Woodhouse C, Dominguez F, Chang H, Carrillo C, Griffin D. 2013. Dominant pattern of U.S. warm season precipitation variability in a fine resolution observational record with focus on the southwest. *International Journal of Climatology*. DOI:10.1002/joc.3716.

Cook BI, Seager R, 2013: The response of the North American Monsoon to increased greenhouse gas forcing. *J. Geophys. Res.*, in press, doi:10.1002/jgrd.50111.

Ding Q, Wang B. 2005. Circumglobal teleconnection in the Northern Hemisphere summer. *Journal of Climate* **18**: 3483-3505.

Ding Q, Wang B, Wallace JM, Branstator G. 2011. Tropical-extratropical teleconnections in boreal summer: observed interannual variability. *Journal of Climate* **24**: 1878-1896.

Garfin, G, Jardine A, Merideth R, Black M, Leroy S, eds. 2013. *Assessment of Climate Change in the Southwest United States: A Report Prepared for the National Climate Assessment*. A report by the Southwest Climate Alliance. Washington, DC: Island Press.

- Geil KL, Serra YL, Zeng X. 2013. Assessment of CMIP5 Model Simulations of the North American Monsoon System. *Journal of Climate* **26**: 8787-8801. DOI:<http://dx.doi.org/10.1175/JCLI-D-13-00044.1>
- Ghil M, Allen MR, Dettinger MD, Ide K, Kondrashov D, Mann ME, Robertson AW, Saunders A, Tian Y, Varadi F, Yiou P. 2002. Advanced spectral methods for climatic time series. *Reviews of Geophysics* **40**(1): 1-41. DOI:10.1029/2000RG000092.
- Gochis D, Schemm J, Shi W, Long L, Higgins W, Douglas A. 2009. A Forum for Evaluating Forecasts of the North American Monsoon. *EOS Transactions American Geophysical Union* **90**(29): 249. DOI:10.1029/2009EO290002.
- Gutzler DS, Coauthors. 2005. The North American monsoon model assessment project. *Bulletin of the American Meteorological Society* **86**: 1423–1429.
- Gutzler DS, Coauthors. 2009. Simulations of the 2004 North American monsoon: NAMA2. *Journal of Climate* **22**: 6716–6740.
- Hu Z-Z, Kumar A, Jha B, Huang B. 2012. An Analysis of Forced and Internal Variability in a Warmer Climate in CCSM3. *Journal of Climate* **25**: 2356–2373.
- Kanamitsu M, A Kumar, H-M H Juang, JK Schemm, W Wang, F Yang, S-Y Hong, P Peng, W Chen, S Moorthi, M Ji. 2002. Ncep dynamical seasonal forecast system 2000. *Bulletin of the American Meteorological Society* **83**: 1019–1037.
- Liang XL, Zhu J, Kunkel KE, Ting M, Wang JXL. 2008: Do CGCMs Simulate the North American Monsoon Precipitation Seasonal Interannual Variability? *Journal of Climate* **21**: 4424-4448.
- Livezey RE, Chen WY. 1983. Statistical Field Significance and its Determination by Monte Carlo Techniques. *Monthly Weather Review* **111**: 46–59.
- Mann ME, Lees JM. 1996. Robust Estimation of background noise and signal detection in climatic time series. *Climate Change* **33**: 409-445.
- McKee TB, Doesken NJ, Kleist J. 1993. The relationship of drought frequency and duration to time scales. *Eight Conference on Applied Climatology*. 17-22 January. Anahelm. California.
- Mearns LO, Arritt R, Biner S, Bukovsky MS, McGinnis S, Sain S, Caya D, Correia J, Flory D, Gutowski W, Takle ES, Jones R, Leung R, Moufouma-Okia W, McDaniel L, Nunes AMB, Qian Y, Roads J, Sloan L, Snyder M. 2012. The North American Regional Climate Change Assessment Program: overview of phase I results. *Bulletin of the American Meteorological Society* **93**: 1337-1362.

Mearns, LO, Gutowski WJ, Barsugli JJ, Buja L, Garfin GM, Lettenmaier DP, Leung L. 2013. The Development of North American CORDEX. *American Geophysical Union, Fall Meeting 2013*: abstract #A41L-05.

Pierce DW, Barnett TP, Santer BD, Gleckler PJ. 2009. Selecting global climate models for regional climate change studies. *Proceedings of the National Academy of Sciences* **106**: 8441-8446.

PRISM Climate Group. 2004. Parameter-elevation Regressions on Independent Slopes Model monthly precipitation grid. *Oregon State University*.
<http://www.prism.oregonstate.edu>.

Rajagolapan B, Mann ME, Lall U. 1998. A multivariate frequency-domain approach to long-lead climatic forecasting. *Weather and Forecasting* **13**: 58-74.

Ray AJ, Garfin GM, Wilder M, Vasquez-Leon M, Lenart M, Comrie AC. 2007. Applications of Monsoon research: Opportunities to inform decision making and reduce regional vulnerability. *Journal of Climate* **20**:1608-1626.

Rockel B, Castro CL, Pielke RA Sr, Von Storch H, Leoncini G. 2008. Dynamical downscaling: Assessment of model system dependent retained and added variability for two different regional climate models. *Journal of Geophysics Research* **113**: D21107. DOI: 10.1029/2007JD009461.

Shamir E, Sharon BM, Carrillo C, Castro CL, Chang H-I, Chief K, Corkhill FE, Eden S, Georgakakos KP, Nelson KM, Prietto J. 2014. Climate change and water resources management in the Upper Santa Cruz River, Arizona. *Journal of Hydrology*. In press.

Sheffield J, SJ Camargo, R Fu, Q Hu, X Jiang, N Johnson, KB Karnauskas, ST Kim, J Kinter, S Kumar, B Langenbrunner, E Maloney, A Mariott, JE Meyerson, JD Neelin, S Nigam, Z Pan, A Ruiz-Barradas, R Seager, YL Serra, D-Z Sun, C Wang, S-P Xie, J-Y Yu, T Zhang, M Zhao. 2013. North American Climate in CMIP5 Experiments. Part II: Evaluation of Historical Simulations of Intraseasonal to Decadal Variability. *Journal of Climate* **26**: 9247-9290.

Smith TM, Reynolds RW, Peterson TC, Lawrimore J. 2008. Improvements to NOAA's historical merged land-ocean surface temperature analysis (1880-2006). *Journal of Climate* **21**: 2283-2296.

Taylor KE, Stouffer RJ, Meehl GA. 2012. An Overview of CMIP5 and the Experiment Design. *Bulletin of the American Meteorological Society* **93**: 485-498.

Wilks DS. 2006. *Statistical Methods in the Atmospheric Sciences*. Elsevier: Burlington, MA

Tables

CCSM	Community Climate System Model
CGCM3	Third Generation Coupled Global Climate Model
GFDL	Geophysical Fluid Dynamics Laboratory GCM
HadCM3	Hadley Centre Coupled Model, Version 3

Table 1: General Circulation Models

CRCM	Canadian Regional Climate Model	Spectral nudged
ECP2	Experimental Climate Prediction Center Regional Spectral Model	Spectral nudged
HRM3	Hadley Regional Model 3	Non-spectral nudged
RCM3	Regional Climate Model Version 3	Non-spectral nudged
WRFG	Weather Research & Forecasting Model	Non-spectral nudged
MM5I	PSU/NCAR mesoscale model at Iowa State University	Non-spectral nudged

Table 2: Regional Climate Models

1	WRFG-CGCM3	WRFG driven by CGCM3
2	RCM3-CGCM3	RCM3 driven by CGCM3
3	CRCM-CGCM3	CRCM driven by CGCM3
4	RCM3-GFDL	RCM3 driven by GFDL
5	ECP2-GFDL	ECP2 driven by GFDL
6	CRCM-CCSM	CRCM driven by CCSM
7	WRFG-CCSM	WRFG driven by CCSM
8	HRM3-HadCM3	HRM3 driven by HadCM3

Table 3: NARCCAP simulations

	20C	21C
CGCM3	0.05	0.02
CCSM	0.16	0.30
HadCM3	0.57	0.44
GFDL	0.66	0.72

Table 4: correlation of spatial patterns of 500-mb GPHA between observed and NARCCAP GCMs. 500-mb GPHA patterns were obtained by regressing original GPHA against the SST ENSO mode obtained with MTM-SVD.

Figure Captions

Figure 1: Upper panel: annual cycle of NARCCAP precipitation for the NAM region for all the NARCCAP models (left) and selected models which best represent the monsoon (right) both for the 20th century. Histogram is for observed precipitation. Lower panel: as in upper panel but for the 21st century.

Figure 2: Seasonal mean (July-August) of NARCCAP precipitation for the 20th century (left panel), 21st century (central panel), and difference between 20th minus 21st century (right panel) for each NARCCAP model. The units for the mean and difference precipitation is mm/day.

Figure 3: Seasonal mean (July-August) of NARCCAP precipitation for individual NARCCAP simulations for the 20th century (yellow bars) and the 21st century (red bars). Dark blue background highlight positive change (wet) and light-blue background negative change (dry). In grey background are the multi-model ensemble mean for both cases: all models (ALL) and well-performing (WELL). The area average is highlighted by the blue box in the upper right corner. Error bars are calculated as ± 1 standard error of the mean for each case.

Figure 4: SPI area average time series for each NARCCAP model for the 20th century (left panel) and the 21st century (right panel). NARCCAP simulations with same GCM boundary condition forcing are grouped with same color. Correlation between a time series and the leader of the group is indicated in the plot by σ .

Figure 5: Right panel: EOF leading mode of spatial variability for observed (top) and IPCC GCM SST (below: gfdl, hadcm3, ccsm, and cpcm3) for summer (JJ) SST for the 1951-2000 period—but 1968-2008 for hadcm3. Left panel: MTM spectrum of the temporal leading mode, PC1, of the cases defined in the right panel. Significance levels of 90% and 99% confidence are superimposed in cyan lines.

Figure 6: Upper: LFV spectrum of the spatiotemporal leading MTM-SVD mode for observed JJ SST (a). Lower: Spatial correlation between the JJ SST gridded dataset and the MTM-SVD reconstructed temporal pattern of JJ SST for the ENSO spectral band (b), the PDV spectral band (c), and the combined ENSO-PDV band (d). Local significance is shown with oblique lines and field significance in percentage in lower left corner.

Figure 7: LFV spectrum of the spatiotemporal leading MTM-SVD mode for JJ SST for each IPCC GCMs used to force NARCCAP models during the 20th century: from 1951 to 2000—but from 1968 to 2008 for hadcm3. Peaks statistically significant passing the 90% level of confidence are highlighted with yellow. Right panel: Spatial correlation between the JJ SST gridded dataset and the MTM-SVD reconstructed temporal pattern of JJ SST for the ENSO spectral band. Local significance is shown with oblique lines and field significance in percentage in lower left corner.

Figure 8: Similar to Fig. 7 but for the 21st century: from 2021 to 2070.

Figure 9: Spatial correlation between the JA GPHA at 500 mb and the MTM-SVD reconstructed temporal pattern of JJ SST for the ENSO (a) and combined ENSO-PDV (b) spectral bands. Local significance is shown with oblique lines with oblique lines and field significance in percentage in lower left corner.

Figure 10: Spatial correlation between the JA NARCCAP GPHA at 500 mb and the MTM-SVD reconstructed temporal pattern of JJ NARCCAP SST for the ENSO spectral band: cgm3(a), hadcm3(b), gfdl(c), and ccsm(d) during the 20th century. Local significance is shown with oblique lines with oblique lines and field significance in percentage in lower left corner.

Figure 11: Similar to Fig. 10 but for the 21st century.

Figure 12: Spatial correlation between the JA SPI gridded dataset and the MTM-SVD reconstructed temporal pattern of JJ SST for the ENSO spectral band (a), the PDV spectral band (b), and the combined ENSO-PDV spectral band (c). Local significance is shown with oblique lines.

Figure 13: Spatial correlation between the JA SPI for each NARCCAP model dynamically downscaled with NCEP-Reanalysis and the MTM-SVD reconstructed temporal pattern of JJ NCEP-Reanalysis SST for the ENSO (left panel) and PDV (right) spectral bands. Local significance is denoted with oblique lines and spatial correlation with the corresponding observed spatial pattern (from Figs. 12a and 12b) are indicated in the lower right corner. The bottom two panels are the spectral nudged cases: CRCM and ECP2.

Figure 14: As in Fig. 13 except for the combined ENSO-PDV mode.

Figure 15: Similar to Fig. 13 but for JA SPI for each NARCCAP model dynamically downscaled with IPCC GCMs for the 20th century (left panel) and 21st century (right panel). For both centuries only ENSO spectral band spatial pattern is shown.

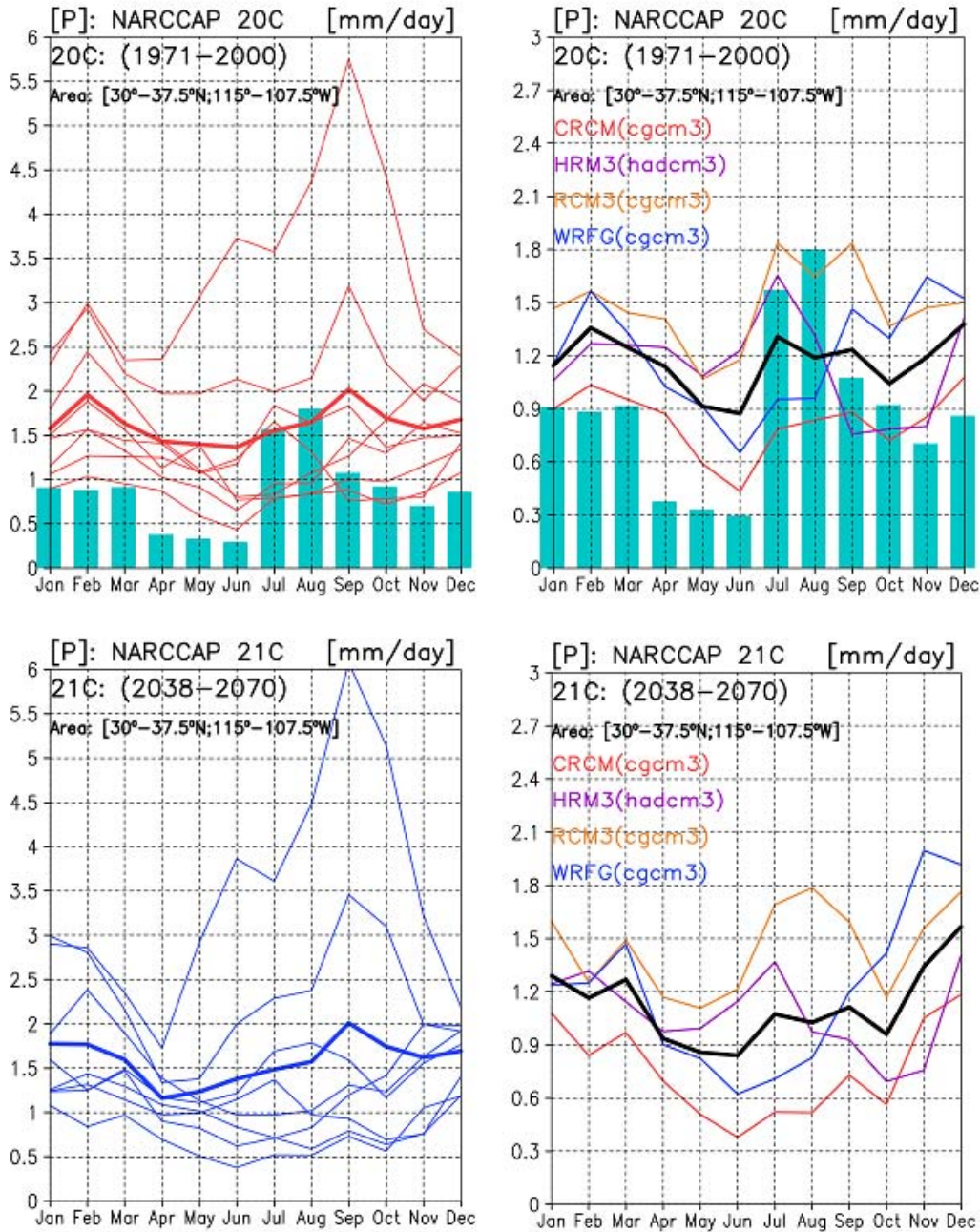


Figure 1: Upper panel: annual cycle of NARCCAP precipitation for the NAM region for all the NARCCAP models (left) and selected models which best represent the monsoon (right) both for the 20th century. Histogram is for observed precipitation. Lower panel: as in upper panel but for the 21st century.

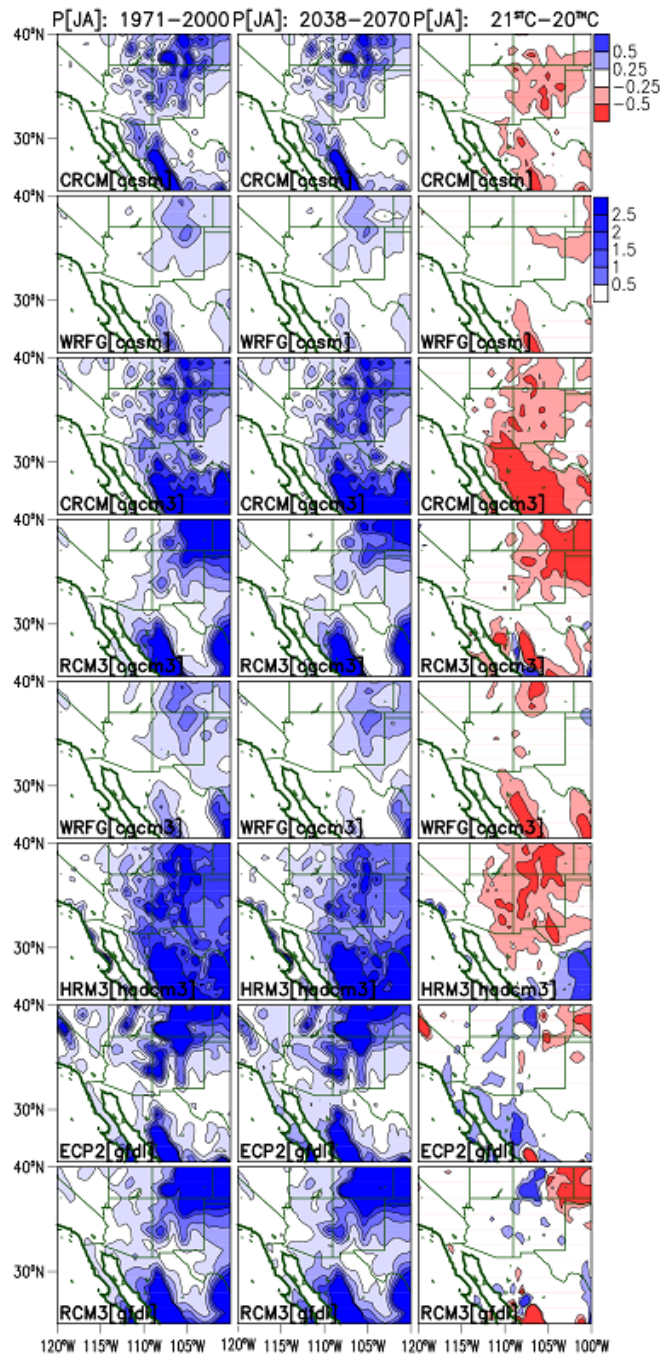


Figure 2: Seasonal mean (July-August) of NARCCAP precipitation for the 20th century (left panel), 21st century (central panel), and difference between 20th minus 21st century (right panel) for each NARCCAP model. The units for the mean and difference precipitation is mm/day.

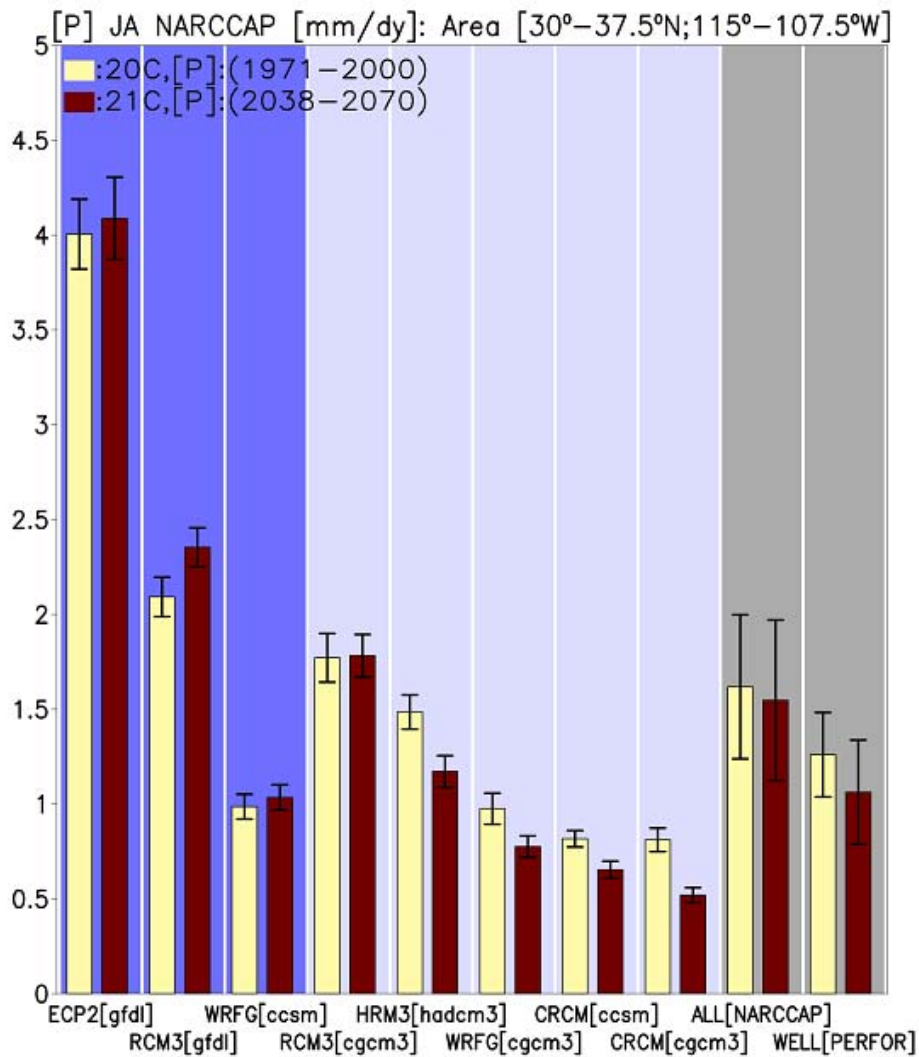


Figure 3: Seasonal mean (July-August) of NARCCAP precipitation for individual NARCCAP simulations for the 20th century (yellow bars) and the 21st century (red bars). Dark blue background highlight positive change (wet) and light-blue background negative change (dry). In grey background are the multi-model ensemble mean for both cases: all models (ALL) and well-performing (WELL). The area average is highlighted by the blue box in the upper right corner. Error bars are calculated as ± 1 standard error of the mean for each case.

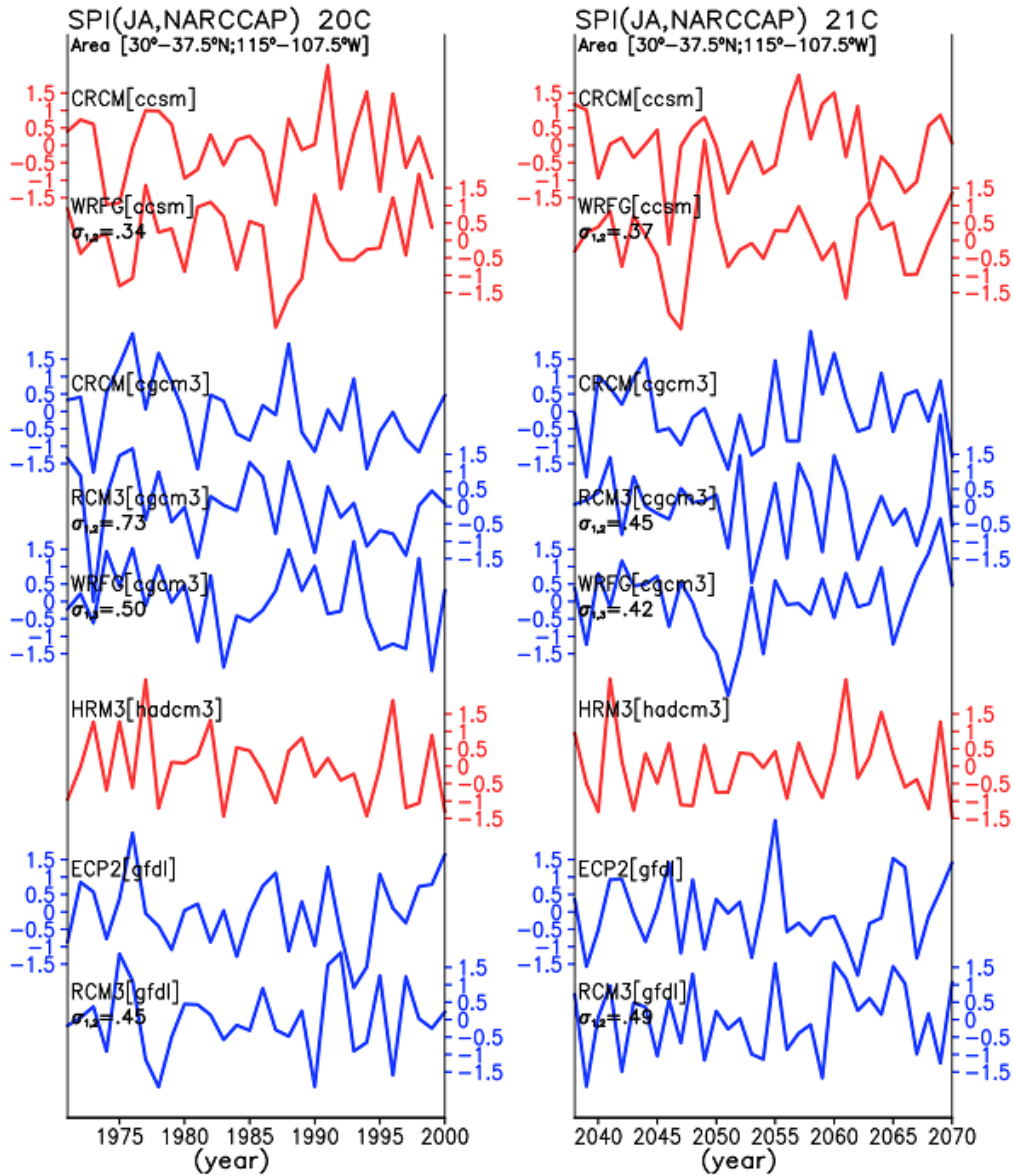


Figure 4: SPI area average time series for each NARCCAP model for the 20th century (left panel) and the 21st century (right panel). NARCCAP simulations with same GCM boundary condition forcing are grouped with same color. Correlation between a time series and the leader of the group is indicated in the plot by σ .

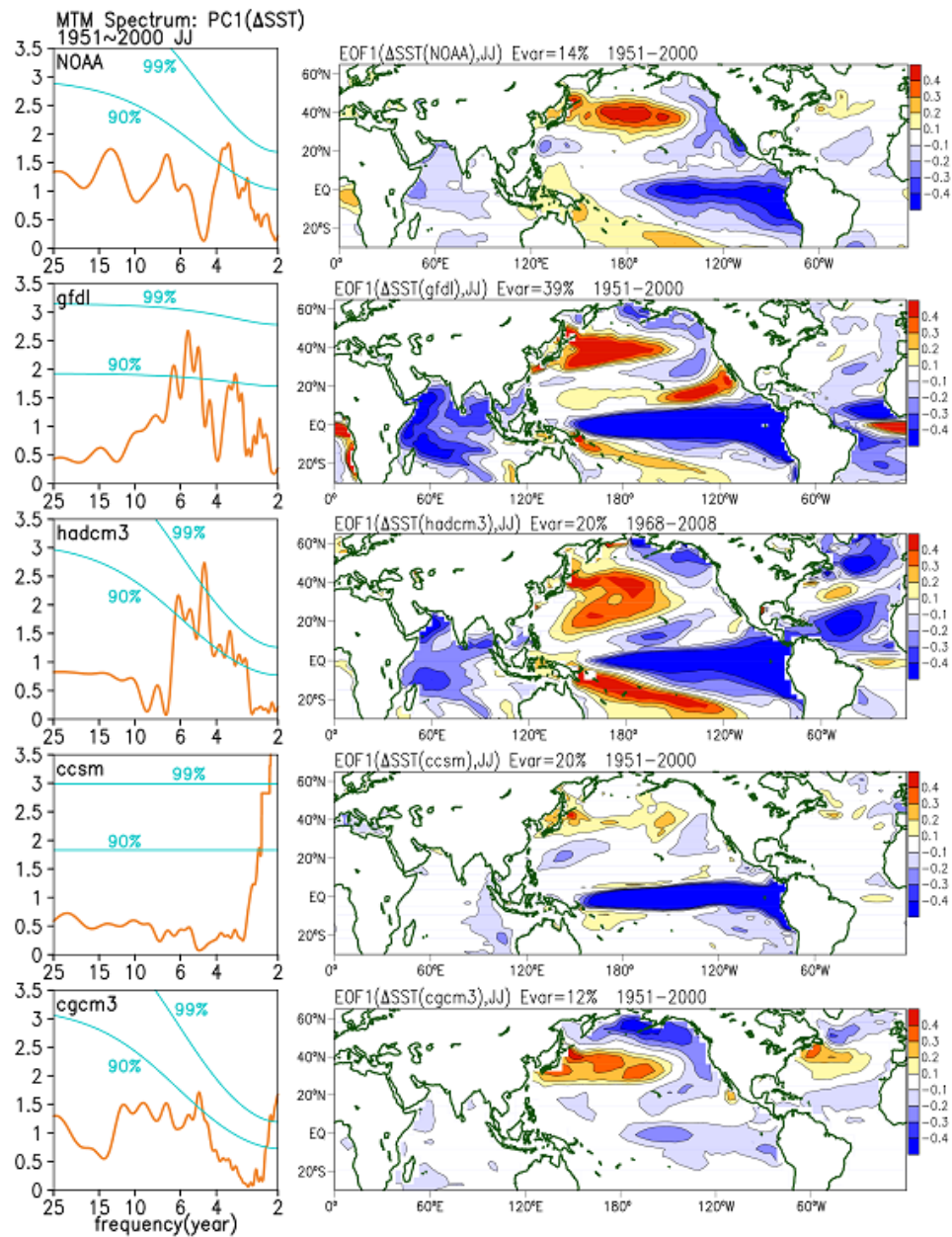


Figure 5: Right panel: EOF leading mode of spatial variability for observed (top) and IPCC GCM SST (below: gfdl, hadcm3, ccsm, and cgcm3) for summer (JJ) SST for the 1951-2000 period—but 1968-2008 for hadcm3. Left panel: MTM spectrum of the temporal leading mode, PC1, of the cases defined in the right panel. Significance levels of 90% and 99% confidence are superimposed in cyan lines.

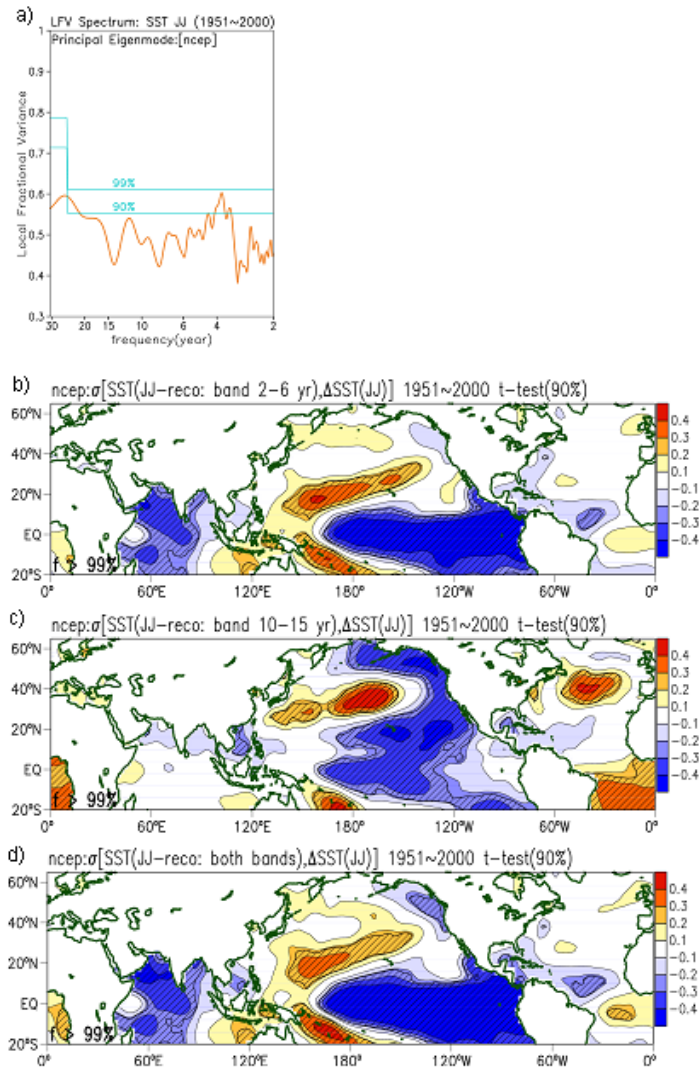


Figure 6: Upper: LFV spectrum of the spatiotemporal leading MTM-SVD mode for observed JJ SST (a). Lower: Spatial correlation between the JJ SST gridded dataset and the MTM-SVD reconstructed temporal pattern of JJ SST for the ENSO spectral band (b), the PDV spectral band (c), and the combined ENSO-PDV band (d). Local significance is shown with oblique lines and field significance in percentage in lower left corner.

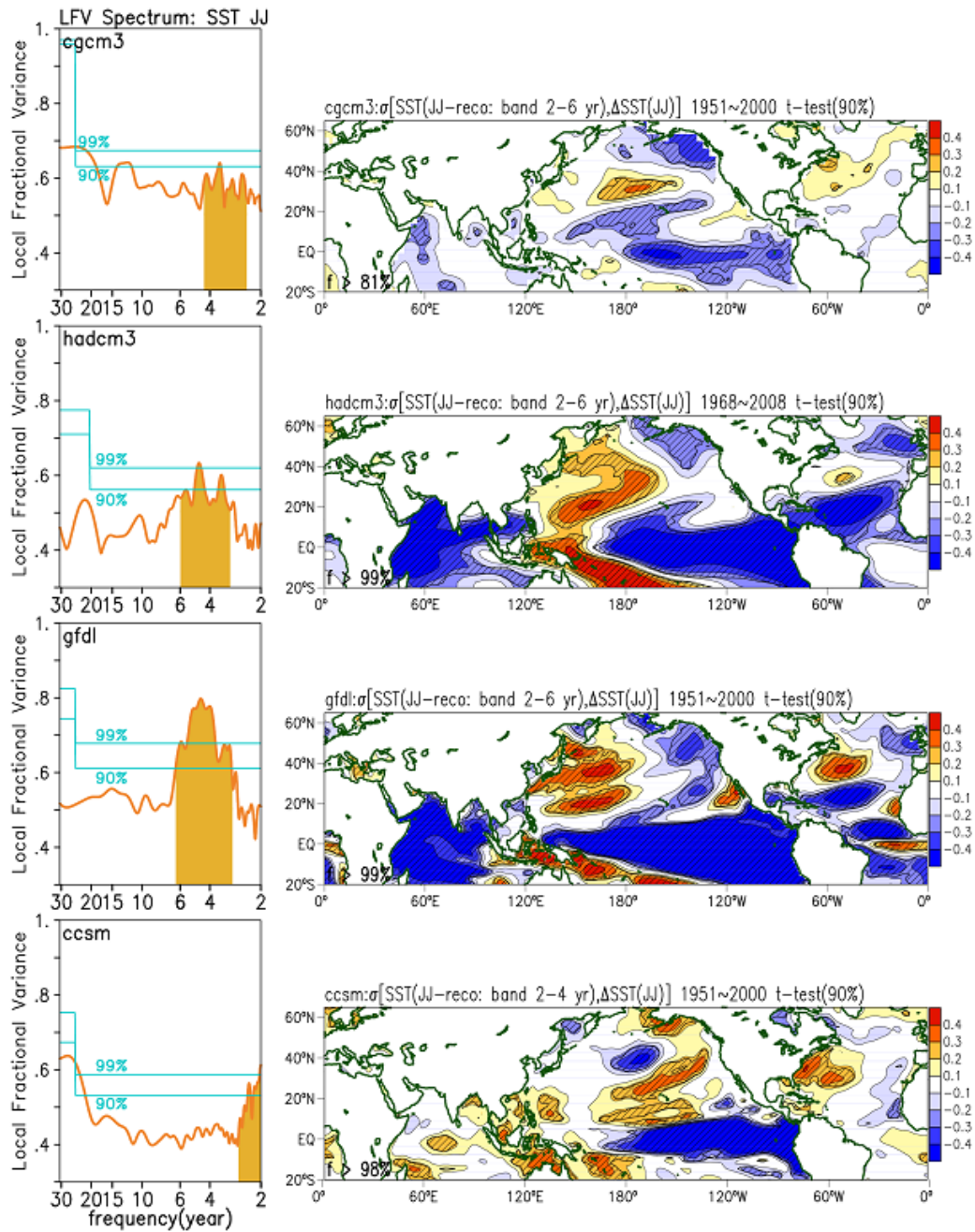


Figure 7: LFV spectrum of the spatiotemporal leading MTM-SVD mode for JJ SST for each IPCC GCMs used to force NARCCAP models during the 20th century: from 1951 to 2000—but from 1968 to 2008 for hadcm3. Peaks statistically significant passing the 90% level of confidence are highlighted with yellow. Right panel: Spatial correlation between the JJ SST gridded dataset and the MTM-SVD reconstructed temporal pattern of JJ SST for the ENSO spectral band. Local significance is shown with oblique lines and field significance in percentage in lower left corner.

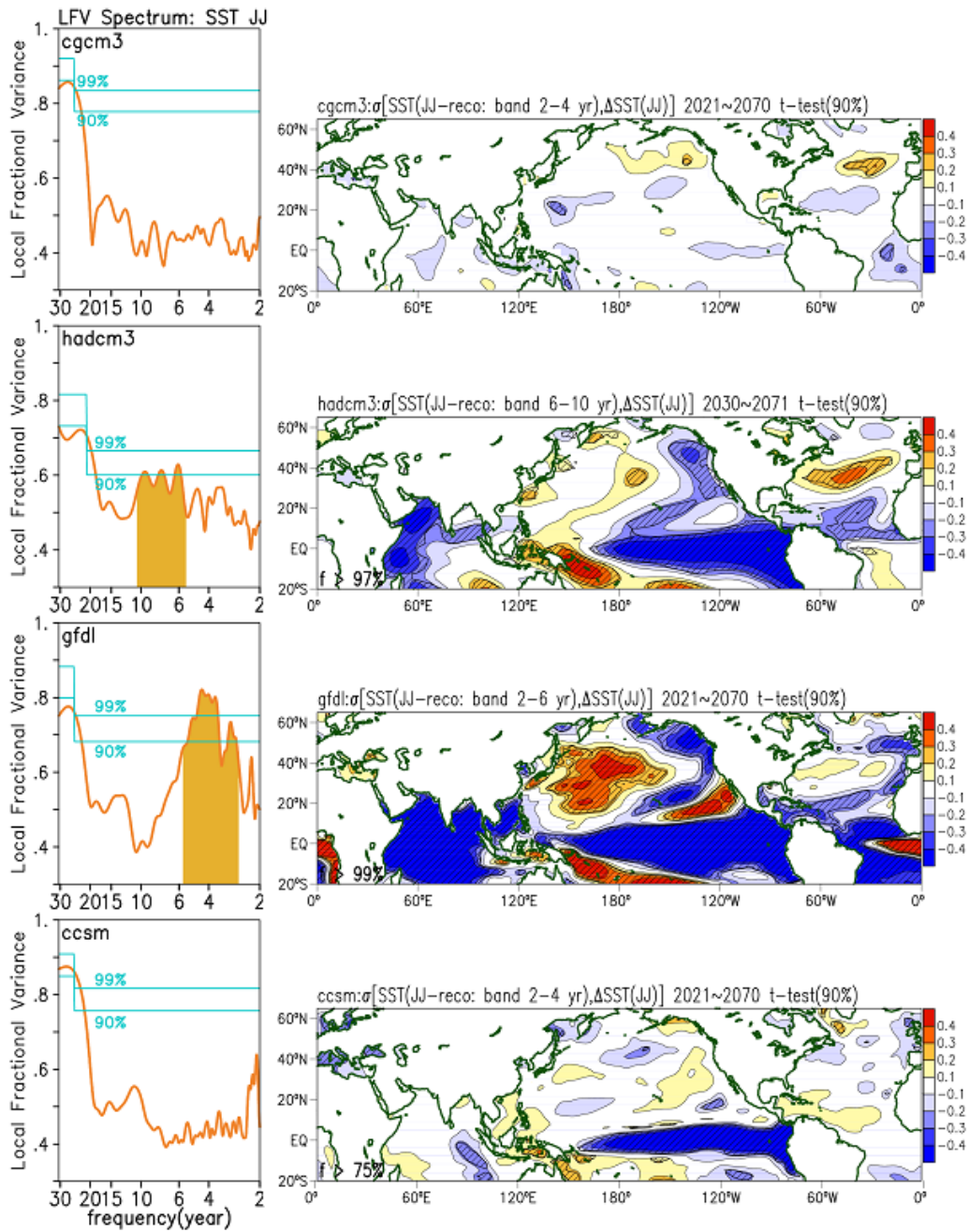


Figure 8: Similar to Fig. 7 but for the 21st century: from 2021 to 2070.

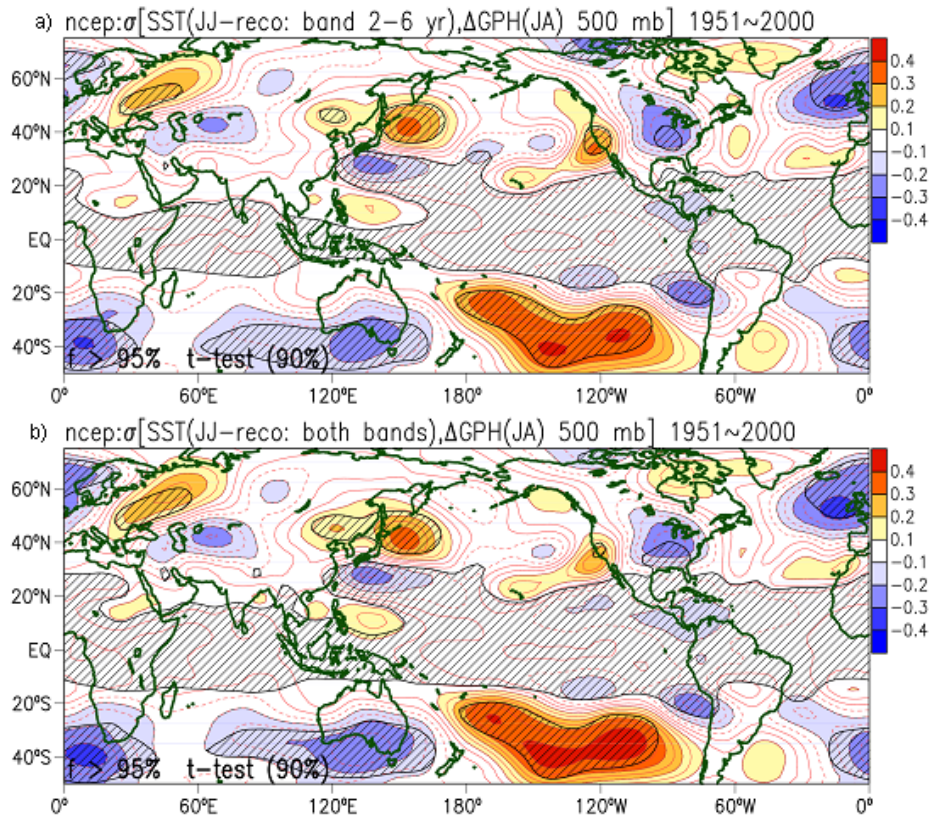


Figure 9: Spatial correlation between the JA GPHA at 500 mb and the MTM-SVD reconstructed temporal pattern of JJ SST for the ENSO (a) and combined ENSO-PDV (b) spectral bands. Local significance is shown with oblique lines with oblique lines and field significance in percentage in lower left corner.

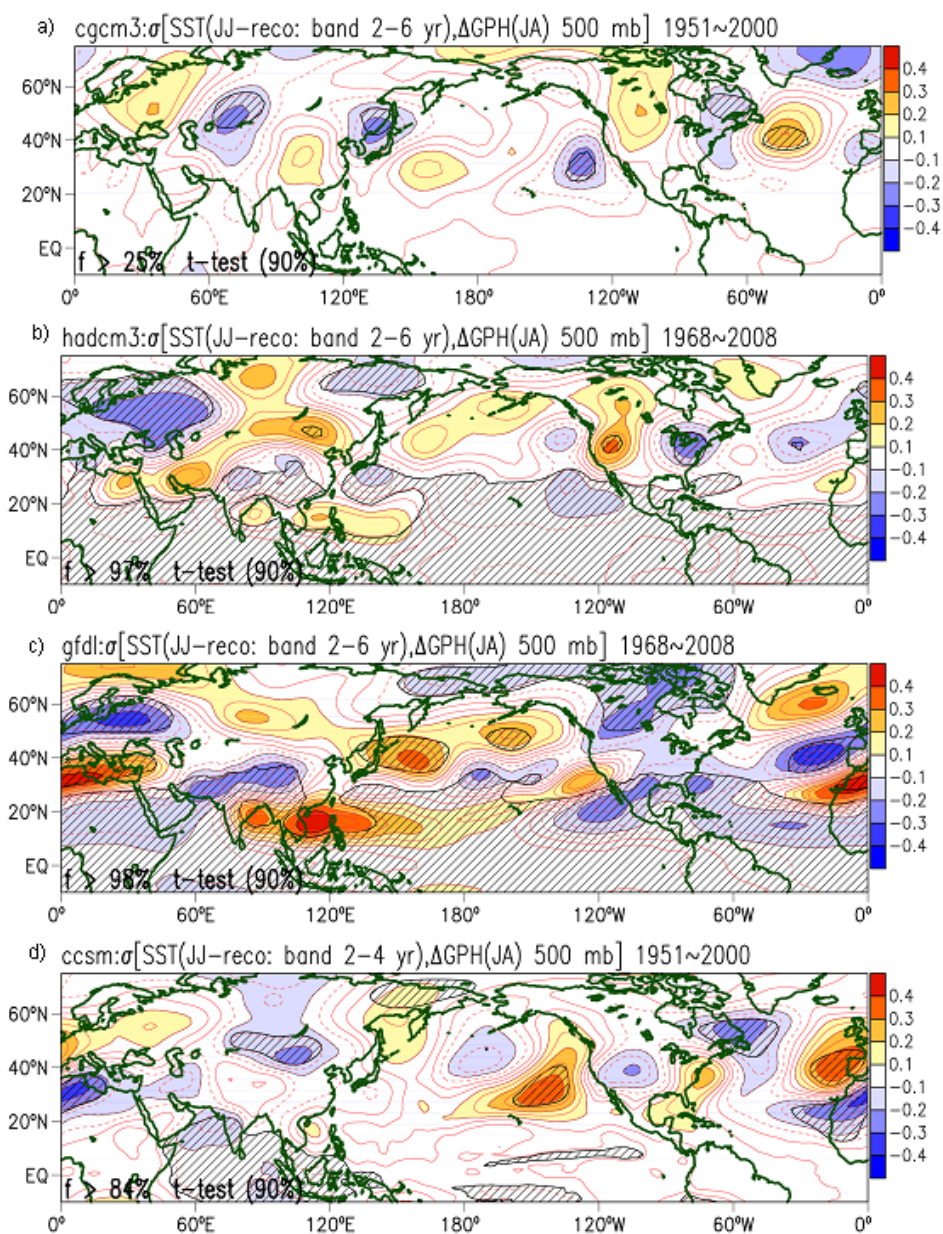


Figure 10: Spatial correlation between the JA NARCCAP GPHA at 500 mb and the MTM-SVD reconstructed temporal pattern of JJ NARCCAP SST for the ENSO spectral band: cgcm3(a), hadcm3(b), gfdl(c), and ccsm(d) during the 20th century. Local significance is shown with oblique lines with oblique lines and field significance in percentage in lower left corner.

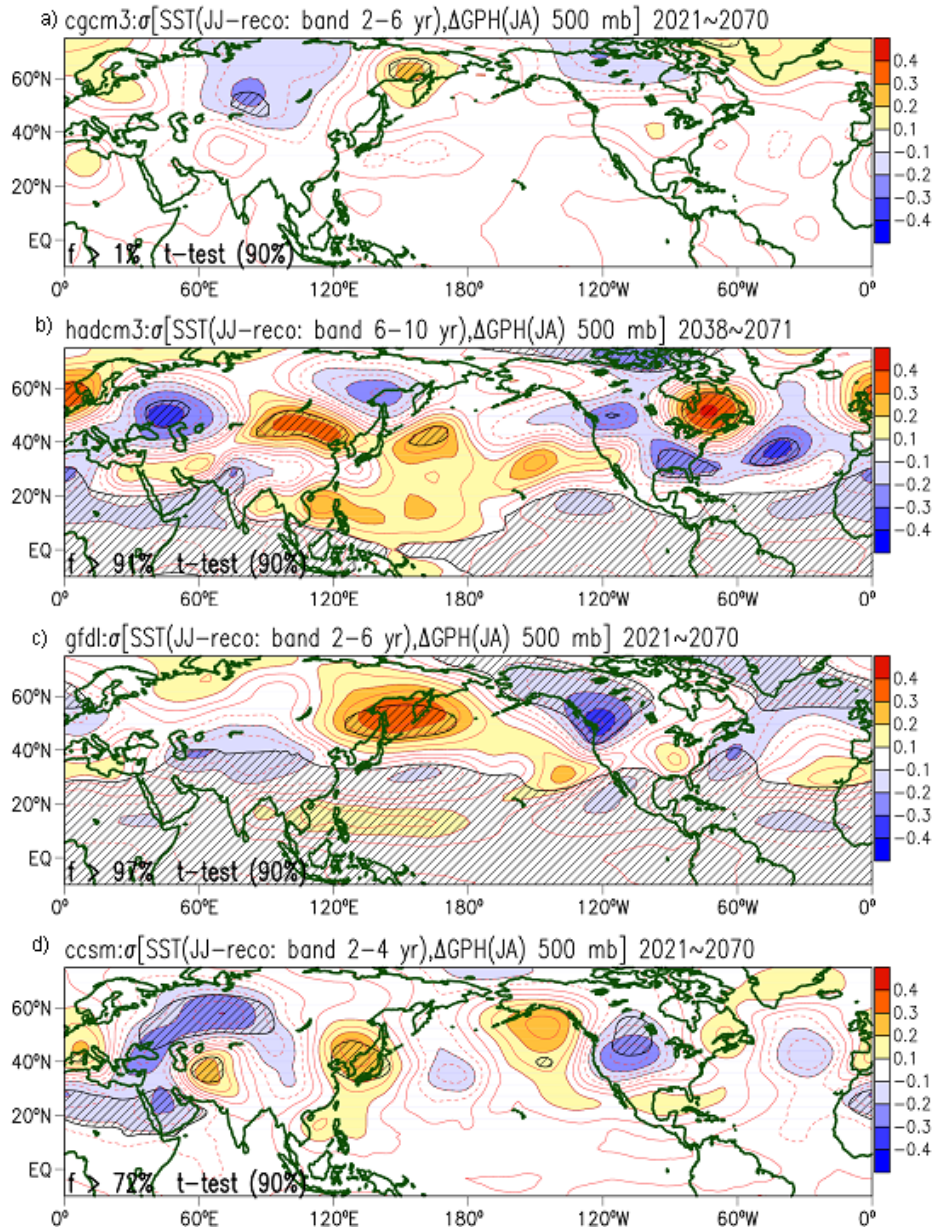


Figure 11: Similar to Fig. 10 but for the 21st century.

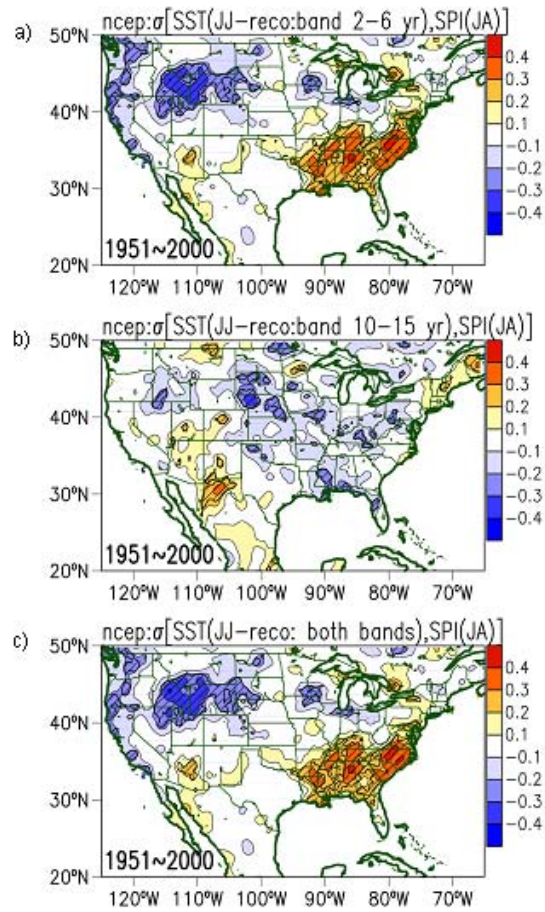


Figure 12: Spatial correlation between the JA SPI gridded dataset and the MTM-SVD reconstructed temporal pattern of JJ SST for the ENSO spectral band (a), the PDV spectral band (b), and the combined ENSO-PDV spectral band (c). Local significance is shown with oblique lines.

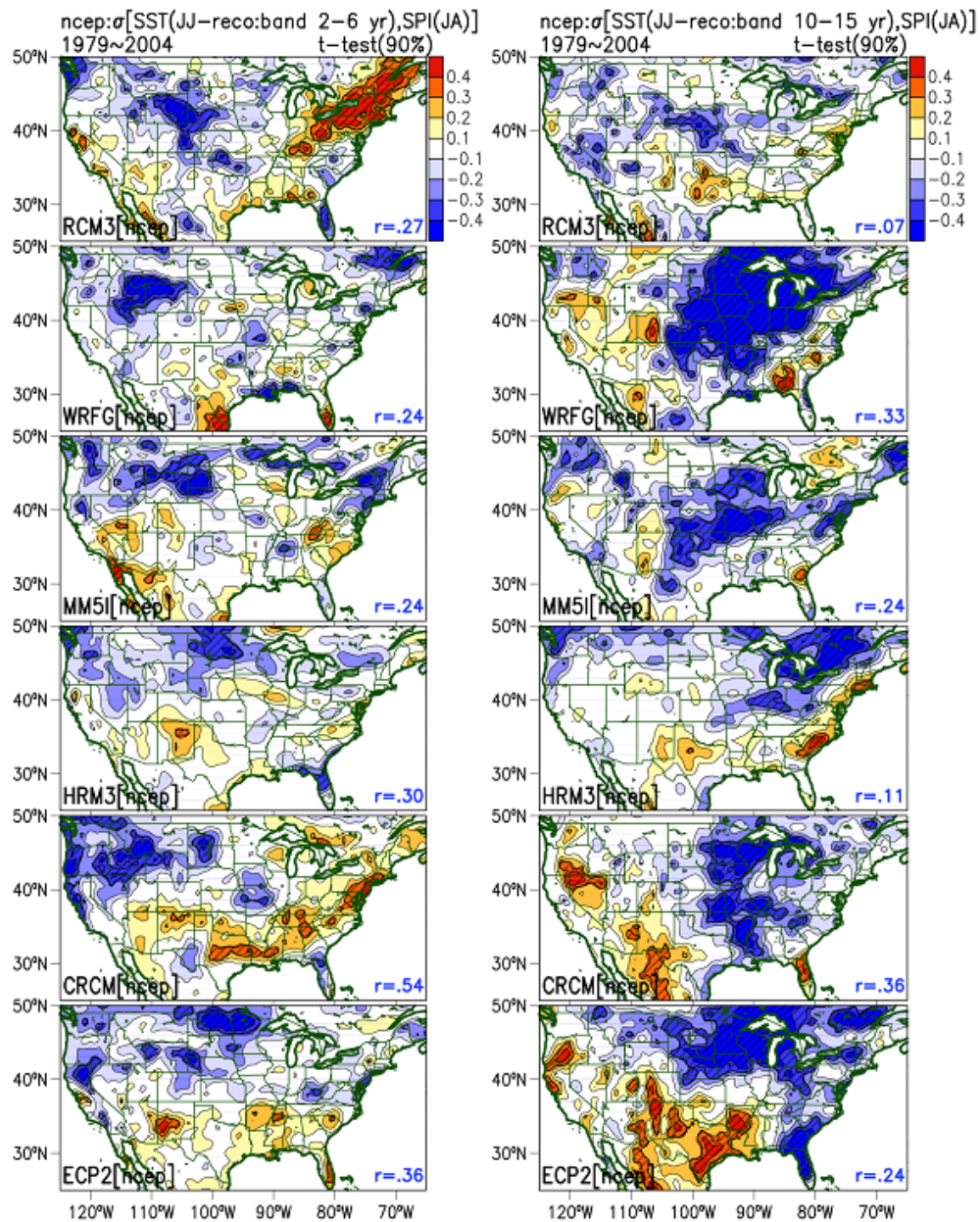


Figure 13: Spatial correlation between the JA SPI for each NARCCAP model dynamically downscaled with NCEP-Reanalysis and the MTM-SVD reconstructed temporal pattern of JJ NCEP-Reanalysis SST for the ENSO (left panel) and PDV (right) spectral bands. Local significance is denoted with oblique lines and spatial correlation with the corresponding observed spatial pattern (from Figs. 12a and 12b) are indicated in the lower right corner. The bottom two panels are the spectral nudged cases: CRCM and ECP2.

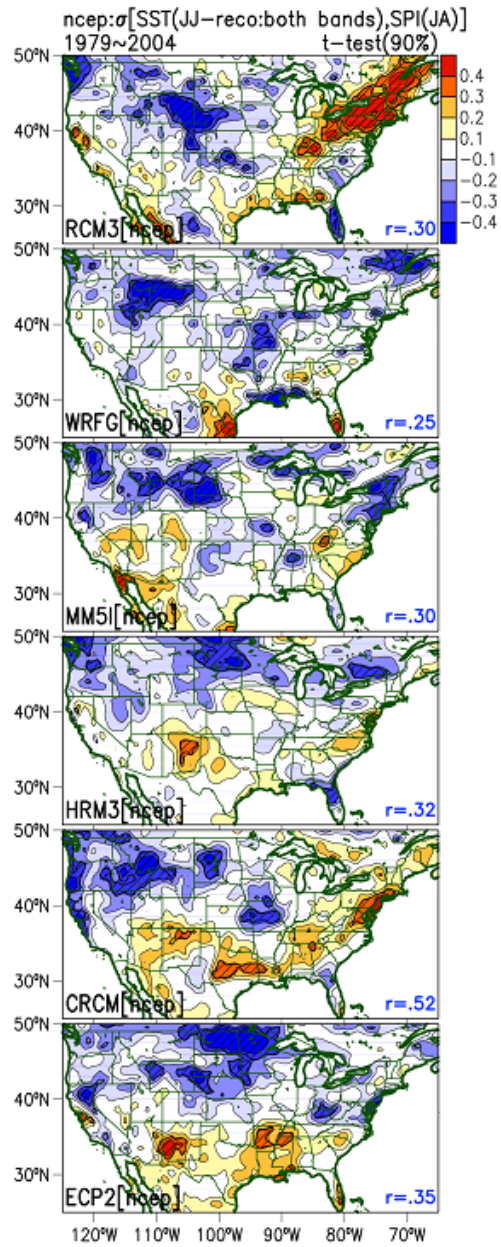


Figure 14: As in Fig. 13 except for the combined ENSO-PDV mode.

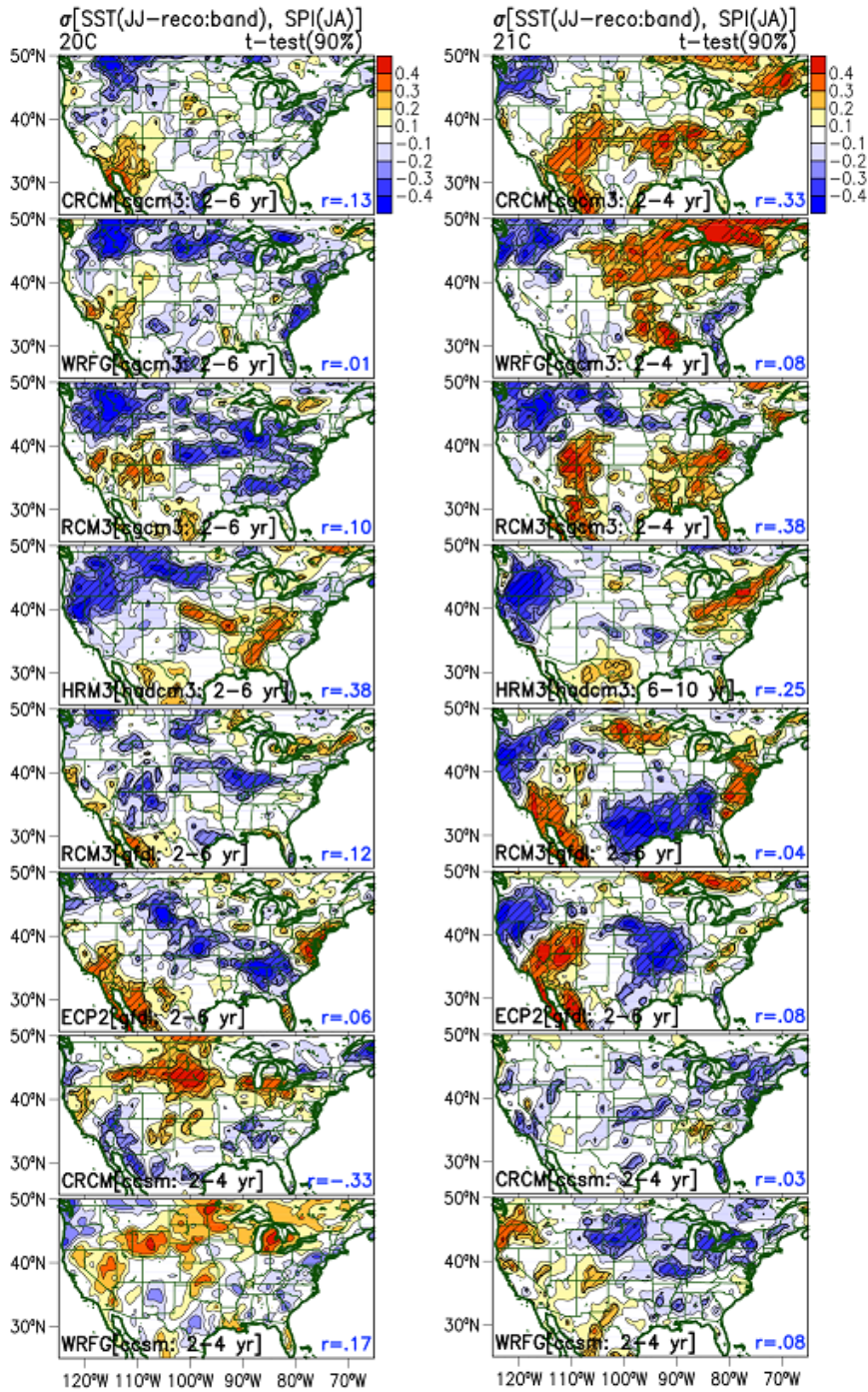


Figure 15: Similar to Fig. 13 but for JA SPI for each NARCCAP model dynamically downscaled with IPCC GCMs for the 20th century (left panel) and 21st century (right panel). For both centuries only ENSO spectral band spatial pattern is shown.

**APPENDIX C: LOW FREQUENCY CLIMATE VARIABILITY IN
WESTERN NORTH AMERICA AS DIAGNOSED IN A
DYNAMICALLY DOWNSCALED TWENTIETH CENTURY
REANALYSIS**

Carlos M. Carrillo¹, Christopher L. Castro¹, Hsin-I Chang¹, and Thang Luong¹

¹Department of Atmospheric Sciences, the University of Arizona, Tucson, Arizona

To be submitted to *International Journal of Climatology*

Version December 7, 2014

Corresponding author address: Carlos M. Carrillo, Department of Atmospheric Sciences, University of Arizona, Physics and Atmospheric Sciences Building, Rm. 536, 1118 East Fourth Street, Tucson, Arizona 85721. E-mail: carlosgc@email.arizona.edu, phone: (520) 626-6329, fax: (520) 621-6833.

Abstract

Our previous work considered North American monsoon climate variability with a monsoon-sensitive network of tree-ring chronologies in the Southwest. We were able to identify a very low-frequency centennial scale climate signal responsible for megadroughts of the past four centuries. Here we continue to investigate very low-frequency climate variability, at the decadal scale and longer, within the context of a twentieth-century atmospheric reanalysis that has been dynamically downscaled with the Weather Research and Forecasting (WRF) model. We apply spectral domain matrix methods technique (Multiple-Taper-Method Singular Value Decomposition; MTM-SVD) to these data to identify dominant and statistically significant spatiotemporal cool and warm season precipitation patterns. Our main question of interest is to ascertain whether the major western U.S. droughts in the last 140 years are driven by very low-frequency climate variability on the decadal to centennial time scale. We present evidence that the answer to this question is affirmative and that major droughts are tied to coherent changes in atmospheric circulation at a planetary scale in this very-low frequency regime. Use of a regional atmospheric model is necessary to resolve the spatial variability in precipitation patterns that are associated with the droughts. The downscaled 20th century reanalysis product is thus suitable to be applied to a hydrologic model to estimate impacts of historical dry and wet periods in the 20th century on water resources.

1. Introduction

Droughts in the southwestern U.S. have been a recurrent hindrance to economic development and living conditions in the region (e.g. Garfin et al., 2013). It has been historically documented that extreme and prolonged drought may be the major cause of the migration and eventual loss of the Anasazi people (Dean, 1994). In terms of monetary loss, it has been estimated that a fluctuation of about 3.4% of the annual U.S economic activity is attributable to weather and climate variability (Lazo et al., 2011). At the state level, the current 2014 drought in California has cost 2.2 billion dollars and 17100 seasonal jobs (Howitt et al., 2014). Therefore, a better understanding about the variability and causes of American southwestern droughts is critical so our society can develop more resilient strategies for natural hazard management, agriculture, public health, and water management (Ray et al., 2007).

One major limitation for understanding of long-term drought dynamics is the scarcity of reliable information that can account for long-term climate variability, at the timescale of several centuries. However, in recent decades, an intensive effort has been taken to understand mechanisms that govern droughts, particularly with the use of proxies that record long-term variability of climate (e.g. Woodhouse and Overpeck, 1998). In most of these studies, historical documents, lake-core sediments (Laird et al., 1996), geomorphic data, and tree-ring chronologies (Grissino-Meyer, 1996) have been used. Tree-ring chronologies are particularly advantageous as a climate proxy because of their ability to register the climate variability from year to year (Douglas, 1914). This advantage had been used to reconstruct climate parameters as far as several millennia

(D'Arrigo and Jacoby, 1991; Herweijer et al., 2007; Meko et al., 2007; Stahle et al., 2009).

In the southwestern United States, summer and winter variability of decadal droughts have been identified using earlywood and latewood chronologies for the last five centuries. Griffin et al. (2013) showed that the 1570s, 1660s, 1770s, 1820s, 1890s, and early 2000s droughts not only experienced a cool-season precipitation deficit but also a monsoonal precipitation failure. In their study, they explored the ability of latewood width tree-rings to explain monsoonal precipitation variability (Meko and Basin, 2001; Griffin et al., 2011) and discovered that monsoon drought events in the previous centuries were more extreme than during the instrumental era. The American Southwest drought is not an isolated phenomenon, but part of a continental-scale pattern of climate variability. An out-of-phase relationship of precipitation anomalies exist between northern Mexico (near the southwestern U.S.) and Central America (Méndez and Magaña, 2010; their Fig. 2) regions at low temporal frequencies has been proposed. During the 1950s, relatively dry conditions occurred in northern Mexico that contrasted with the anomalous wet conditions further south. Similarly, using a 500 years record of reconstructed tree-ring Palmer Drought Severe Index (PDSI; Cook et al. 2004) they also showed that persistent droughts in northern Mexico correspond with wet conditions in Central America.

The causes of the American droughts at the seasonal timescale are fairly well understood, but persistent droughts of several years (e.g. 1930s) and decadal order are not (Woodhouse and Overpeck, 1998). Recently, two major mechanisms have been proposed as relevant to explain multiyear droughts in the instrumental era: oceanic forcing and internal atmospheric variability (Seager and Hoerling, 2014). For example, the 1930s

drought has been related to cool tropical SST and warm North Atlantic SST (Schubert et al., 2004), which confirms the influence of the Pacific Decadal Oscillation (PDO; Mantua et al., 1997) and the Atlantic Multidecadal Oscillation (AMO; Enfield et al., 2001) as the sources of American droughts. Similarly, drought in Central America seems to be also related to out-of-phase configuration between the positive PDO and negative AMO phases (Méndez and Magaña, 2010).

By using tree-ring chronologies to explore the low-frequency climate variability, Griffin et al. (2013) have found an important characteristic of the climate variability in the southwestern United States: a dual summer-winter season coherence co-variability on tree-rings that characterized simultaneous cool-season precipitation deficit and failure of summer monsoon precipitation. This characteristic might be relevant to explain the occurrence of persistent droughts during the last five centuries in the Southwest. However, they also discuss three major caveats on the approach used to reconstruct the precipitation: 1) tree physiology related to root and crown mass (Fritts, 2001), 2) standardization of the ring-width time series (Cook et al., 1995), and 3) true low-frequency climate variability. All of these factors may adversely bear on the ability to characterize low-frequency climate variability in tree-ring records. Carrillo et al., (2014a, in preparation) provide additional evidence to support possible existence of this dual-season drought signal. By using an alternative statistical approach, they explicitly isolated this very low-frequency drought signal, and showed it to be statistically significant and spatially coherent within the Southwest. In addition, a seesaw spatial pattern at a continental scale between the Southwest and central U.S. was found to be associated with this drought signal during the observational era. However, the significance of these

results on precipitation only could not be assessed because of the short length of record. Exploring the continental spatiotemporal pattern of the drought signal only with tree-rings is a challenge as the tree-ring network is confined into the southwestern American region.

Therefore to assess the reliability of this low-frequency climate variability it is critically important to understand the mechanisms of persistent droughts. Can drought behavior in tree-ring dataset be confirmed in an independent dataset? In this work, we take an alternative approach to address low-frequency climate variability using a dynamical modeling approach. Based on our previous research, we assert that the best option at present is to consider the entire record of the new twentieth century reanalysis (20CR; Compo et al. 2011). Although the 20CR is limited to about 140 years in length it might be sufficient to capture several cycles of long-term drought (Cook et al. 2010). The major limitation found in 20CR is the improper representation of the precipitation features at regional and local scale. However, to bypass this limitation another variable, such as moisture flux convergence, may be used in lieu of precipitation (e.g. Castro et al., 2001). In addition, we dynamically downscale the 20CR, as to better simulate the physical mechanism of precipitation generation on the mesoscale. The utility of dynamical downscaling of atmospheric reanalyses to represent North American climate in the cool and warm season has been firmly established by a wide body of literature and research efforts (Gutzler et al., 2005 and 2009; Castro et al., 2007 and 2012; Bukovsky et al., 2013). The North American Regional Climate Change Assessment Program (NARCCAP; Mearns et al. 2012) is a recent example. This would include a reasonable representation of climate variability due to coupled-ocean atmosphere interactions, as we

showed for NARCCAP regional climate models in Carrillo et al. (2014b, in preparation). In this research we hypothesize that very low-frequency variability may potentially be found in both the 20CR and DD-20CR, as a dominant mode of variability that explains droughts in the southwestern U.S. during the cool and warm season. If we can show that this low-frequency variability exist in a RCM as tree-ring suggest, we can use the model data to potentially assess drought dynamics related to this low-frequency variability at a continental scale.

This paper is organized as follows. The data and methodology are described in sections 2 and 3. The dominant low-frequency mode diagnosed on moisture flux convergence simulated by 20th century Reanalysis is explained in section 4a and 4b. A description of the simulated annual cycle and variance of the dynamically downscaled 20th-century Reanalysis is presented in section 4c. The low-frequency precipitation mode in dynamically downscaled 20th-century Reanalysis as well as the drought covariability signal between summer and winter are explored in section 4d. Teleconnection patterns associated with sea surface temperature and geopotential height are described in section 4.e. Concluding points are presented in section 5.

2. Data

a. Twentieth-century reanalysis

We use the version 2 of the NCEP-NCAR Twentieth Century Reanalysis (20CR) project dataset, which is an international effort to produce a retrospective analysis from 1871 to the present. 20CR data are available every 6 hours at 2° degree resolution (Compo et al., 2011). The 20CR is the longest atmospheric reanalysis product currently available, and has already been used to investigate long-term climate variations. For

example Version 1 20CR has been used to investigate the U.S. Dust Bowl of the 1930s (Cook et al., 2010). The 20CR assimilates available observational data by use of an Ensemble Kalman Filter (Whitaker and Hamill, 2002). Ingested observations include surface pressure from the International Surface Pressure Databank and monthly sea surface temperature and sea-ice concentration from the Hadley Centre Sea Ice and SST dataset (Rayner et al., 2003).

b. Sea surface temperature and geopotential height data

Sea surface temperature (SST) from the Hadley Centre Sea Ice SST dataset (Rayner et al., 2003), is used for two purposes in this study: 1) to specify the surface boundary condition in the regional climate model and 2) to link large-scale remote forcing RCM-simulated precipitation. The SST is averaged for respective warm and cool season period of July-August (JA) and November to April (NA) during 1871 to 2010. We investigate the different large-scale modes of variability precipitation in North America related to sea surface temperatures, similar to our previous work (Castro et al. 2001, Castro et al. 2007, Ciancarelli et al. 2013). The atmospheric response to SST forcing is also analyzed using geopotential height anomalies (GPHA) at 500-mb from 20CR.

c. Dynamical downscaling of 20CR with WRF

The 20CR is dynamically downscaled with the Weather Research and Forecasting (WRF) model (DD-20CR). A continuous simulation is performed over a domain that extends the contiguous U.S. and Mexico with 35 km grid spacing. Boundary conditions are updated every six hours. The WRF model is used with similar parameterizations to the operational forecasting configuration of the Department of Atmospheric Sciences at the University of Arizona, as previously described in Castro et al. (2012). We include

one important update to the WRF model simulation design from Castro et al. (2012), within the Gulf of California (GoC), sea surface temperatures are bias corrected to the observed satellite record. If this is not performed, GoC sea surface temperature will be too cold and act to suppress convective precipitation during the warm season, consistent with Mitchell et al. (2002). We also emphasize that spectral nudging is imposed on the interior of the RCM domain to conserve the large-scale synoptic variability, including any stationary wave train atmospheric teleconnections, from the driving 20CR. Prior studies have generally found better skill in the representation of the climate variability in North America when implementing the spectral nudging approach (e.g. Castro et al., 2012; Mearns et al., 2012; Bukovsky et al., 2013; Carrillo et al., 2014b).

d. Precipitation data

Precipitation data is from a new 0.5° gridded National Oceanic and Atmospheric Administration (NOAA) product (P-NOAA), provided by Drs. Russ Vose and Richard Heim. P-NOAA covers the entire area of study (U.S and Mexico) and incorporates a terrain correction interpolation function, similar to the Parameter-elevation Regressions on Independent Slopes Model (PRISM Climate Group, 2004), beneficial for the complex terrain of the Southwest. We previously considered the P-NOAA product in Castro et al. (2012) in evaluation of a dynamically downscaled global seasonal forecast model for the warm season period.

3. Statistical Analysis Methodologies

a. Moisture flux convergence and water vapor budget analysis

In lieu of precipitation from the 20CR, as in Castro et al. (2001) and Castro et al. (2007), we consider moisture flux convergence (MFC) because of its stronger tie to the

underlying atmospheric dynamics. Evaporation, precipitation, and MFC are directly related to the water vapor budget equation (Schmitz and Mullen, 1996; Higgins et al., 1997).

$$\frac{\partial W}{\partial t} + \nabla \cdot \vec{Q} = E - P \quad (1)$$

Where, E=Evaporation, P=Precipitation, $\vec{Q} = \frac{1}{g} \int_0^{P_s} \vec{V} dp$ = water vapor flux, q = specific humidity, p=pressure, g=gravity, \vec{V} = velocity, and $W = \frac{1}{g} \int_0^{P_s} q dp$ = precipitable water. MFC from 20CR is used to identify the regions that are associated with spatial variability in precipitation on continental and larger scales.

b. Standardized Precipitation Index (SPI)

The standardized precipitation index (SPI) is used to specify precipitation during the period 1871 to 2010. SPI is a gamma-normalized value that characterizes anomalous precipitation (McKee et al., 1993), and was originally designed to characterize droughts in the western United States. Cool season SPI is defined for the period November to April (NA) and warm season SPI is defined from July to August (JA). SPI has been used to monitor short and long term droughts in the United States (Heim, 2002). Its main advantage is the ability to identify spatial patterns of precipitation variability at regional and continental scales (e.g. Castro et al. 2009). We used the same methodology to compute SPI as in Castro et al. (2009) and Ciancarelli et al. (2013) in P-NOAA and the DD-20CR.

c. MTM-SVD analysis

Multi-Taper-Method Singular Value Decomposition (MTM-SVD) (Mann and Park, 1994 and 1996; Mann and Lees, 1996; Rajagopalan et al., 1998) is used to determine the dominant spatiotemporal variability of MFC, observed SPI, and DD-20CR SPI. The MTM-SVD technique and implementation is explained in further detail in Rajagolapan et al. (1998). In our analysis, we consider the Local Fractional Variance (LFV) spectrum, the reconstructed spatial pattern, and the reconstructed temporal time series (Mann and Park, 1996). The LFV is a form of a power spectrum where the temporal and spatial variation is accounted for simultaneously. Statistically significant spectral peaks in the LFV spectrum are identified by statistical significance intervals determined by bootstrap re-sampling (Rajagolapan et al., 1998). The reconstructed spatial pattern represents the spatial variability associated with a specific spectral band, or specific frequency. For our analyses, we consider the reconstructed spatial pattern for spectral bands that are statistically significant at the 90% level or above. The reconstructed spatial patterns are plotted as correlation maps, where the correlation fields were computed by Pearson correlation between the raw field and the reconstructed temporal time series. The reconstructed temporal time series are obtained at point in the domain specified at reference point. The reference point for both datasets analyzed is located at the center of the North American Monsoon Experiment region 2 (NAME 2) (32.75°N, 110.25°W) (Gochis et al., 2009). We used the same methodology to compute MTM-SVD as in Castro et al. (2009) and the codes we obtained from the website of Professor Michael Mann at the Pennsylvania State University.

d. Correlation, local significance, and field significance

Spatial correlation patterns for MFC, observed SPI, DD-20CR SPI, SSTA, and GPHA are portrayed by the Pearson correlation coefficient. Local significance is determined by a Student's t-test and field significance is assessed as in as in Livezey and Chen (1983). The threshold for local significance is the 90% confidence level ($p < 0.10$) and the field significance is obtained by a Monte Carlo technique that randomizes the maps of 500 times. The field significance value, displayed as a percentage, is indicated on each correlation map. The methodology is quite consistent with our prior work in Castro et al. (2007b) and Ciancarelli et al. (2013).

4. Results

The major purpose of this paper is to show whether 20CR and DD-20CR are able to reasonably represent drought variability in at low temporal frequencies that is maybe responsible of multiyear precipitation deficit. The major problem we face is the limitation of 20CR to produce realistic precipitation in the Southwest. However, the 20CR and moisture flux still reflects atmospheric circulation variability at continental and global scales (Compo et al., 2011; Cook et al., 2010). In this analysis, two steps were used to validate the existence of low-frequency climate variability. First, we analyze the low-frequency variability on 20CR. Second, the same analysis is applied to the dynamically downscaled 20CR. The first step is necessary to guarantee that low-frequency climate variability exists within the 20CR and it is able to be transferred to the DD-20CR. The second step is relevant to obtain an improved precipitation in the spatial and temporal domain, especially in regions with terrain-related thunderstorms such as the Southwest during the monsoon.

a. Evidence of the dominant low-frequency drought mode as diagnosed by moisture flux convergence

Moisture flux convergence (MFC) can be used as alternative parameter instead of precipitation to evaluate 20CR moisture variability on global and continental scales. As previously mentioned in the Introduction, persistent droughts in the Southwest show a seesaw pattern with Central America and Great Plains (Méndez and Magaña, 2010; Cook et al., 2004). The association in the climatology (annual cycle) between the Southwest and Central America is not that evident. Central America has a bimodal summer precipitation, with one peak during June-July and the other in September (Magaña et al., 1999; Karnauskas and Busalacchi, 2009), a decrease in between corresponding to the period of the midsummer drought (Mosiño and Garcia, 1966; Hastenrath, 1967). In contrast, the southwestern U.S. presents a mono-modal summer precipitation peak with an abrupt transition in late June and early July, driven by the onset of the North American monsoon (Adams and Comrie, 1997).

MFC has been used to characterize NAM variability with Reanalysis I (Castro et al., 2001). They found that MFC can portray NAM interannual variability related to ENSO and PDV. The variability in MFC is associated with changes in tropical convection, in the central tropical Pacific (Fig. 1). In reference to our North American analysis here, we consider the location of local maximum variability in MFC located over Central America during the warm season. This is highlighted by the red box labeled as CA in Fig. 1, which will be target of further analysis here. We calculated the combined Pacific SST variability index (P-SST), from Castro et al. (2001) their equation 1, for 20CR cool and warm season. P-SST is correlated with cool and warm season MFC in

Figure 2 to analyze convective activity associated to SST forcing at large scale.

Irrespective of the season, there is a clear out-of-phase (seesaw) pattern in the MFC and P-SST correlation field between the central Pacific and both the western Pacific and equatorial Atlantic that generally reflects the dominant influence of ENSO on precipitation in the tropics and the mid-latitudes during the cool and warm seasons (Ropelewski and Halpert, 1986 and 1987). Therefore, 20CR MFC is a good proxy to capture at least the global scale distribution of precipitation associated with ENSO, so it probably also contains information on low-frequency climate variability.

We consider the region of local maximum MFC variability in Central America (CA) as target to explore the low-frequency variability on 20CR. The 10-year running mean filtered and raw time series of JA MFC spatially averaged over CA is shown at the bottom of Fig. 3. We can infer that the 10-year running mean captures only low-frequency climate variability. The positive sign of MFC is associated with a pluvial and a negative sign a drought in Central America as confirmed in Fig. 5. We identify three distinct periods of interest in which the low-frequency variability is dominant: the 1888-1901 pluvial, 1917-1932 drought, and the 1942-1952 pluvial (Méndez and Magaña, 2010). The composite spatial patterns of MFC for these three periods are shown at the top of Figure 3. Positive values represent convergence and negative divergence, which are emphasized with vectors. In general, wet (dry) periods in Central America are associated with moisture flux divergence (convergence) in the central equatorial Pacific, which would be consistent with La Niña-like (El Niño-like) conditions. There is a more inconsistent relationship with MFC in areas near the Indian Monsoon region. Even this region shows opposite values during the Central American pluvials (1888-1901 and

1942-1952). However, the phases agree in Central America and central tropical Pacific for all three periods. Fig. 4 shows the same information as Fig. 3 but for the cool season (NA). As in the warm season, MFC over Central America during the identified droughts and pluvials shows the same inverse relationship with MFC over the central equatorial Pacific at least for the 1917-1932 and 1942-1952 periods. It is important to note that the time series (Fig. 4) does not show the pronounced peak in this period. The summer and winter seasonal patterns of the drought and pluvial are in-phase in the low-frequency in a similar way proposed by Griffin et al. (2013) in the Southwest. The cool season droughts and pluvials are also in phase with the warm season ones. The warm season precipitation anomalies (Fig. 5) during the identified droughts and pluvials in Central America show that enhanced (suppressed) precipitation occurs with a more northward displacement of the Intertropical Convergence Zone (ITCZ; Karnauskas and Busalacchi, 2009) that would again tend to occur with more La Niña-like (El Niño-like) conditions (Giannini et al., 2000). Albeit with parameterized precipitation physics, the 20CR is able to capture this salient difference in ITCZ positioning. The precipitation anomaly in Central America during JA matches the signal in MFC shown earlier in Fig. 3. We will show later in the manuscript that the ENSO signatures in Pacific SST are present at least for two of these periods.

Our previous investigations of cool and warm season precipitation variability in the southwestern U.S. (Griffin et al. 2013, Carrillo et al., 2014a in preparation) considered EW and LW_{adj} tree-ring indices for a 400-year record to describe statistically significant low-frequency climate variability, as shown in Carrillo et al. (2014a in preparation; their Fig. 18). By comparing these results we assert that major droughts and

pluvials in the Southwest are inversely related to MFC and precipitation in Central America within the 20CR record as in Méndez and Magaña (2010). Thus, the long-term droughts in the Southwest would be associated with persistent La Niña-like conditions in the Pacific, consistent with Herweijer et al. (2007). Though the 20CR precipitation signal in Central America is quite evident in Fig. 5, there is not a comparably inverse relationship in 20CR precipitation over southwestern North America. We will later demonstrate that the DD-20CR is able to capture this out-of-phase relationship in a way that supports the analysis of the southwestern U.S. tree-ring record.

b. Assessment of statistically significant low-frequency variability in 20CR MFC using MTM-SVD

The composite analyses of MFC during major droughts and pluvials are quite physically suggestive of low-frequency climate variability. Basically an anti-phase relationship between MFC in Central America and the central tropical Pacific tied to ENSO exist. Is this spatiotemporal variability in MFC statistically significant at the decadal timescale and longer? We apply MTM-SVD to the JA global MFC field for the entire record of the 20CR. Three main results are shown in Fig. 6: the LFV spectrum, the reconstructed time series for low-frequencies (decadal and longer) in the Central America region, and the pattern correlation map of the reconstructed time series with MFC. The LFV reveals statistically significant low-frequency variability, particularly in the range of 25-50 years. The reconstructed time-series of low-frequency MFC reveals a very similar result as shown in the previous section with time 10-year running mean time series. The spatial correlation map in Fig. 6b also shows essentially a similar anti-phase relationship in MFC between Central America and the central tropical Pacific, but the negative center

is shifted south at 40° S. Therefore we conclude that low-frequency climate variability exist in the 20CR dataset that drives the droughts and pluvials in Central America and the southwestern U.S. and it is statistically significant (Méndez and Magaña, 2010).

Repeating the same exact analysis on a more restrictive 25-50 year band yields basically the same result with an even stronger spatial loading pattern in the MFC correlation map (Fig. 7). To verify that this global-scale pattern of MFC is associated with southwestern U.S. drought during the warm season, the MFC reconstructed time series (Fig. 7b) is correlated with JA SPI (from P-NOAA). A statistically significant negative correlation with JA SPI exists throughout much of the southwestern U.S., demarcating the geographic areas with the U.S. that are influenced by the North American monsoon (e.g. Adams and Comrie, 1997). When performed the MTM-SVD analysis for the cool season (Fig. 8), the results are similar to the warm season in terms of the pattern of MFC, though the statistically significant spatiotemporal variability at low frequencies is only apparent in a 10-15 year band. Cool season variability in NA SPI will be considered later when analyzing the DD-20CR.

c. Precipitation annual cycle in WRF DD-20CR

Though the 20CR can portray the global-scale low-frequency variability in MFC, MFC and 20CR are probably not sufficient to characterize the climatology of the continental U.S., based on our prior comparisons of the NCEP-NCAR reanalysis to observed and RCM-generated warm season precipitation (Castro et al. 2007b). A necessary requirement of a robust physical modeling system must be a reasonable climatological representation of precipitation, prior to any consideration of year-to-year variability. Fig. 9 shows variance of monthly precipitation for the period 1985-2010 for

P-NOAA, DD-CR, and 20CR. Note that the 20CR tends to underestimate precipitation variability in the southwestern U.S. and this is improved upon in the DD-20CR. In general, DD-20CR shows more precipitation variability with a clear terrain influence throughout the western U.S. and northern Mexico. We consider the annual cycle of monthly precipitation in the western Pacific Northwest (A1) and Arizona (A2) regions (Fig. 10) for P-NOAA, DD-20CR and 20CR. In the western Pacific Northwest the monthly mean precipitation is nearly identical between the 20CR and DD-20CR. Both products underestimate cool season precipitation, especially during the DJF period. In Arizona, DD-20CR does a better job of reproducing the annual cycle of precipitation. In comparison to 20CR, DD-20CR helps to reduce the positive winter precipitation bias and, more importantly, simulates a distinct North American monsoon where none exists in the 20CR. The value added of a RCM to represent the North American monsoon by dynamically downscaling an atmospheric reanalysis is entirely consistent with prior work from the North American Monsoon Experiment (Gutzler et al. 2009) as well as Castro et al. (2007a). The differences in precipitation variability in Fig. 11 are mainly accounted for by differences during the warm season.

d. The low-frequency variability in the DD-20CR

It seems reasonable to expect that the statistically significant low-frequency spatiotemporal variability in precipitation would be nearly identical between P-NOAA and DD-20CR precipitation. After all, 20CR just has an additional 30 years of data prior to 1900. MTM-SVD analysis of P-NOAA JA SPI is shown in Fig. 12. The only statistically significant low-frequency variability occurs at a timescale of 15 years. The regressed pattern of JA SPI does show an expected anti-phase relationship between

precipitation in the southwestern U.S. and central U.S./Pacific Northwest that is driven in great part by ENSO and Pacific Decadal Variability (e.g. Castro et al., 2001; Castro et al. 2007b; Castro et al. 2009). Performing the identical analysis on DD-20CR precipitation reveals a somewhat different result, however (Fig. 13). The LFV spectra has more statistically significant temporal variability beyond a timescale of 10 years and the spatial loadings in the SPI correlation maps show several new characteristics. The continuity between the Southwest and northern Mexico is better resolved, but the negative sign over the Great Plains is shifted north. The loading over western Pacific Northwest is lost but the out-of-phase relationship between Central America and the Southwest is explicitly resolved for both seasons. The reconstructed time series also more closely matches the known sequencing of droughts and pluvials in southwestern U.S. from the tree-ring record, as described earlier. Why might DD-20CR precipitation yield a result for low-frequency precipitation variability in North America that has better correspondence with the tree-ring record and global MFC, in comparison to P-NOAA? Most obvious is the fact that the additional time length of 20CR allows for consideration of the late 1890s drought, so even the seemingly inconsequential addition of 30 years of data actually does allow us to capture an important climate event that P-NOAA cannot. But perhaps less obvious is the fact that the dynamically downscaled precipitation is a result of consistent large-scale dynamical forcing mechanisms (i.e. atmospheric teleconnections) as input boundary forcing to the RCM. Though we consider P-NOAA as observational truth, it is subject to data limitations in the station site availability where precipitation data would have been recorded, especially during the early part of its record. An identical analysis performed for the cool season is shown in Fig. 14 for just the DD-20CR. Statistically

significant low-frequency spatiotemporal variability in cool season precipitation is in phase with that of the warm season, with the peaks of the 1890s drought, 1917-1932 pluvial and 1942-1952 drought present.

This synergistic phasing in the low-frequency regime is statistically assessed by the temporal ($r=0.58$) and spatial ($\rho=0.43$) correlations between the winter and summer spatiotemporal patterns. How this could impact on our understanding of the climate of the Southwest? The ability to simulate the spatiotemporal pattern of low-frequency climate variability in DD-20CR is important because: 1) it confirms the low-frequency variability in EW and LW_{adj} tree-ring data from the Southwest U.S. network is not an artifact of the biological processes in the trees themselves, 2) it permits consideration of the possible forcing mechanisms for the variability with a consistent physical modeling framework, and 3) it demonstrates that long-term droughts and pluvials in the southwestern U.S. is a result of the synergistic phasing of cool and warm season precipitation anomalies.

e. Associated sea surface temperature anomalies and atmospheric teleconnections

The associated sea surface temperature anomalies during the identified droughts and pluvials are shown in Figs. 15 and 16, respectively for the warm and cool seasons. The SSTA patterns between two periods are quite consistent (1917-1932 and 1942-1952). An ENSO-like signal is present in the central tropical Pacific for the 1917-1932 (El Niño) and 1942-1952 (La Niña) periods, consistent with the change in ITCZ positioning noted earlier and North American drought variability described by Herweijer et al. (2007). However, there is no ENSO signal apparent for the 1888-1901 drought. As has been pointed out by Seager and Hoerling (2014), the 1888-1901 drought is most related to internal atmosphere variability. There do not appear clear and consistent linkages to PDO

for these droughts either, at least by the composite analysis. More physically consistent results are revealed by correlated the reconstructed low-frequency SPI time series for the Southwest U.S. for warm and cool season with global SSTA (top of Figs. 17 and 18). Low frequency cool season precipitation variability in the Southwest is associated with El Niño-like conditions in the central equatorial Pacific and Pacific Decadal Variability. The corresponding warm season precipitation variability is more associated with just Pacific Decadal Variability, but the pattern is not field significant. In contrast to the composite analysis, the SSTA associated with sustained dual season drought in the Southwest U.S. do not appear to be persistent from the cool to warm season, in agreement with Griffin et al. (2013).

Finally, we regressed the warm and cool season SPI on the corresponding 500-mb 20CR geopotential height anomalies (lower panels of Figs. 17 and 18). Coherent stationary wavetrains are present for both seasons, field significant above the 80% level. During the cool season, a circumglobal PNA-like pattern is observed over western North America, which has connection to ENSO. During the warm season, the Western Pacific North America (WPNA) pattern is present, as described in Ding et al. (2011) and Ciancarelli et al. (2013). Somewhat similar to the PNA pattern in winter, WPNA is a quasi-stationary Rossby wavetrain that emanates from the western tropical Pacific and Indian monsoon region and modulates the strength and positioning of the North American monsoon ridge. Castro et al. (2007) and Ciancarelli et al. (2013) suggest this warm season teleconnection response is more connected to ENSO-PDV variability in the early part of summer (JJ). Though the exact physical mechanism(s) of how WPNA is generated during the warm season is still a subject of active research, it clearly bears

heavily on low-frequency variability in Southwest U.S. monsoon precipitation. The teleconnection patterns just described considering the DD-20CR also appear in a similar way with respect to the dominant modes of EW and LWadj tree-ring data in the Southwest U.S. network (Carrillo et al., 2014a in preparation).

5. Concluding points

The major purpose of this investigation was to evaluate whether there is coherency in warm and cool season precipitation variability at low frequencies in the Southwest that may be responsible for decadal droughts. As has been described previously with a new monsoon-sensitive network of tree-ring chronologies (Griffin et al., 2013; Carrillo et al., 2014a), our study present solid evidence to support this idea. We took an alternative approach by using not only the new Twentieth-Century Reanalysis (20CR), but also its dynamically downscaled product. In the first part, we utilized MFC because of the limitation of 20CR precipitation to resolve terrain-related convective precipitation. MFC resolves well the water budget on tropical regions, so a good strategy is to validate the low-frequency variability in 20CR by exploring the ability of MFC to describe the persistent drought in Central America, because they are related to the Southwest droughts at low frequencies (Méndez and Magaña, 2010). In the second part, we have used a dynamically downscaled version of the Twentieth-Century Reanalysis (DD-20CR) to investigate the low-frequency climate variability associated with droughts on the NAM region. The dynamically downscaled of 20CR was done with the WRF model with the purpose of incorporating the best representation of the terrain-forced summer monsoonal precipitation highly dependent on the mesoscale and large-scale teleconnections.

We have hypothesized that 20CR contains low-frequency variability. By using the moist flux convergence (MFC), as moist integrator variable, we were able to show that 20CR contains similar low-frequency variability as previously identified in Carrillo et al. (2014a) with tree-ring chronologies. This is fundamentally important, because a RCM such as WRF is not able to generate this variability as part of its internal dynamics, because the low-frequency regime must be part of a large-scale process. The answer to our research question related to whether multiyear persistent Southwest droughts are driven by very low-frequency climate variability is a categorical yes. Using enhanced monsoonal precipitation by the DD WRF on 20CR, we portrayed how low-frequency variability modulates the American Southwest droughts. Therefore, the evidence presented in this paper suggests this possibility. An evaluation of the climatology shows that the DD-20CR can reproduce well the annual cycle and summer/winter interannual variability with some caveats. This makes possible to use 20CR and DD-20CR to explore the NAM climate variability at low frequencies. The precipitation generated by the DD-20CR is synchronized with the low-frequency variability in the 20CR. This evidence suggests that the low-frequency drought signal is part of the climate system not only in the Southwest, but part of a continental-scale pattern.

From a seasonal perspective, 20CR MFC and DD-20CR precipitation confirm the coherence of summer and winter co-variability at the low frequencies. It was found that this dual-season low frequency regime can be responsible for persistent droughts in the Southwest. Thus, the modeling approach provides additional support to confirm the existence of this dual-season precipitation covariability. The drought and pluvial temporal phases and spatial patterns over the Southwest and central U.S. are observed;

however, the spectral 50-100 year signature is not completely solved, as can be the case with tree-ring chronologies, due to the length record limitation in 20CR but the phases are evident.

The forcing mechanism for the cool season seems to be related to the El Niño-like variability in central tropical Pacific. However, for the warm season it seems to be more related to the high latitude Pacific Decadal Variability. The covariability between seasons that is suggested by the composite analysis is complicated to assess because of the limitation of the time series length. In addition, the atmospheric teleconnection for summer shows a CGT type of Rossby wave trains as in Ding et al. (2011) and in Ciancarelli et al. (2013), and for winter a circumglobal PNA-like pattern is observed.

As this longest retrospective reanalysis is able to capture the low-frequency variability in a quite similar manner tree-ring chronologies do, we propose it could be potentially used to evaluate the synergistic impact on extreme droughts by natural variability on a warming future climate in the Southwest. We suggest that by explicitly including these changes in a pseudo global warming modeling framework (DD-20CR) that already is able to simulate drought variability, it can be a better approach to evaluate the impact of extreme droughts under a future climate in change. Maybe we can benefit more from this approach than current CMIP5 model simulation, which struggle to reproduce variability in the order of decadal scale due to the complexity of fully coupled AOCGMs.

Acknowledgments

This research was funded by the Department of Interior, Bureau of Reclamation, Salt River Project, and Central Arizona Project. Additional funding was provided by the Water Sustainability Graduate Student Fellowship Program at the University of Arizona. We thank Twentieth Century Reanalysis Project for providing the dataset. The 20CR Project is funded by the DOE and NOAA. We are grateful to Drs. Russ Vose and Richard Heim for access to the gridded precipitation dataset.

6. References

- Adams DK, Comrie AC. 1997. The North American Monsoon. *Bulletin of the American Meteorological Society* **10**: 2197-2213.
- Bukovsky MS, DJ Gochis, LO Mearns. 2013. Towards assessing narccap regional climate model credibility for the north american monsoon: current climate simulations. *Journal of Climate* **26**: 8802-8826.
- Carrillo CM, Castro CL, Woodhouse CA, Griffin D. 2014a: Low frequency variability of the North American Monsoon as diagnosed through earlywood and latewood tree-ring chronologies in the Southwest U.S. *International Journal of Climatology*. To be submitted.
- Carrillo CM, Castro CL, Garfin G, Chang H-I, Bukovsky MS. 2014b: Pacific SST-related teleconnective influences on North American monsoon precipitation within North American Regional Climate Change Assessment Program (NARCCAP) models. *International Journal of Climatology*. To be submitted.
- Castro LC, TB McKee, RA Pielke. 2001. The relationship of the North American monsoon to tropical and north pacific sea surface temperature as revealed by observational analysis. *Journal of Climate* **14**: 4449-4473.
- Castro CL, Pielke Sr RA, Adegoke JO. 2007a: Investigation of the summer climate of the contiguous United States and Mexico using the Regional Atmospheric Modeling System (RAMS). Part I: Model climatology (1950–2002). *Journal of Climate* **20**: 3844–3865.
- Castro CL, RA Pielke Sr, JO Adegoke, SD Schubert, PJ Pegion. 2007b. Investigation of the Summer Climate of the Contiguous U.S. and Mexico Using the Regional

Atmospheric Modeling System (RAMS). Part II: Model Climate Variability. *Journal of Climate* **20**: 3866-3887.

Castro CL, Beltrán-Prezekurat AB, Pielke Sr. RA. 2009. Spatiotemporal variability of precipitation, modeled soil moisture, and vegetation greenness in North America within the recent observational record. *Journal of Hydrometeorology* **10**: 1355-1378. DOI: 10.1175/2009JHM1123.1.

Castro CL, H Chang, F Dominguez, C Carrillo, J Kyung-Schemm, HH-M Juang. 2012. Can a regional climate model improve warm season forecasts in North America? *Journal of Climate* **25**: 8212-8237.

Ciancarelli B, CL Castro, C Woodhouse, F Dominguez, H Chang, C Carrillo, D Griffin. 2013. Dominant pattern of U.S. warm season precipitation variability in a fine resolution observational record with focus on the southwest. *International Journal of Climatology*. doi:10.1002/joc.3716.

Compo GP, JS Whitaker, PD Sardeshmukh, N Matsui, RJ Allan, X Yin, BE Gleason, RS Vose, G Rutledge, P Bessemoulin, S Brönnimann, M Brunet, RI Crouthamel, AN Grant, PY Groisman, PD Jones, M Kruk, AC Kruger, GJ Marshall, M Maugeri, HY Mok, Ø Nordli, TF Ross, RM Trigo, XL Wang, SD Woodruff, SJ Worley. 2011. The Twentieth Century Reanalysis Project. *Quarterly Journal of the Royal Meteorological Society* **137**: 1-28. doi: 10.1002/qj.776

Cook ER, Briffa KR, Meko DM, Graybill DA, Funkhouser G. 1995. The segment length curse in long tree-ring chronology development for palaeoclimatic studies. *The Holocene* **5(2)**: 229-237.

Cook BI, Seager R, Miller RL. 2010. Atmospheric circulation anomalies during two persistent North American droughts: 1932-1939 and 1948-1957. *Climate Dynamics*. DOI: 10.1007/s00382-010-0807-1.

Cook ER, Woodhouse CA, Eakin CM, Meko DM, Stahle DW. 2004. Long-term aridity changes in the western United States. *Science* **306**: 1015-1018.

D'Arrigo RD, Jacoby GC. 1991. A 1000-year record of winter precipitation from northwestern New Mexico, USA: a reconstruction from tree-rings and its relationship to El Niño and the Southern Oscillation. *Holocene* **1**: 95-101.

Dean JS. 1994. The medieval warm period on the southern Colorado plateau. *Climate Change* **26**: 225-241

Ding Q, Wang B, Wallace JM, Branstator G. 2011. Tropical-extratropical teleconnections in boreal summer: observed interannual variability. *Journal of Climate* **24**: 1878-1896.

- Douglas AE. 1914. A method of estimating rainfall by the growth of trees. *The Climatic Factor*, E. Huntington Editors, Carnegie Institute 101-122.
- Enfield DB, Mestas-Nunez AM, Trimble PJ. 2001. The Atlantic Multidecadal Oscillation and its relationship to rainfall and river flows in the continental US. *Geophysical Research Letters* **28**: 2077-2080.
- Fritts HC. 2001. Tree Rings and Climate. *Blackburn Press*, Caldwell, New Jersey. (Originally published 1976, Academic Press London).
- Garfin, G, Jardine A, Merideth R, Black M, Leroy S, eds. 2013. *Assessment of Climate Change in the Southwest United States: A Report Prepared for the National Climate Assessment*. A report by the Southwest Climate Alliance. Washington, DC: Island Press.
- Giannini A, Kushnir Y, Cane MA. 2000. Interannual Variability of Caribbean Rainfall, ENSO, and the Atlantic Ocean. *Journal of Climate* **13** :297–311.
- Gochis, D., Schemm J, Shi W, Long L, Higgins W, Douglas A. 2009. A Forum for Evaluating Forecasts of the North American Monsoon. *EOS Transactions American Geophysical Union* **90**(29): 249. DOI:10.1029/2009EO290002.
- Griffin D, DM Meko, R Touchan, S Leavitt, CA Woodhouse. 2011. Latewood chronology development for summer-moisture reconstruction in the US Southwest. *Tree-ring Research* **67**(2): 87-11.
- Griffin D, CA Woodhouse, DM Meko, DW Stable, HL Faulstich, C Carrillo, R Touchan, CL Castro, SW Leavitt. 2013. North American monsoon precipitation reconstructed from tree-ring latewood. *Geophysical Research Letters*. doi:10.1002/grl.50184.
- Grissino-Mayer HD. 1996. A 2129-year reconstruction of precipitation for northwestern New Mexico, USA. *Tree-rings, Environmental and Humanity, Radiocarbon*, Tucson AZ, 191-204.
- Gutzler DS, Coauthors. 2005. The North American monsoon model assessment project. *Bulletin of the American Meteorological Society* **86**: 1423–1429.
- Gutzler DS, LN Long, J Schemm, SB Roy, M Bosilovich, JC Collier, M Kanamitsu, P Kelly, D Lawrence, M-I Lee, RL Sánchez, B Mapes, K Mo, A Nunes, EA Ritchie, J Roads, S Schubert, H Wei, GJ Zhang. 2009. Simulations of the 2004 North American Monsoon: NAMAP2. *Journal of Climate* **22**: 6716–6740.
- Hastenrath S. 1967. Rainfall distribution and regime in Central America. *Arch. Meteor. Geophys. Bioklimatol.* **15B**: 201-241.
- Heim RR. 2002. A review of Twentieth-Century Drought Indices Used in the United States. *Bulletin of the American Meteorological Society* **83**: 1149-1165.

- Herweijer C, R Seager, ER Cook, J Emile-Geay. 2007. North American droughts of the last millenium from a gridded network of tree-ring data. *Journal of Climate* **20**: 1353-1376.
- Higgins RW, Shi W, Wang XL, 1997. Influence of the North American monsoon system on the U.S. summer precipitation regime. *Journal of Climate*, **10**:2600–2622.
- Howitt RE, Medellin-Azuara J, MacEwan D, Lund JR, Sumner DA. 2014. Economic analysis of the 2014 drought for California agriculture. University of California – Davis CA. 20p: <http://watershed.ucdavis.edu>
- Karnauskas KB, Busalacchi AJ. 2009. The Role of SST in the East Pacific Warm Pool in the Interannual Variability of Central American Rainfall. *Journal of Climate* **22**: 2605–2623.
- Laird KR, Fritz SC, Maasch KA, Cumming BF. 1996. Greater drought intensity and frequency before A.D. 1200 in the northern Great Plains, USA. *Nature* **384**: 552-554.
- Lazo JK, Lawson M, Larsen PH, Waldman DM. 2011. U.S. economic sensitivity to weather variability. *Bulletin of the American Meteorological Society* **92**: 709-720.
- Livezey RE, Chen WY. 1983. Statistical Field Significance and its Determination by Monte Carlo Techniques. *Monthly Weather Review* **111**: 46–59.
- Magaña V, Amador JA, Medina S. 1999. The Midsummer Drought over Mexico and Central America. *Journal of Climate* **12**: 1577-1588.
- Mann ME, Lees JM. 1996. Robust Estimation of background noise and signal detection in climatic time series. *Climate Change* **33**: 409-445.
- Mann ME, Park J. 1994. Global-scale modes of surface temperature variability on interannual to centennial timescales. *Journal of Geophysical Research* **99**: 1055-1058.
- Mann ME, Park J. 1996. Joint spatiotemporal modes of surface temperature and sea level pressure variability in the Northern Hemisphere during the last century. *Journal of Climate* **9**: 2137-2162.
- Mantua NJ, Hare SR, Zhang Y, Wallace JM, Francis RC. 1997. A Pacific interdecadal climate oscillation with impacts on salmon production. *Bulletin of the American Meteorological Society* **78**: 1069-1079.
- McKee TB, Doesken NJ, Kleist J. 1993. The relationship of drought frequency and duration to time scales. *Eight Conference on Applied Climatology*. 17-22 January. Anahelm. California.

Mearns LO, coauthors. 2012. The North American Regional Climate Change Assessment Program: overview of phase I results. *Bulletin of the American Meteorological Society* **93**:1337-1362.

Meko DM, CH Baisan. 2001. Pilot study of latewood-width of conifers as an indicator of variability of summer rainfall in the North American monsoon region. *International Journal of Climatology* **12**: 697-708.

Meko DM, CA Woodhouse, CA Baisan, T Knight, JJ Lukas, MK Hughes, MW Salzer. 2007. Medieval drought in the upper Colorado River Basin. *Journal of Geophysical Research* **34**: 1-5. L10705, doi:10.1029/2007GL029988.

Méndez M, Magaña V. 2010. Regional aspects of prolonged meteorological droughts over Mexico and Central America. *Journal of Climate* **23**: 1175-1188.

Mitchell DL, Ivanova D, Rabin R, Brown TJ, Redmond K. 2002. Gulf of California Sea Surface Temperatures and the North American Monsoon: Mechanistic Implications from Observations. *Journal of Climate* **15**: 2261–2281.

Mosiño AP, García E. 1966. Evaluación de la sequía intraestival en la República Mexicana. *Proc. Conf. Reg. Latinoamericana Union Geogr. Int.* **3**: 500-516.

PRISM Climate Group. 2004. Parameter-elevation Regressions on Independent Slopes Model monthly precipitation grid. *Oregon State University*.
<http://www.prism.oregonstate.edu>.

Rajagolapan B, Mann ME, Lall U. 1998. A multivariate frequency-domain approach to long-lead climatic forecasting. *Weather and Forecasting* **13**: 58-74.

Ray AJ., Garfin GM, Wilder M, Vasquez-Leon M, Lenart M, Comrie AC. 2007. Applications of Monsoon research: Opportunities to inform decision making and reduce regional vulnerability. *Journal of Climate* **20**:1608-1626.

Rayner NA, Parker DE, Horton EB, Folland CK, Alexander LV, Rowell DP, Kent EC, Kaplan A. 2003. Global Analyses of sea surface temperature, sea ice, and night marine air temperature since the late nineteenth century. *Journal of Geophysical Research* **108**(D14): 4407. DOI:10.1029/2002JD002670.

Ropelewski CF, MS Halpert. 1986. North American precipitation and temperature associated with El Niño/Southern Oscillation (ENSO). *Monthly Weather Review* **114**: 2352-2363.

Ropelewski CF, MS Halpert. 1987. Global and regional scale precipitation patterns associated with El Niño/Southern Oscillation (ENSO). *Monthly Weather Review* **115**: 1606-1626.

Schmitz JT, Mullen S. 1996. Water vapor transport associated with the summertime North American monsoon as depicted by ECMWF analyses. *Journal of Climate* **9**: 1621-1632.

Seager R, Hoerling M. 2014. Atmospheric and oceanic origin of North American droughts. *Journal of Climate* **27**: 4581-4606.

Schubert SD, Suarez MJ, Pegion PJ, Koster RD, Bacmeister JT. 2004. On the causes of the 1930s Dust Bowl. *Science* **303**: 1855-1859.

Stahle DW, MK Cleaveland, HD Grissino-Mayer, RD Griffin, FK Fye, MD Therrell, DJ Burnette, DM Meko, JV Diaz. 2009. Cool- and warm-season precipitation reconstructions over western New Mexico. *Journal of Climate* **22**: 3729-3750.

Whitaker JS, Hamill TM. 2002. Ensemble data assimilation without perturbed observations. *Monthly Weather Review* **130**: 1913-1924.

Woodhouse CA, JT Overpeck. 1998. 2000 Years of Drought Variability in the Central United States. *Bulletin of the American Meteorological Society* **79**: 2693-2714.

Figure Captions

Figure 1: Variance of Moisture Flux Convergence for the Twentieth Century Reanalysis (20CR). Summer (top) is defined during July-August and winter (bottom) during November-April. A box in Central America is defined as CA for analysis.

Figure 2: Spatial correlation between the combined Pacific SST index (P-SST) as defined in Castro et al. (2001) and the cool and warm Moisture Flux Convergence (MFC) for summer (top) and winter (bottom) during the period 1871-2012. Local significance is shown with oblique lines and field significance with percentage in lower left corner.

Figure 3: JA MFC composite anomaly for the periods 1888-1901, 1917-1932, 1942-1952 (upper), which are defined for the positive and negative anomalies in the JA MFC time series (bottom). Vectors show the convergence/divergence of the flux. The JA MFC time series is calculated over the Central America (CA) area in Fig. 1. Arrows highlight the intensity of these peaks associated with pluvial and drought regimes. Bars are the interannual variation and solid line the 10-year running mean.

Figure 4: Similar to Fig. 3 but for the cool season.

Figure 5: Similar to Fig. 3 but for 20CR precipitation anomaly. Vector of the MFC in Fig. 3 is conserved for comparison purpose.

Figure 6: LFV spectrum of the spatiotemporal leading MTM-SVD mode for the warm 20CR MFC (a). Spatial correlation between JA 20CR MFC and its reconstructed

temporal pattern for frequencies greater than 10 years (b). Local significance is shown with oblique lines and field significance in percentage. Reconstructed JA 20CR MFC temporal pattern for frequencies greater than 10 years (c). Same boxes and arrow defined in Fig. 3 are superimposed.

Figure 7: Spatial correlation between JA 20CR MFC and its reconstructed temporal pattern for the 25-50 year spectral band (a). Reconstructed JA 20CR MFC temporal pattern for the 25-50 year spectral band (b). Spatial correlation between time series defined in (b) and JA SPI (from P-NOAA). Local significance is shown with oblique lines and field significance in percentage.

Figure 8: Similar to Fig. 6 but for the cold season.

Figure 9: Variance of monthly precipitation for P-NOAA (a), DD-20CR (b), and 20CR (c). During periods 1985-2010 for P-NOAA and 1871-2010 for both DD-20CR and 20CR. Two boxes are highlighted A1 defined at [35-50°N; 125-120°W] and A2 at [30-37.5°N; 115-107.5°W].

Figure 10: Annual cycle of monthly precipitation for the western Pacific Northwest (A1; first column) and Arizona (A2; second column) regions as defined in Fig. 9 for P-NOAA (a), DD-20CR (b), and 20CR (c).

Figure 11: Variance of summer (JA, first column) and winter (NA, second column) precipitation for P-NOAA (upper), DD-20CR (middle), and 20CR (bottom).

Figure 12: LFV of the spatiotemporal leading mode for observed JA SPI (a). The reconstructed temporal mode for frequencies higher than 10 years (b). Spatial correlation between the reconstructed time series defined in (b) and the original observed JA SPI (c). Local significance is shown in oblique lines.

Figure 13: Similar to Fig. 2 but for JA DD-20CR.

Figure 14: Similar to Fig. 13 but for winter (NA).

Figure 15: Warm season (JA) composite sea surface temperature (SST) anomalies for periods 1888-1901, 1917-1932, and 1942-1952 as defined in Fig. 3.

Figure 16: Similar to Fig. 15 but for the cold season (NA).

Figure 17: Warm season spatial correlation between the reconstructed time series of JA DD-20CR SPI defined in Fig. 13b and both JA sea surface temperature (upper) and JA geopotential height at 500 mb (bottom). Local significance is shown in oblique lines and field significance in percentage.

Figure 18: Similar to Fig. 17 but for the cool season (NA).

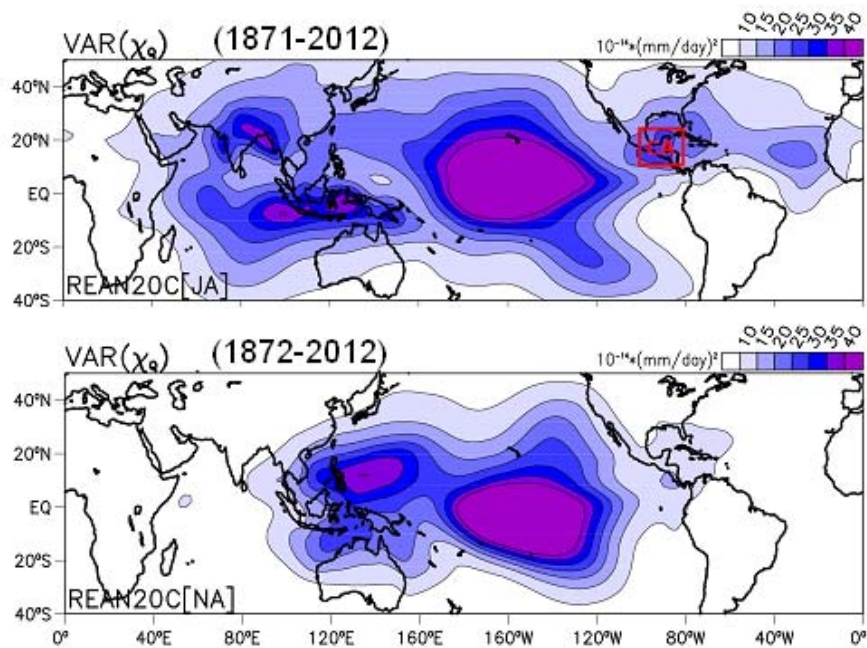


Figure 1: Variance of Moisture Flux Convergence for the Twentieth Century Reanalysis (20CR). Summer (top) is defined during July-August and winter (bottom) during November-April. A box in Central America is defined as CA for analysis.

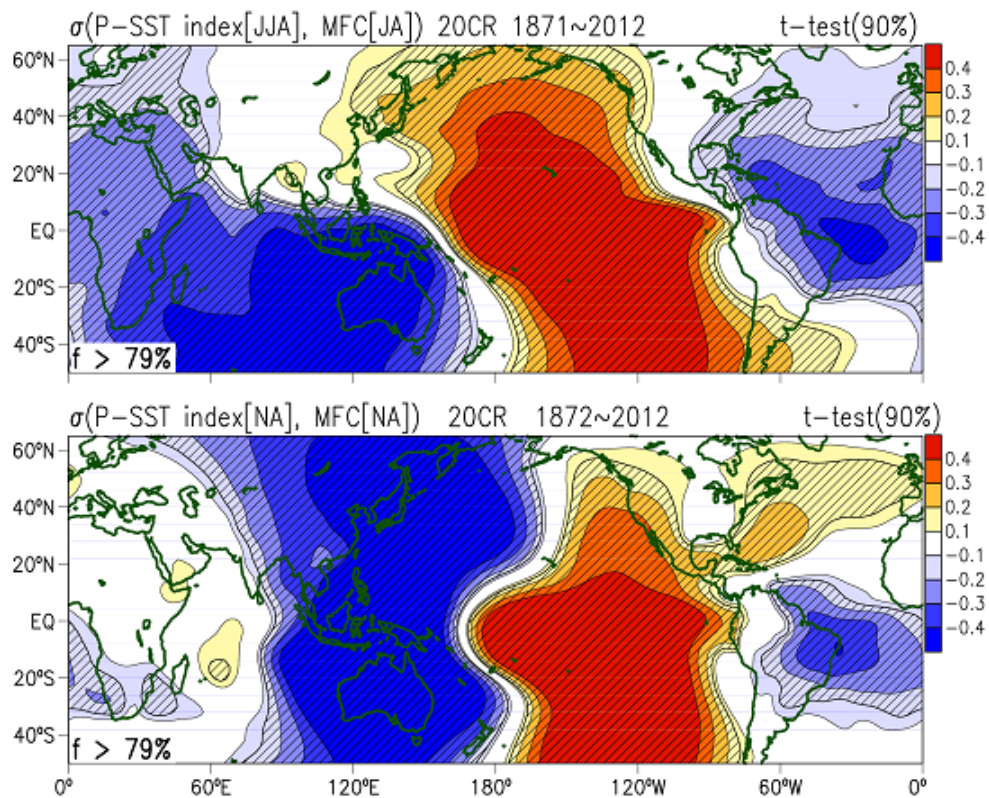


Figure 2: Spatial correlation between the combined Pacific SST index (P-SST) as defined in Castro et al. (2001) and the cool and warm Moisture Flux Convergence (MFC) for summer (top) and winter (bottom) during the period 1871-2012. Local significance is shown with oblique lines and field significance with percentage in lower left corner.

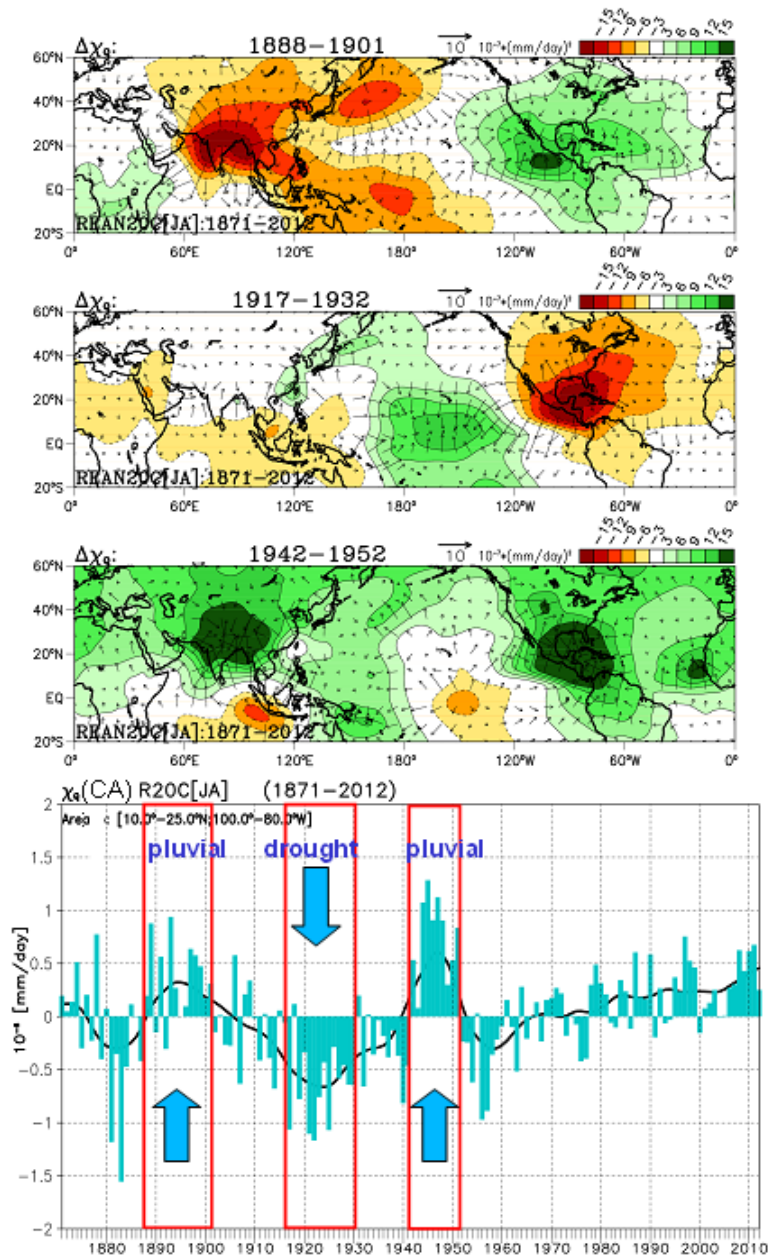


Figure 3: JA MFC composite anomaly for the periods 1888-1901, 1917-1932, 1942-1952 (upper), which are defined for the positive and negative anomalies in the JA MFC time series (bottom). Vectors show the convergence/divergence of the flux. The JA MFC time series is calculated over the Central America (CA) area in Fig. 1. Arrows highlight the intensity of these peaks associated with pluvial and drought regimes. Bars are the interannual variation and solid line the 10-year running mean.

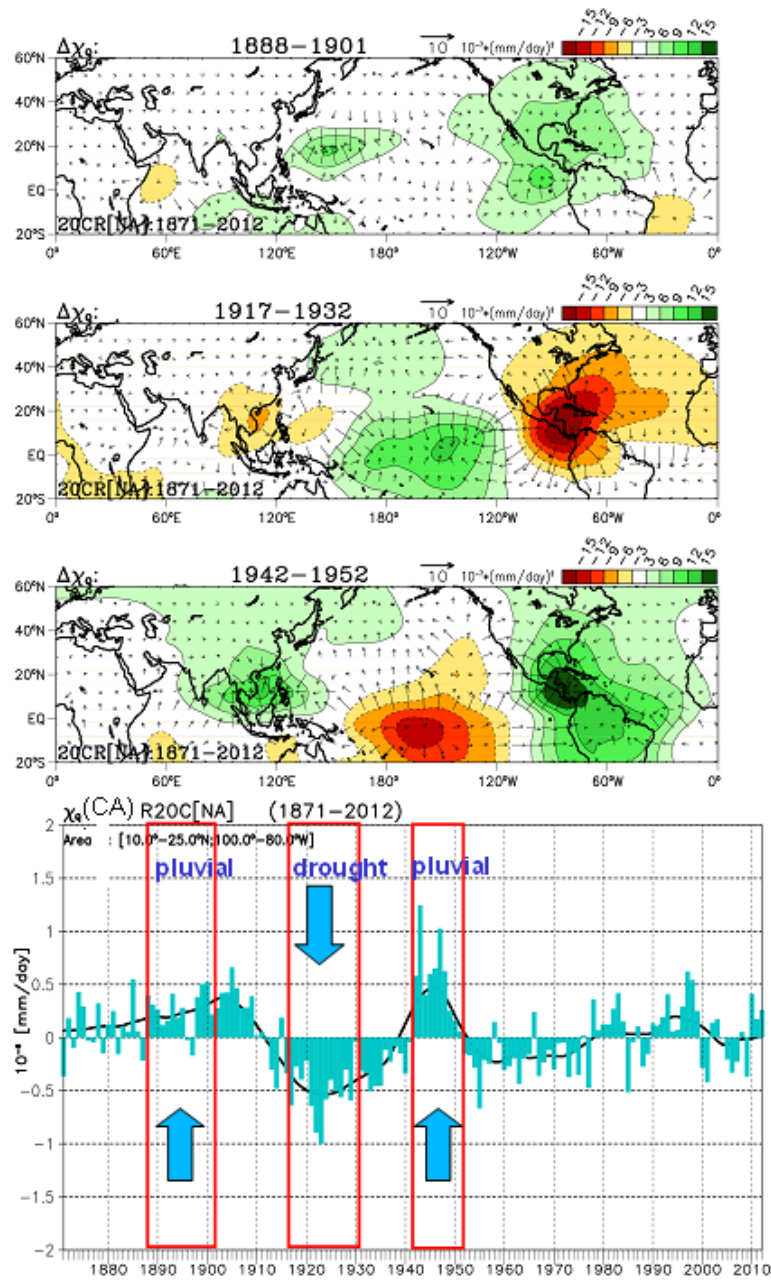


Figure 4: Similar to Fig. 3 but for the cool season.

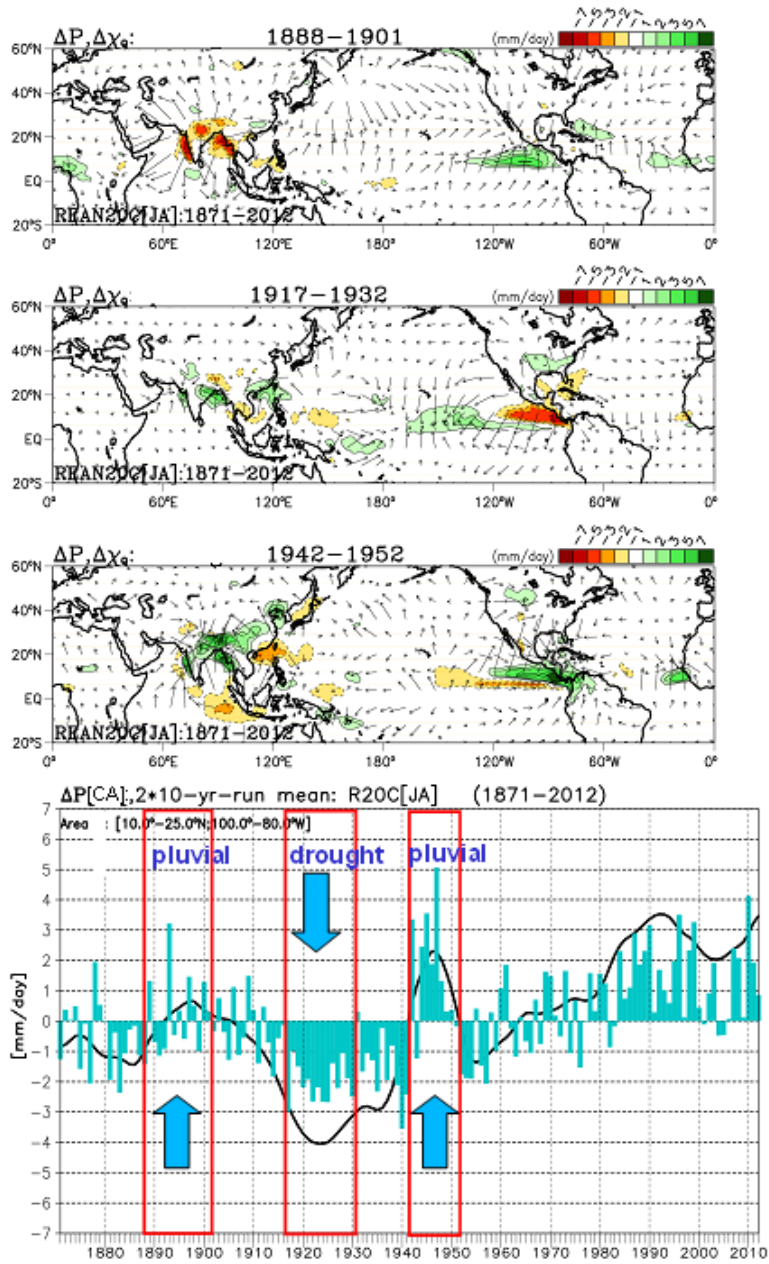


Figure 5: Similar to Fig. 3 but for 20CR precipitation anomaly. Vector of the MFC in Fig. 3 is conserved for comparison purpose.

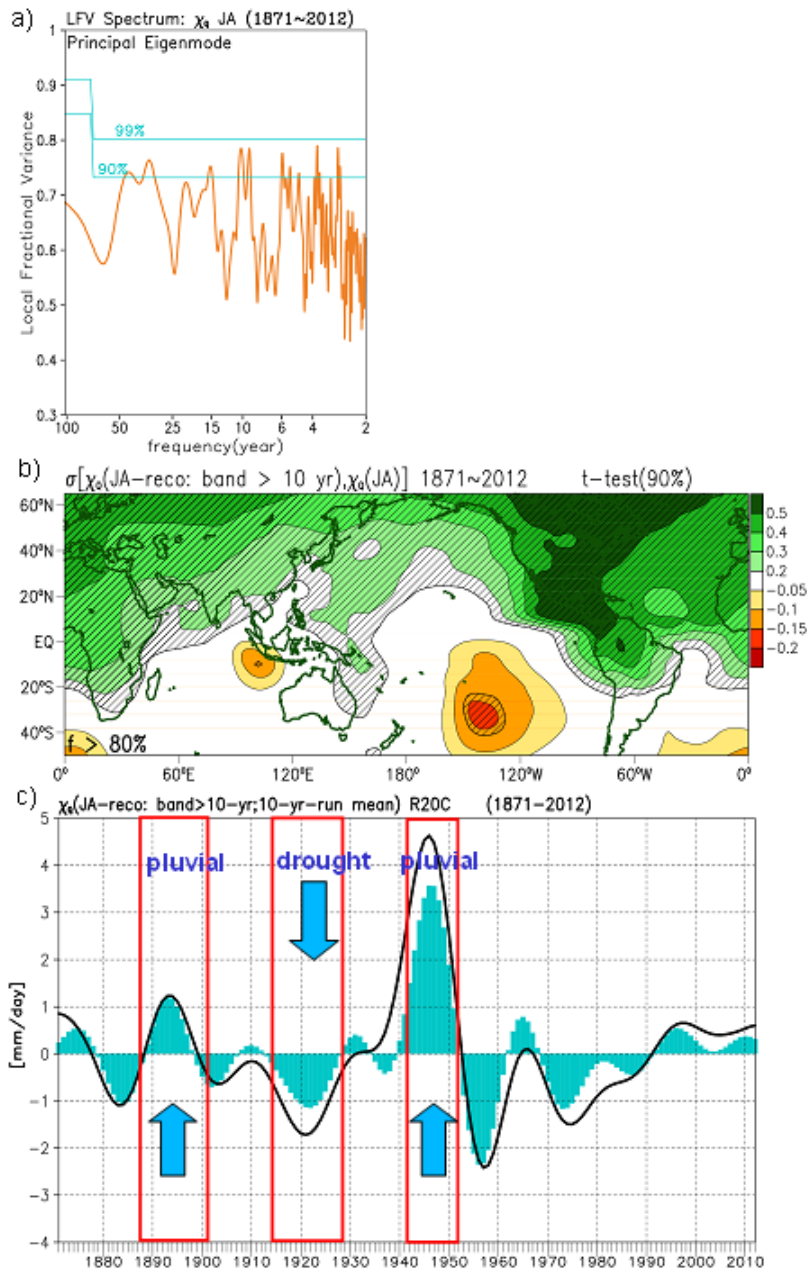


Figure 6: LFV spectrum of the spatiotemporal leading MTM-SVD mode for the warm 20CR MFC (a). Spatial correlation between JA 20CR MFC and its reconstructed temporal pattern for frequencies greater than 10 years (b). Local significance is shown with oblique lines and field significance in percentage. Reconstructed JA 20CR MFC temporal pattern for frequencies greater than 10 years (c). Same boxes and arrow defined in Fig. 3 are superimposed.

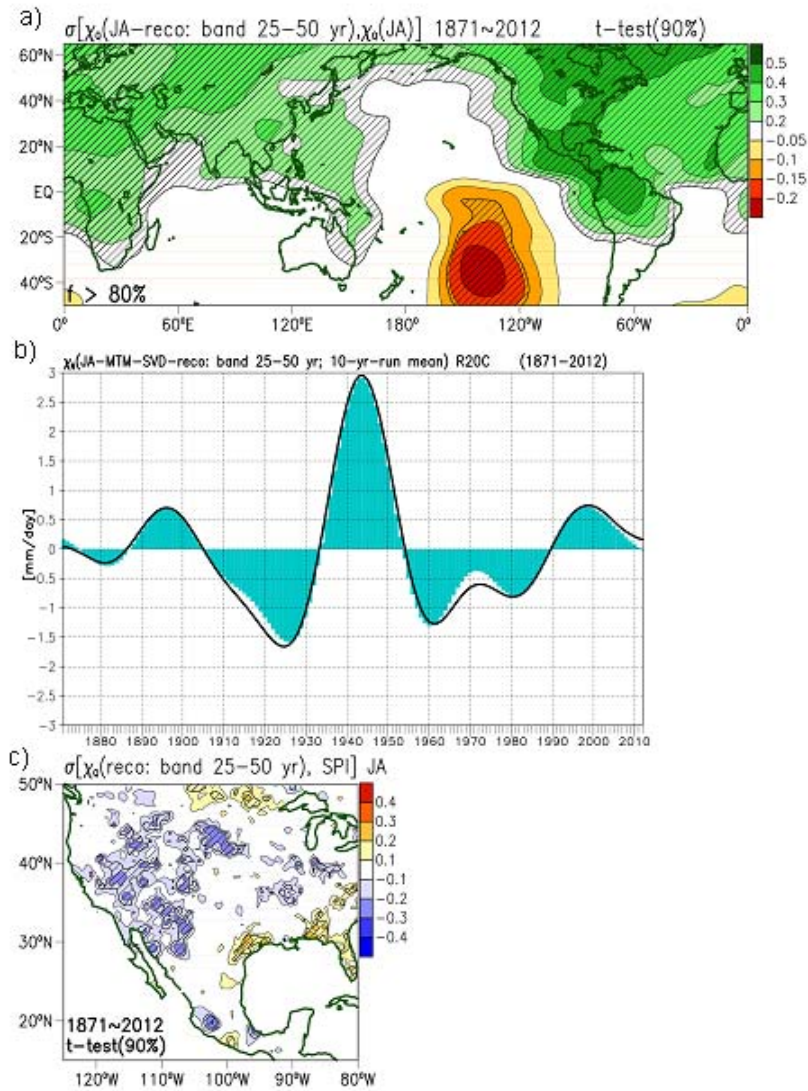


Figure 7: Spatial correlation between JA 20CR MFC and its reconstructed temporal pattern for the 25-50 year spectral band (a). Reconstructed JA 20CR MFC temporal pattern for the 25-50 year spectral band (b). Spatial correlation between time series defined in (b) and JA SPI (from P-NOAA). Local significance is shown with oblique lines and field significance in percentage.

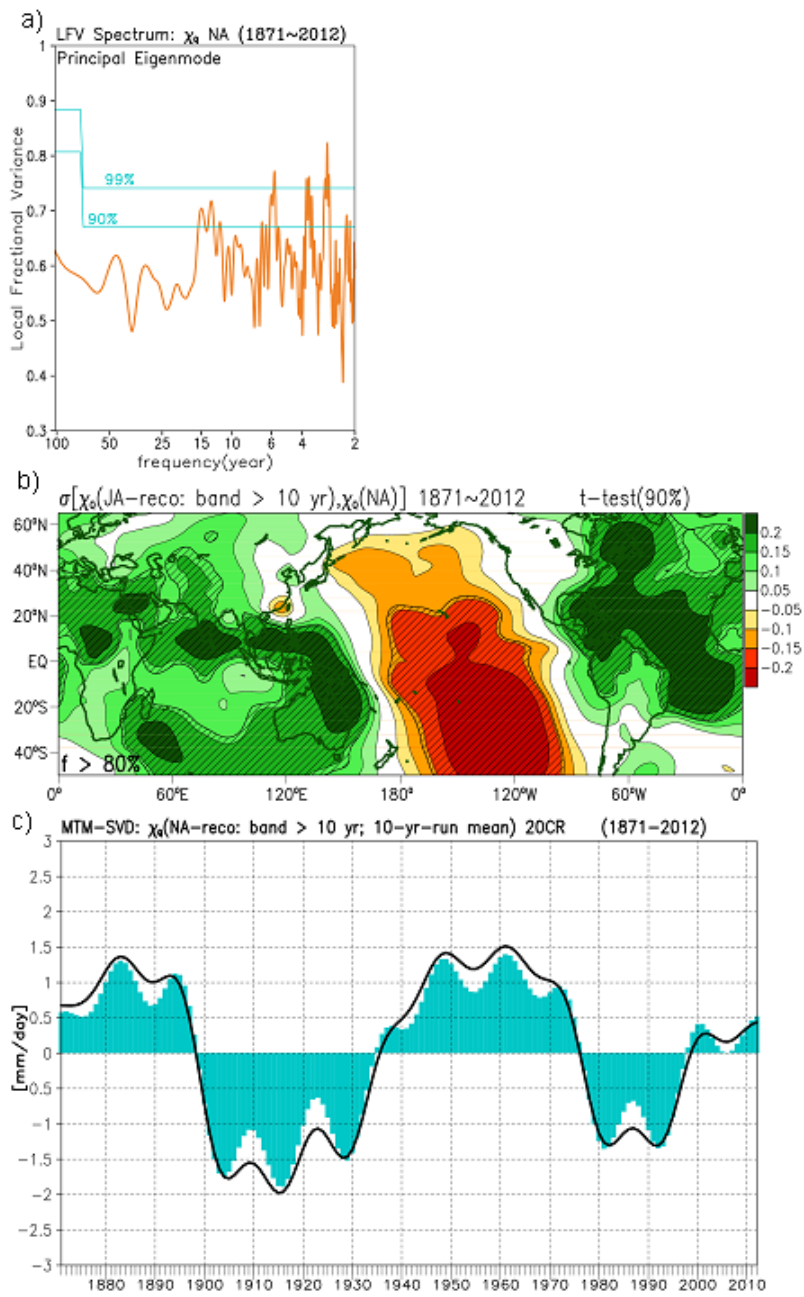


Figure 8: Similar to Fig. 6 but for the cold season.

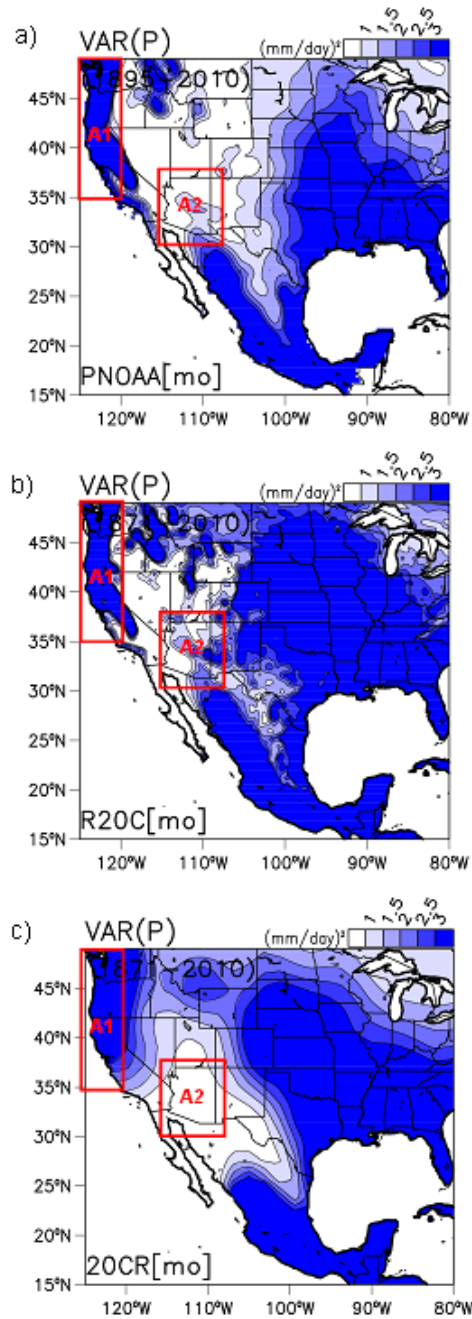


Figure 9: Variance of monthly precipitation for P-NOAA (a), DD-20CR (b), and 20CR (c). During periods 1985-2010 for P-NOAA and 1871-2010 for both DD-20CR and 20CR. Two boxes are highlighted A1 defined at [35-50°N;125-120°W] and A2 at [30-37.5°N;115-107.5°W].

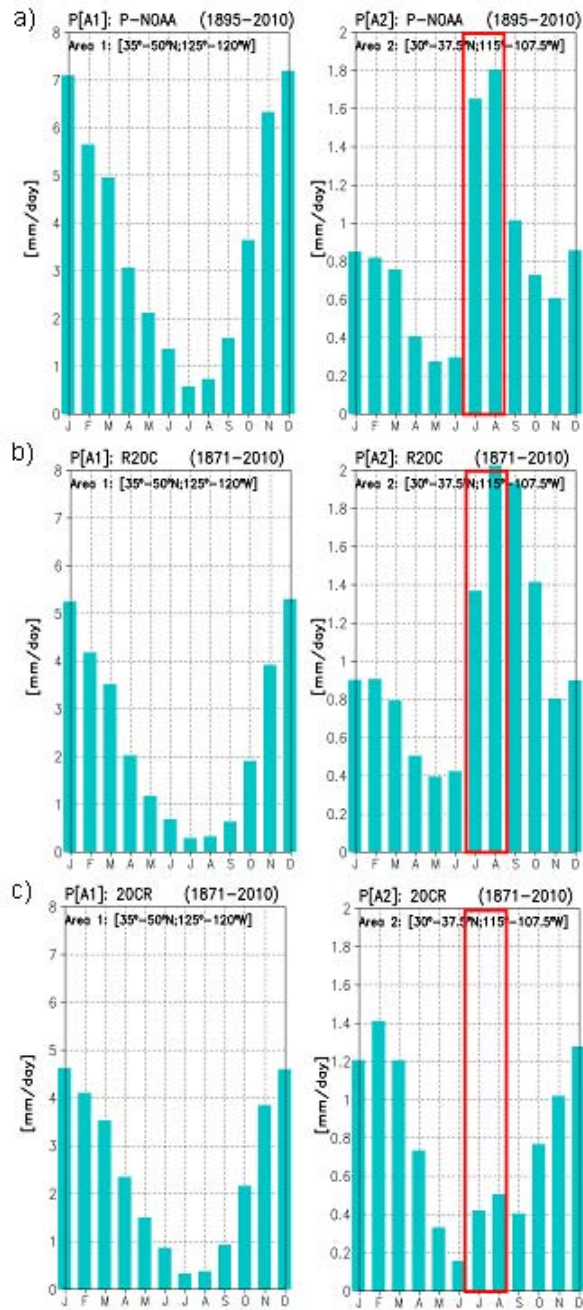


Figure 10: Annual cycle of monthly precipitation for the western Pacific Northwest (A1; first column) and Arizona (A2; second column) regions as defined in Fig. 9 for P-NOAA (a), DD-20CR (b), and 20CR (c).

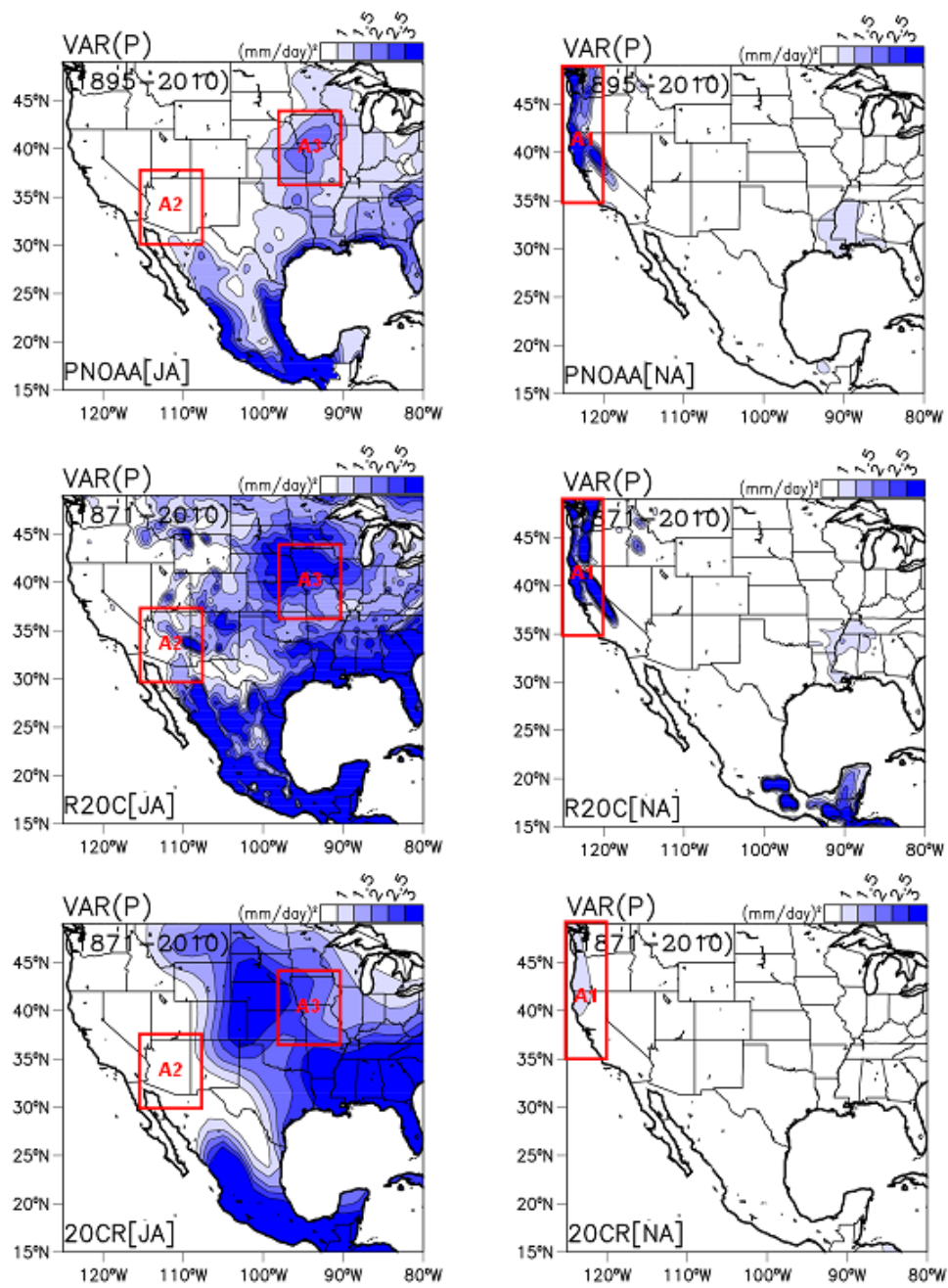


Figure 11: Variance of summer (JA, first column) and winter (NA, second column) precipitation for P-NOAA (upper), DD-20CR (middle), and 20CR (bottom).

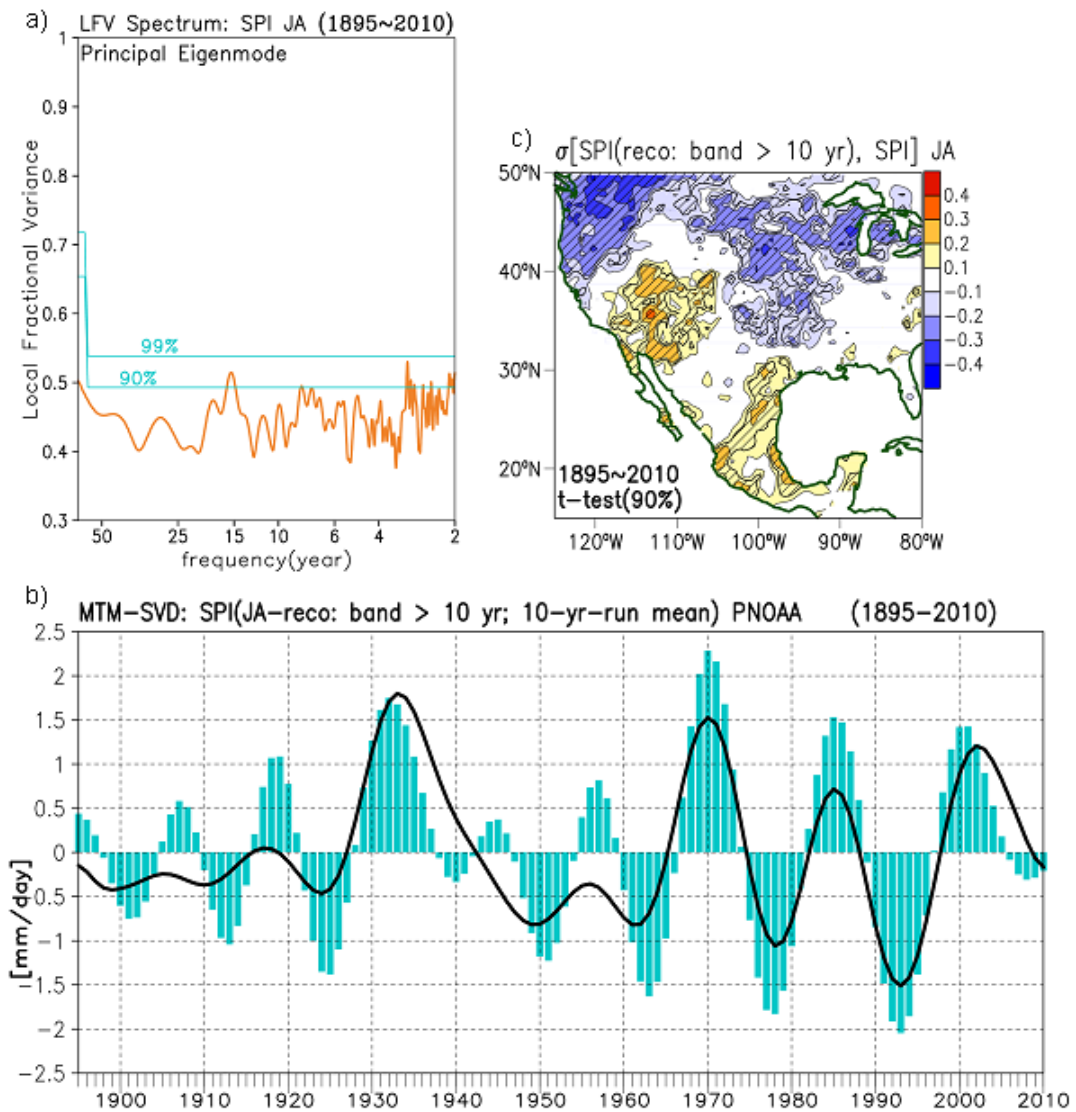


Figure 12: LFV of the spatiotemporal leading mode for observed JA SPI (a). The reconstructed temporal mode for frequencies higher than 10 years (b). Spatial correlation between the reconstructed time series defined in (b) and the original observed JA SPI (c). Local significance is shown in oblique lines.

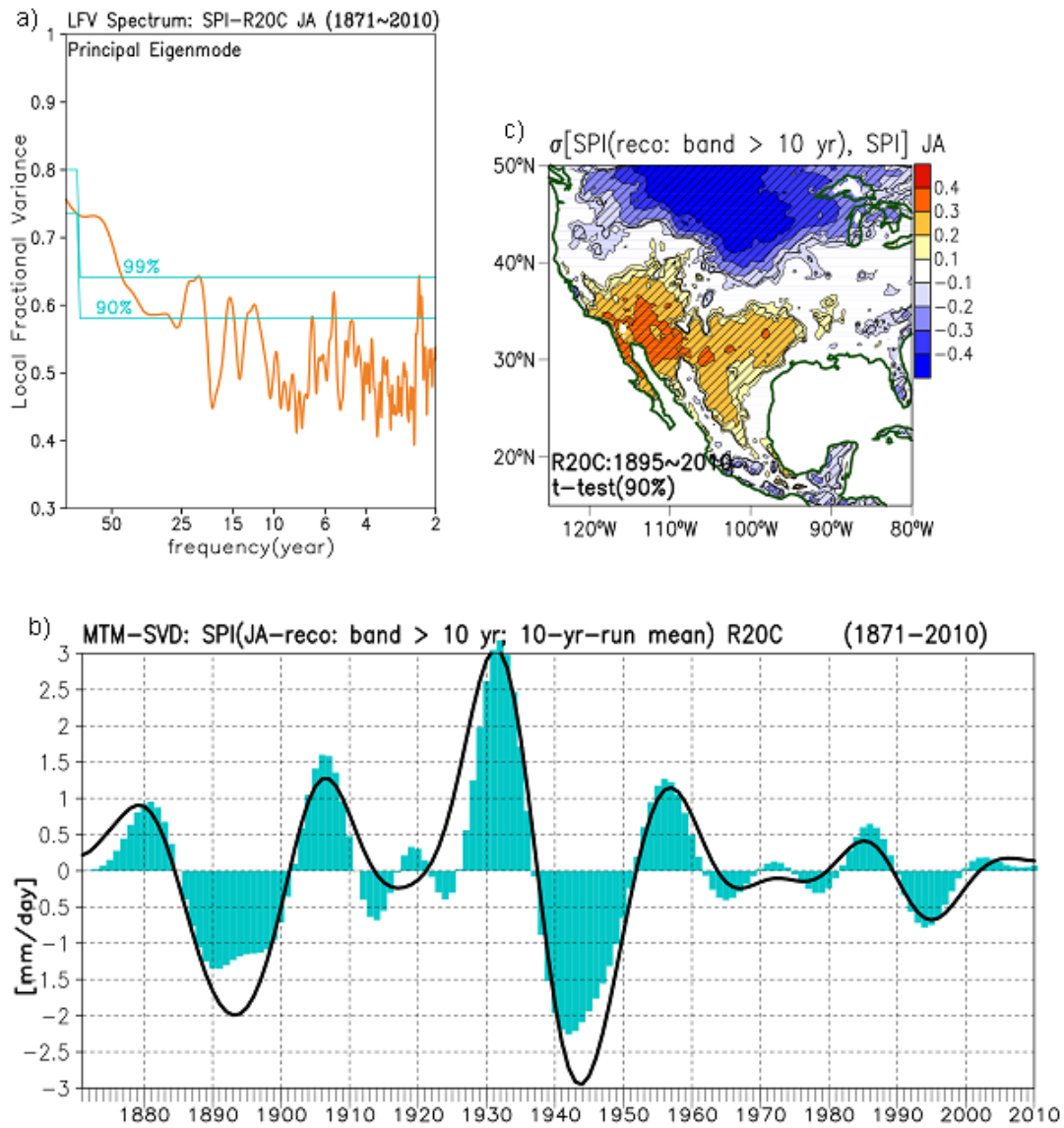


Figure 13: Similar to Fig. 2 but for JA DD-20CR.

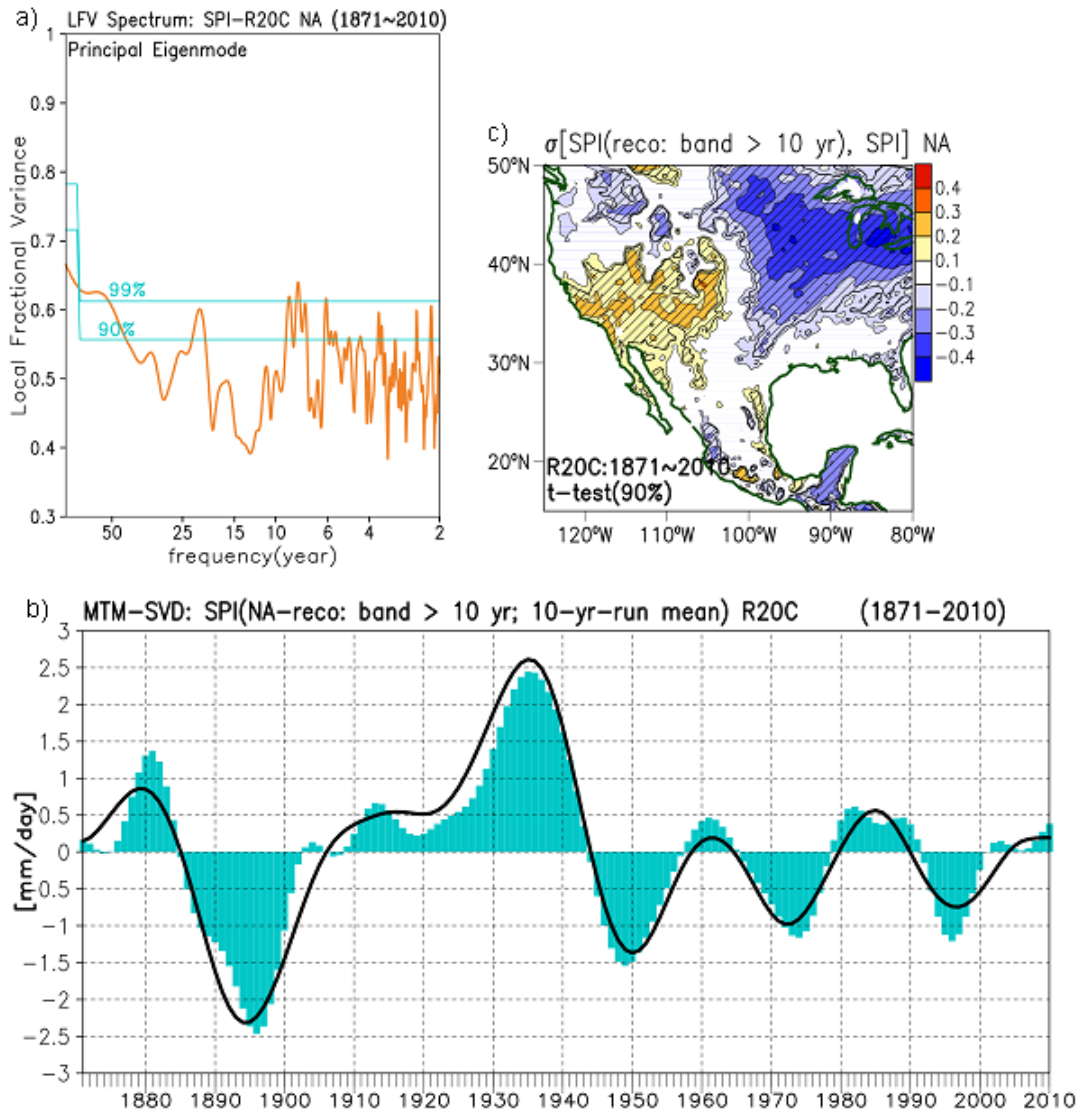


Figure 14: Similar to Fig. 13 but for winter (NA).

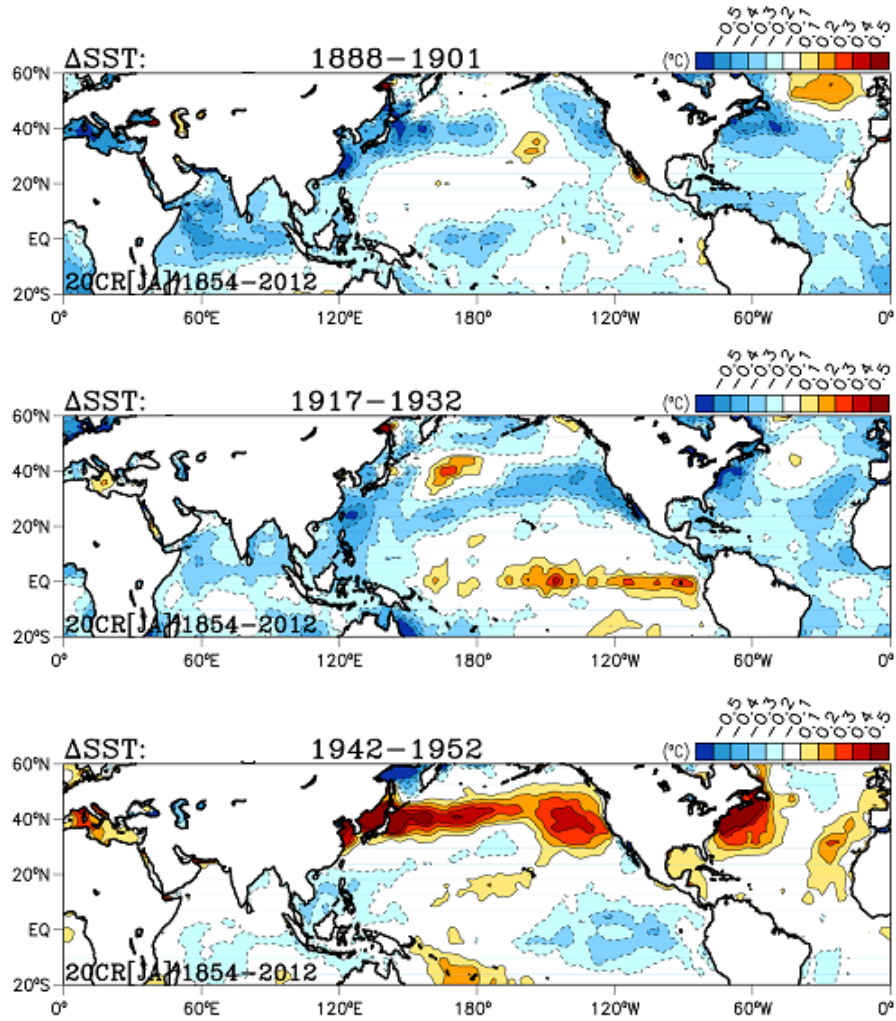


Figure 15: Warm season (JA) composite sea surface temperature (SST) anomalies for periods 1888-1901, 1917-1932, and 1942-1952 as defined in Fig. 3.

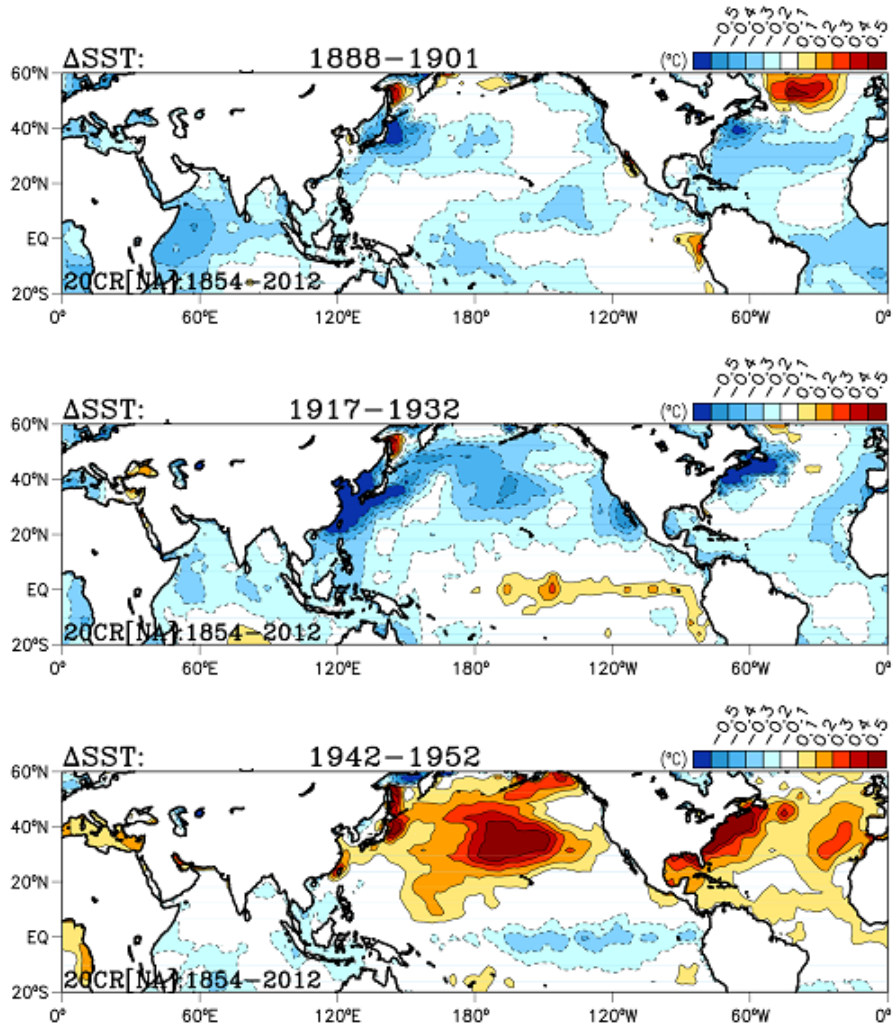


Figure 16: Similar to Fig. 15 but for the cool season (NA).

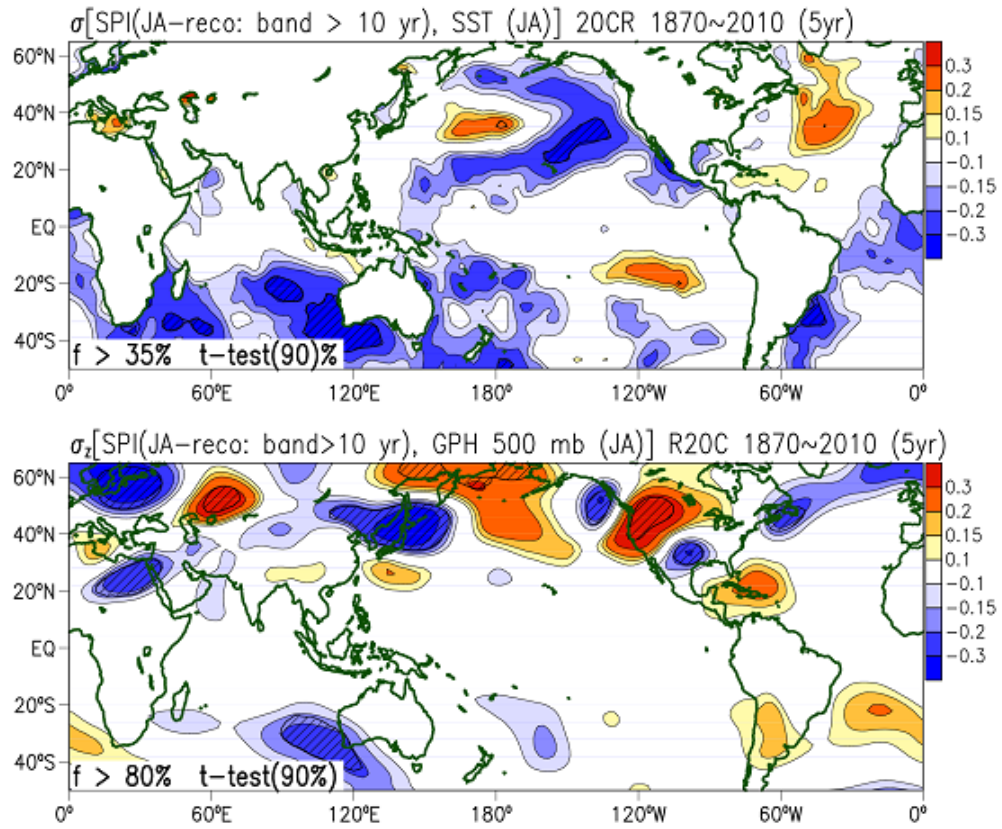


Figure 17: Warm season spatial correlation between the reconstructed time series of JA DD-20CR SPI defined in Fig. 13b and both JA sea surface temperature (upper) and JA geopotential height at 500 mb (bottom). Local significance is shown in oblique lines and filed significance in percentage.

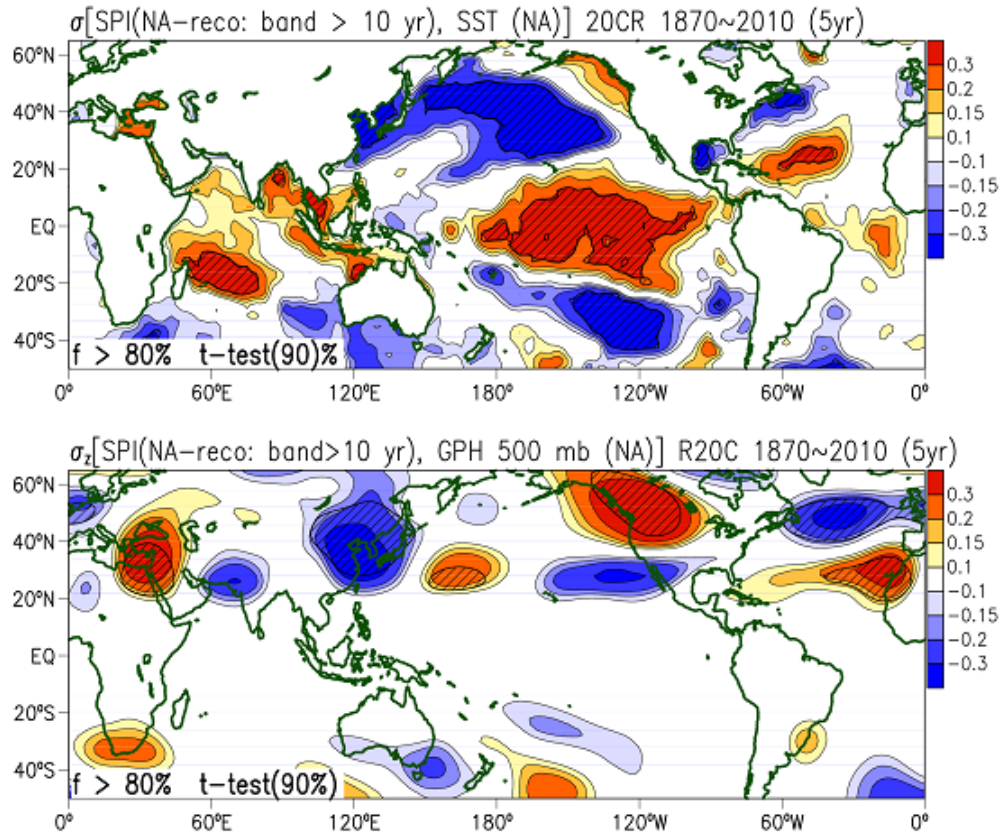


Figure 18: Similar to Fig. 17 but for the cold season (NA).